Influence of Solvent Removal Rate and Polymer Concentration on Ordering Kinetics of Block Copolymers in Solution

Alicia Pape

Dissertation submitted to the faculty of the Virginia Polytechnic Institute and State University in partial fulfillment of the requirements for the degree of

DOCTOR OF PHILOSOPHY

in

Chemical Engineering

Stephen M. Martin - Chair

Donald G. Baird

Herve Marand

Richey M. Davis

February 27, 2017

Blacksburg, VA

Keywords: Block copolymers; self-assembly; polymer solutions; kinetics; polymer physical chemistry

Influence of Solvent Removal Rate and Polymer Concentration on Ordering Kinetics of Block Copolymers in Solution

Alicia Pape

ABSTRACT

An examination of the ordering process of block copolymer microstructure with respect to concentration was performed. Specifically, the process of solution casting block copolymer films was studied using small-angle X-ray scattering (SAXS). A method for determining the volume fraction of ordered phase in solution as the system dried was developed and used to analyze the solution casting process in several different block copolymer films in the neutral solvent toluene; these polymers include poly(styrene-*b*-butadiene), poly(styrene-*b*-isoprene-*b*-styrene), poly(styrene-*b*-butadiene-*b*-styrene), and several poly(methyl methacrylate-*b*-butyl acrylate-*b*-methyl methacrylate) polymers with different block fractions. A method was also developed for studying different drying rates of these films at a constant temperature. Temperature quenches of poly(styrene-*b*-isoprene-*b*-styrene) were performed to evaluate the effect of concentration on ordering rate.

In all cases studied, an ordering layer was observed where self-assembly was thermodynamically favorable. This layer steadily grew until it reached the bottom substrate, resulting in a two-step ordering process. In the case of the styrene/diene copolymers, a constant polymer concentration was observed in the ordering layer as it grew to encompass the entire film. Kinetic entrapment was observed in the case of the diblock copolymer, as the system with a medium drying rate with respect to the other two experienced faster kinetics than the other two systems. For the two triblock copolymers, it was found that similar kinetics were observed with respect to the ordering layer concentration, largely due to skinning on the surface allowing time for lower sections of the film to order more completely.

In the acrylate copolymers studied, the kinetics were not able to be evaluated with respect to drying rate. This was due to domain compression that cause a disordering of ordered microstructure as solvent was removed. This disordering was attributed to interfacial disruption caused by the compression in the film. In addition, a significant decrease in domain spacing was observed to occur in the vertical direction as a result of compression in that direction and pinning of the film to the substrate in the horizontal direction.

Finally, the Avrami kinetic model was fit to several concentration of styrene/isoprene triblock copolymers as they ordered after a temperature quench. A U-shaped curve was observed in the system, as a result of competition between chain mobility effects and thermodynamic effects that occur as polymer concentration increases away from the C_{ODT}. It was found that the Avrami exponent remained constant over all concentrations, and an empirical model was fit to find the various rate constants at each polymer concentration.

Influence of Solvent Removal Rate and Polymer Concentration on Ordering Kinetics of Block Copolymers in Solution

Alicia Pape

GENERAL AUDIENCE ABSTRACT

Block copolymers are polymers consisting of two or more separate regions made up of different types of polymer chains. Under favorable conditions, these chains will phase separate into ordered structures, with different components being made up of each block. Because they are attached to each other, these structures are in the size range of 10-100nm. For example, a phase separated styrene/butadiene block copolymer of a particular composition can form cylindrical structures where the cylinders are made up of polystyrene, and the surrounding matrix is made up of polybutadiene. These structures can greatly influence the properties of block copolymers, allowing them to be used for everything from lithography to fuel cell membranes.

A common method for the production of block copolymer films for applications such as fuel cell membranes is solution casting, where a polymer in a solvent is spread on a surface and the solvent is allowed to dry. The rate of this drying is a parameter that is not often taken into account when designing a process, despite the fact that it can have an effect on the resulting structure. Thus, insight into how the ordering of structures in a film during film drying can be used to improve processing of these materials.

Using a computer model to determine the concentration profile of solvent throughout the film, and combining this with x-ray scattering data taken during drying at different rates, it was determined that there was a layer in which ordering could proceed, or ordering layer, that steadily grew as the film dried. This ordering layer continued to grow until it encompassed the entire film. In the diblock (styrene/butadiene) copolymer that was studied, it was found that a medium drying rate produced the fastest ordering. This drying condition balanced the driving force for ordering created by the increased drying rate and the ability of the chains to arrange, which would have been reduced upon faster drying. This effect was not seen in the two triblock copolymers (styrene/butadiene/styrene and styrene/isoprene/styrene). In the triblock copolymers, the ordering rate only depended on bulk ordering layer concentration. This was attributed to the presence of a skin on the surface, which slowed ordering

throughout the films. In the case of the acrylate triblocks that were studied, the ordering rate trend could not be determined, as compression in the film due to the removal of solvent caused ordered structures to disorder after they formed.

Finally, a model was fit to the styrene/isoprene/styrene at different solvent concentrations. The different concentrations produced a U-shaped curve with respect to ordering time, resulting again from competition between driving force and the ability of the chains to rearrange.

Acknowledgements

This work would not have been possible without support from a number of people. I would like to thank my advisor, Dr. Stephen M. Martin for his continued guidance and support throughout my time at Virginia Tech. I would also like to thank Dr. Herve Marand for his insight and advice, and especially for his help later in the project. I am grateful to Dr. Donald Baird for offering his encouragement and critique. Finally, I would like to acknowledge Dr. Richey Davis for providing assistance with several different aspects of the project.

I would like to thank Dr. John Pople for helping to gather data, and Dr. Sue Mecham for her aid in characterization.

In addition, I would like to acknowledge my lab mates and various students that I have worked with over the years.

- Dr. Du Hyun Shin
- Dr. Feras Rabie
- Dr. Ninad Dixit
- Dr. Carlos Landaverde
- Dr. Wai-fong Chan
- Ethan Smith
- Martha Hay
- Mohamed Mohamedali
- Sahel Aminian
- Coogan Thompson
- Victoria Lu

There are several other individuals that I would like to recognize.

- My parents for their continued support and encouragement throughout my life and academic career
- My brother for his companionship
- My extended family for their love and support
- Staff of the Chemical Engineering Department, especially Diane Cannaday

Table of Contents

List of Figures

List of Tables

1 Introduction

Block copolymer films are commonly produced using a solution-casting method. The microphase ordered structures that form in these films are known to be affected by the drying rate used during production.[1,2] Previous work by Heinzer, et al.[3,4] investigated the effect of drying rate on microphase separation kinetics, but utilized temperature to control drying rate, meaning that the effect of concentration changes on ordering were not able to be directly measured. We wish to study the kinetics of microphase separation in thick (>100μm) films that occurs during the drying process.

Several models have been proposed to account for the effects of temperature change in the Avrami kinetic model. Two different approaches are that of Lambrigger[5], and that of Farjas and Roura[6,7]. Both of these approaches apply to temperature ramps, but use very different approaches. Lambrigger relates the Avrami exponent to an apparent reaction order defined by the inflection point. Farjas and Roura utilized a scaling analysis relating dimensionless time to the heating or cooling rate, assuming an Arrhenius relationship between temperature and nucleation and growth rates to obtain Avrami master curves.

The goal of this research is ultimately to relate the kinetics of block copolymer self-assembly in solution during casting to the drying rate. Little work has been done to relate this drying rate and the polymer concentration in solution to ordering kinetics[3,4] despite the fact that microstructure can greatly be affected.[2] It is hoped that this work will ultimately allow for the optimization of solution-casting processes for various applications.

The ultimate questions this research seeks to address are:

1. *What are the overall effects of altering the film drying rate on self-assembly kinetics in solution-cast thick block copolymer films?*
2. *How does concentration affect the kinetics of self-assembly in such films?*

To answer these questions, the following approaches will be taken:

1. To modify a method previously developed by our group for tracking in-situ ordering to more directly control the drying rate of a solution-cast block copolymer film
2. To develop a method of determining volume fraction ordered phase in block copolymer films during solution casting, accounting for changing solvent concentration throughout the film and the partitioning of solvent between blocks
3. To determine the relative ordering rate of solution-cast block copolymer films with respect to drying rate and bulk solvent concentration in the film
4. To determine the effect of the drying process on the self-assembly kinetics in thick block copolymer films
5. To obtain a semi-empirical relationship between concentration and the parameters of the Avrami equation

We created a method of increasing the drying rate of a block copolymer film without changing the temperature of the system. Measurements of the volume fraction of ordered domains, $\phi(t)$, in the films were taken with small-angle X-ray scattering (SAXS). SAXS was used in-situ to study ordering in block copolymer films during drying and was combined with a drying model to determine the effect of changing concentration on ordering in the films. We modified the Avrami equation to account for the effects of solvent concentration under iso-concentration conditions.

The format of this dissertation is as follows:

A review of relevant literature is provided in Chapter 3.

Chapter 4 describes the drying model and solvent partitioning used to determine the volume fraction of ordered phase. It also examines the ordering rate in a cast poly(styrene-*b*-butadiene) solution in the neutral solvent, toluene.

Chapter 5 discusses the ordering kinetics of two styrene/diene triblock copolymers in toluene. These are poly(styrene-*b*-butadiene-*b*-styrene), and poly(styrene-*b*-isoprene-*b*-styrene). Both of these polymer solutions exhibit slower toluene diffusivity than the diblock copolymer.

Chapter 6 discusses the phenomenon of domain compression and subsequent disordering observed in PMMA/PBA triblock copolymer of varying block fraction.

Chapter 7 describes the effect of polymer concentration on the half-times of ordering observed during temperature quenches in solutions of varying concentration. These results were then correlated to the Avrami equation.

A summary and a description of potential future work is provided in Chapter 8.

References

1. Huang, H.; Zhang, F.; Hu, Z.; Du, B.; He, T.; Lee, F. K.; Wang, Y.; Tsui, O. K. C., Study on the Origin of Inverted Phase in Drying Solution-Cast Block Copolymer Films. *Macromolecules* **2003,** *36* (11), 4084-4092.
2. Lee, M.; Park, J. K.; Lee, H.-S.; Lane, O.; Moore, R. B.; McGrath, J. E.; Baird, D. G., Effects of block length and solution-casting conditions on the final morphology and properties of disulfonated poly(arylene ether sulfone) multiblock copolymer films for proton exchange membranes. *Polymer* **2009,** *50* (25), 6129-6138.
3. Heinzer, M. J.; Han, S.; Pople, J. A.; Baird, D. G.; Martin, S. M., In Situ Measurement of Block Copolymer Ordering Kinetics during the Drying of Solution-Cast Films Using Small-Angle X-ray Scattering. *Macromolecules* **2012,** *45* (8), 3471-3479.
4. Heinzer, M. J.; Han, S.; Pople, J. A.; Martin, S. M.; Baird, D. G., Iso-concentration ordering kinetics of block copolymers in solution during solvent extraction using dynamic oscillatory measurements. *Polymer* **2012,** *53* (15), 3331-3340.
5. Lambrigger, M., Non-isothermal polymer crystallization kinetics and avrami master curves. *Polymer Engineering and Science* **1998,** *38* (4), 610.
6. Farjas, J.; Roura, P., Modification of the Kolmogorov–Johnson–Mehl–Avrami rate equation for non-isothermal experiments and its analytical solution. *Acta Materialia* **2006,** *54* (20), 5573-5579.
7. Farjas, J.; Roura, P., Solid-phase crystallization under continuous heating: Kinetic and microstructure scaling laws. *Journal of Materials Research* **2008,** *23* (02), 418-426.

2 Literature Review

2.1 Film Drying

The drying of homopolymer films is an important problem in polymer science as film casting is a common method for the production of coatings in industry. The drying process that occurs in an oven or at room temperature includes quite a few parameters that must be considered, for instance: the shrinkage of the film, evaporative cooling, and diffusivity changes as the solvent concentration drops in the film, et cetera. Modeling of this problem has been performed using both molecular dynamics simulations [1] and bulk parameter simulations. [2] [3].

G.A. Buxton and N. Clarke[2] used the finite difference method to simulate phase separation in thin films of polymer blends upon spin coating a 10% solution. It was found that, as the film dried, growth of ordered domains proceeded down from the top of the film via a nucleation and growth mechanism. Later on in the process, spinodal decomposition occurred near the substrate before the ordering front was able to reach the bottom of the film.

M. Tsige and G.S. Grest[1] created a molecular dynamics simulation to simulate the drying of both a homopolymer and heteropolymer in solvent. Skinning was predicted to occur under the conditions that were studied. In addition, the difference in the stiffness of the blocks was found to be important in the rate of solvent evaporation. The rate of evaporation from homopolymer and heteropolymer was found decrease exponentially with respect to time. [1]

J.S. Vrentas and C.M. Vrentas [3] produced an unsteady state model of film drying for a homopolymer film on a moving substrate in an oven with gas above and below the system. They also took into account the changes in temperature of the film that are brought on by solvent evaporation. A schematic of the system considered can be seen below

Vrentas and Vrentas assume no velocity gradients down the film, a steady state drying process, Newtonian

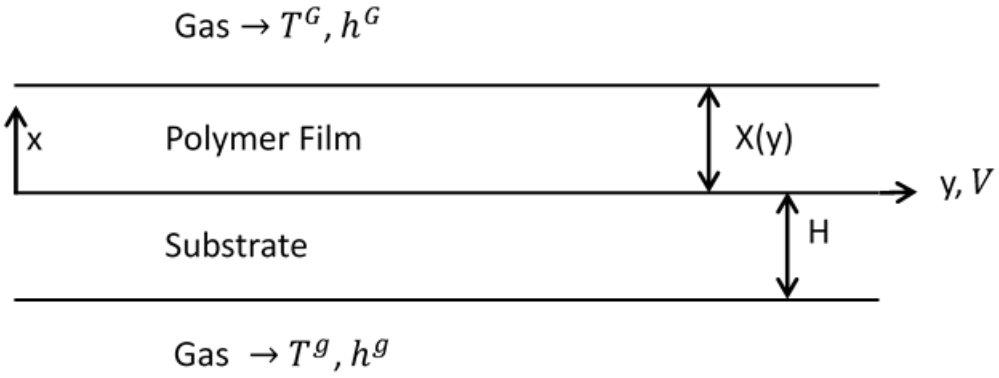

Figure 2-1: Schematic of the model system from [3]

polymer, one polymer and solvent, no excess volume, no gravitational effects, constant density, constant heat capacity, constant thermal conductivity, density is only a function of polymer concentration, no viscous dissipation, uniform substrate temperature, uniform polymer film temperature, no kinetic energy effects at the interfaces, inviscid gas, uniform pressure, a system that isn't in the glassy state, and that momentum transfer via convection is negligible. They use a jump mass balance, a jump momentum balance and a jump energy balance at the interface between the polymer and the gas above it. Using volume rather than mass in this way simplifies the mass, energy, and momentum balances.

A jump mass balance at an interface of phase A and phase B is given as

$$\rho^A(\boldsymbol{v}^A \cdot \boldsymbol{n}^* - \boldsymbol{U}^* \cdot \boldsymbol{n}^*) = \rho^B(\boldsymbol{v}^B \cdot \boldsymbol{n}^* - \boldsymbol{U}^* \cdot \boldsymbol{n}^*) \tag{2-1}$$

with a jump mass balance of species I of

$$\rho_I^A(\boldsymbol{v}_I^A \cdot \boldsymbol{n}^* - \boldsymbol{U}^* \cdot \boldsymbol{n}^*) = \rho_I^B(\boldsymbol{v}_I^B \cdot \boldsymbol{n}^* - \boldsymbol{U}^* \cdot \boldsymbol{n}^*) \tag{2-2}$$

Here, $\boldsymbol{n}^*$ is the unit normal from phase B to phase A, and $\boldsymbol{U}^*$ is the velocity of the phase boundary. For phase J, ρ^J is is the mass density, and $\boldsymbol{v}^J$ is the mass average velocity. Due to the steady state assumption,

$$\boldsymbol{U}^* \cdot \boldsymbol{n}^* = 0 \tag{2-3}$$

The jump linear momentum balance is

$$\rho^A \boldsymbol{v}^A(\boldsymbol{v}^A \cdot \boldsymbol{n}^* - \boldsymbol{U}^* \cdot \boldsymbol{n}^*) - \boldsymbol{\tau}^A \cdot \boldsymbol{n}^* = \rho^B \boldsymbol{v}^B(\boldsymbol{v}^B \cdot \boldsymbol{n}^* - \boldsymbol{U}^* \cdot \boldsymbol{n}^*) - \boldsymbol{\tau}^B \cdot \boldsymbol{n}^* \tag{2-4}$$

The jump energy balance is given as

$$\rho^A \hat{U}^A(\boldsymbol{v}^A \cdot \boldsymbol{n}^* - \boldsymbol{U}^* \cdot \boldsymbol{n}^*) + \boldsymbol{q}^A \cdot \boldsymbol{n}^* - \boldsymbol{v}^A \cdot (\boldsymbol{\tau}^A \cdot \boldsymbol{n}^*) = \rho^B \hat{U}^B(\boldsymbol{v}^B \cdot \boldsymbol{n}^* - \boldsymbol{U}^* \cdot \boldsymbol{n}^*) + \boldsymbol{q}^B \cdot \boldsymbol{n}^* - \boldsymbol{v}^B \cdot (\boldsymbol{\tau}^B \cdot \boldsymbol{n}^*) \tag{2-5}$$

with $\hat{U}^A$ and $\hat{U}^B$ as the specific internal energies of phases A and B, and $\boldsymbol{q}^J$ as the heat flux due to conduction in J. This conductive heat flux can be determined using Fourier's law of conduction for temperature of J, T^J and thermal conductivity k^J

$$\boldsymbol{q}^J = -k^J \nabla T^J \tag{2-6}$$

Here, temperatures across interfaces are assumed to be equal. It is also assumed that there is a no-slip boundary condition, and that, at the interface between phases, the phases are at equilibrium. At the interface, the first two assumptions can be represented as

$$T^A = T^B \tag{2-7}$$

$$\boldsymbol{t} \cdot \boldsymbol{v}^A = \boldsymbol{t} \cdot \boldsymbol{v}^B \tag{2-8}$$

$\boldsymbol{t}$ is the unit vector tangent to the interface.

The partial pressure of component 1 in the gas a the interface.

$$p_{1i}^G = f(\rho_1^P) \tag{2-9}$$

Where ρ_1^P is the mass density of 1 in the film. In addition, at the film/air interface, it is assumed that

$$\boldsymbol{q}^G \cdot \boldsymbol{n}^* = h^G(T^P - T^G) \tag{2-10}$$

$$\rho_1^A(\boldsymbol{v}_1^A \cdot \boldsymbol{n}^* - \boldsymbol{U}^* \cdot \boldsymbol{n}^*) = k_1^G(p_{1i}^G - p_{1b}^G) \tag{2-11}$$

where h^G is the heat transfer coefficient of the air in the oven. The components of the unit normal vector $\boldsymbol{n}^*$ at $x = X(y)$, which can also be expressed as $X(t)$, as, for this system, $y = Vt$, where V is the velocity of the substrate, can be given by

$$\boldsymbol{n}_x^* = \left[1 + \left(\frac{dX}{dy}\right)^2\right]^{-1/2} \approx 1 \tag{2-12}$$

$$\boldsymbol{n}_y^* = -\frac{\frac{dX}{dy}}{\left[1 + \left(\frac{dX}{dy}\right)^2\right]^{1/2}} \approx -\frac{dX}{dy} \tag{2-13}$$

$$\boldsymbol{n}_z^* = 0 \tag{2-14}$$

The mass flux was assumed to occur via diffusion. A velocity field in the film of $v^P = v_y^P = V$ was assumed. Because of this, and the fact that it is assumed that there is no conduction in the y direction, at the upper film interface,

$$\boldsymbol{v}^P \cdot \boldsymbol{n}^* = -\frac{dX}{dt} \tag{2-15}$$

$$\boldsymbol{q}^P \cdot \boldsymbol{n}^* = -k^P \frac{\partial T^P}{\partial x} \tag{2-16}$$

The jump mass balance at $x = X(y)$ can be given as

$$\rho^P \boldsymbol{v}^P \cdot \boldsymbol{n}^* = \rho^G \boldsymbol{v}^G \cdot \boldsymbol{n}^* = Q \tag{2-17}$$

where Q is the volumetric flow rate. At the substrate, the jump energy balance at the interface between substrate and film can be found to be

$$k^P \frac{\partial T^P}{\partial x} = k^S \frac{\partial T^S}{\partial x} \tag{2-18}$$

At $x = X$, it was thus found that the temperature boundary condition was

$$k^P \frac{\partial T^P}{\partial x} = \Delta \widehat{H}_{vap} \rho^P \frac{dX}{dt} + h^G (T^G - T^P) \tag{2-19}$$

where $\Delta \widehat{H}_{vap}$ is the specific enthalpy of vaporization for the solvent. The mass flux of component I in the film is given by

$$\rho_I^P \boldsymbol{v}_I^P = \rho_I^A (\boldsymbol{v}^P)^{\ddagger} - D^P \nabla \rho_I^P \tag{2-20}$$

where D^P is the mutual diffusion coefficient in the film, and $(\boldsymbol{v}^P)^{\ddagger}$ is the volume average velocity in the film. In addition, the density has a second order dependence on temperature, meaning that, throughout the film,

$$\nabla \cdot (\boldsymbol{v}^P)^{\ddagger} = 0 \tag{2-21}$$

and thus,

$$\frac{\partial (\boldsymbol{v}_x^P)^{\ddagger}}{\partial x} = 0 \tag{2-22}$$

It is assumed that there is no bulk velocity in the x direction, and that

$$\frac{\partial \rho_I^P}{\partial x} = 0 \tag{2-23}$$

at the polymer/substrate interface. Furthermore, the jump mass balance at the upper film surface gives a boundary condition of

$$V \frac{dX}{dy} = \frac{D^P \hat{V}_1^P}{\rho_2^P \hat{V}_2^P} \frac{\partial \rho_1^P}{\partial x} \tag{2-24}$$

where $\hat{V}_I^P$ is the specific volume of component I in the polymer film. This equation can be found from

$$(\boldsymbol{j}_1^P)^{\ddagger} \hat{V}_1^P + (\boldsymbol{j}_2^P)^{\ddagger} \hat{V}_2^P = \mathbf{0} \tag{2-25}$$

The film/air interface movement can be expressed in terms of t rather than y as

$$V \frac{dX}{dt} = \frac{D^P \hat{V}_1^P}{1 - \rho_1^P \hat{V}_1^P} \frac{\partial \rho_1^P}{\partial x} \tag{2-26}$$

In addition, the jump mass balance for component 1 at this interface can be represented by

$$-D^P \frac{\partial \rho_1^P}{\partial x} - \rho_1^P \frac{dX}{dt} = k_1^G (p_{1i}^G - p_{1b}^G) \tag{2-27}$$

The unsteady heat transfer equations are

$$\rho^P \hat{C}_P^P \frac{\partial T^P}{\partial t} = k^P \frac{\partial T^P}{\partial x^2} \tag{2-28}$$

$$\rho^S \hat{C}_P^S \frac{\partial T^S}{\partial t} = k^S \frac{\partial T^S}{\partial x^2} \tag{2-29}$$

where, for phase J, $\hat{C}_P^J$ is the specific heat capacity. Integrating these equations over the thickness of the film and substrate respectively and the temperature boundary conditions gives an equation for dimensionless temperature

$$\frac{\partial T^*}{\partial t^*} = \frac{A[1 - T^*] + E + B \frac{dX^*}{dt^*}}{C + X^*} \tag{2-30}$$

where T^*, t^*, and X^* are dimensionless variables, and A, B, C, and E are all defined as

$$T^* = \frac{T - T_0}{T^G - T_0} \tag{2-31}$$

$$t^* = \frac{D_0^P t}{x^2} \tag{2-32}$$

$$X^* = \frac{X}{L} \tag{2-33}$$

$$A = \frac{L(h^G + h^g)}{D_0^P \rho^P \hat{C}_P^P} \tag{2-34}$$

$$B = \frac{\Delta \widehat{H}_{vap}}{\hat{C}_P^P (T^G - T_0)} \tag{2-35}$$

$$C = \frac{\rho^S \hat{C}_P^S H}{\rho^P \hat{C}_P^P L} \tag{2-36}$$

$$E = \frac{h^g (T^g - T^G) L}{D_0^P \rho^P \hat{C}_P^P (T^G - T_0)} \tag{2-37}$$

here, D_0^P is defined as the diffusivity at the initial conditions of the oven, L is the initial thickness of the film, and T_0 is the initial oven temperature. The continuity equation for the solvent becomes

$$\frac{\partial \rho_1^P}{\partial t} = \frac{\partial}{\partial x}\left(D^P \frac{\partial \rho_1^P}{\partial x}\right) \tag{2-38}$$

Putting this equation into a dimensionless form yields

$$\frac{\partial c}{\partial t^*} - \frac{\eta}{X^*}\frac{dX^*}{dt^*}\frac{\partial c}{\partial \eta} = \frac{1}{(X^*)^2}\frac{\partial}{\partial \eta}\frac{D^P}{D_0^P}\frac{\partial c}{\partial \eta} \tag{2-39}$$

where

$$c = \frac{\rho_1^P}{\rho_{10}^P} \tag{2-40}$$

$$\eta = \frac{x}{X(t)} \tag{2-41}$$

At $\eta = 0$,

$$\frac{\partial c}{\partial \eta} = 0 \tag{2-42}$$

In addition

$$c(0, \eta) = 1 \tag{2-43}$$

Integrating the dimensionless form of the mass transfer boundary equation gives

$$\frac{d}{dt^*}\left[X^*\left(\int_0^1 c d\eta\ \right)\right] = -\frac{k_1^G\left(\rho_{1i}^G - \rho_{1b}^G\right)L}{D_0^P \rho_{10}^P} \tag{2-44}$$

The location of the upper interface of the film becomes[3]

$$X^* = \frac{1 - \hat{V}_1^P \rho_{10}^P}{1 - \hat{V}_1^P \rho_{10}^P\left(\int_0^1 c d\eta\ \right)} \tag{2-45}$$

The diffusivity of the solvent in the polymer film behaves differently depending on whether the polymer is above or below the glass transition temperature. Above the glass transition, $D(\phi) \approx D_0$, while below or near the glass transition diffusivity is a strong function of polymer concentration. [1]

2.2 Block Copolymers

2.2.1 Block Copolymers in Melt

2.2.1.1 Ordering

Block copolymers exhibit localized phase separation into various types of domains whose properties depend on the thermodynamics, specifically the incompatibility between the blocks, represented by χN of the phase separation process. The transition between the ordered and disordered states is known as the order-disorder transition (ODT). Subsequently, a transition between one ordered state and another is known as the order-order transition (OOT). Lamellar, cylindrical, and BCC spherical domains encompass the so-called "classical phases", although other phases such as FCC cylinders and a gyroid phase can also occur under various conditions. In melts, the formation of these morphologies depends on block fraction or f, χ, and N. A representation of these different morphologies can be seen in Figure 2-2 below

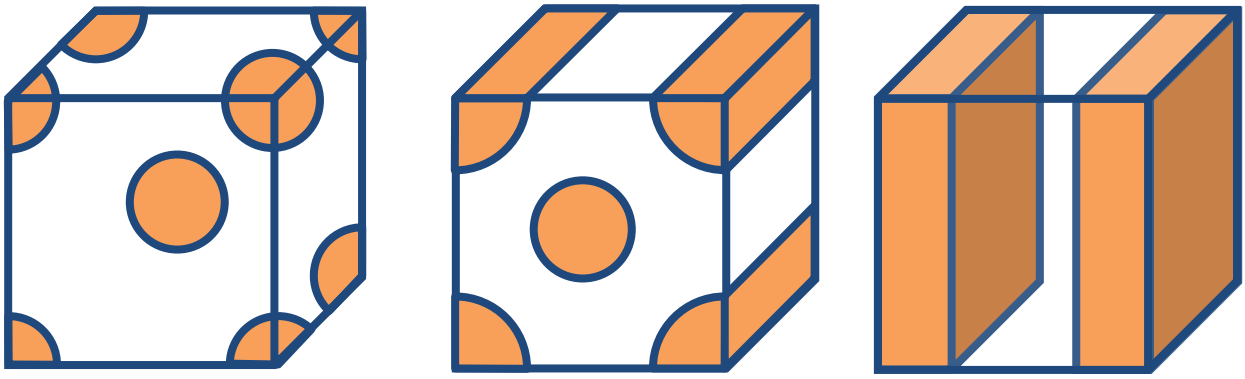

A. BCC Spheres B. HEX Cylinders C. Lamellae

Figure 2-2: (A), (B), and (C) are representations of "classical phases" formed by microphase separated block copolymer domains.

In general, BCC and FCC spheres form at lower block fractions than HEX cylinders, which form at lower block fractions than lamellae.

The characteristics of the equilibrium ordered structures that result and the relative conditions at which these transitions occur have been described by several different models. [4,5,6] These models rely on calculating the relative density of each block by minimizing the system free energy at given conditions. There are two major models with various assumptions that are used; weak segregation and strong segregation. The thermodynamics and equilibrium phase behavior of systems in the weak segregation limit were first characterized in a seminal paper by Leibler [4]. Leibler calculated the free energies of different phases for a system of an incompressible, monodisperse diblock copolymer under equilibrium. The blocks were assumed to have a constant bulk density, and equal Kuhn lengths. The final morphologies

were assumed based on the results from previous experiments. The original morphologies consisted of lamellar domains, hexagonal cylinders, and fcc and bcc spherical domains. Given the proximity to the ODT, sharp phase boundaries were not assumed. The ordering was characterized by an order parameter, given by

$$\psi(\vec{r}) = \langle (1-f)\rho_A(\vec{r}) - f\rho_B(\vec{r}) \rangle \tag{2-46}$$

for an A-B diblock copolymer where $\vec{r}$ is defined as a point, $\rho_i(\vec{r})$ is the ratio of density of monomer i at point $\vec{r}$ to the density of the system, and f is weight fraction of block A. Leibler's model predicted the existence of lamellar, hexagonal cylindrical, and BCC spherical microdomains, although the spherical microdomains existed over a narrow band in the phase diagram and were nearly metastable. Leibler's theory predicted that, in the case of melts, only χN and f were relevant for predicting the microphase behavior of the system. The calculated phase diagram can be seen below

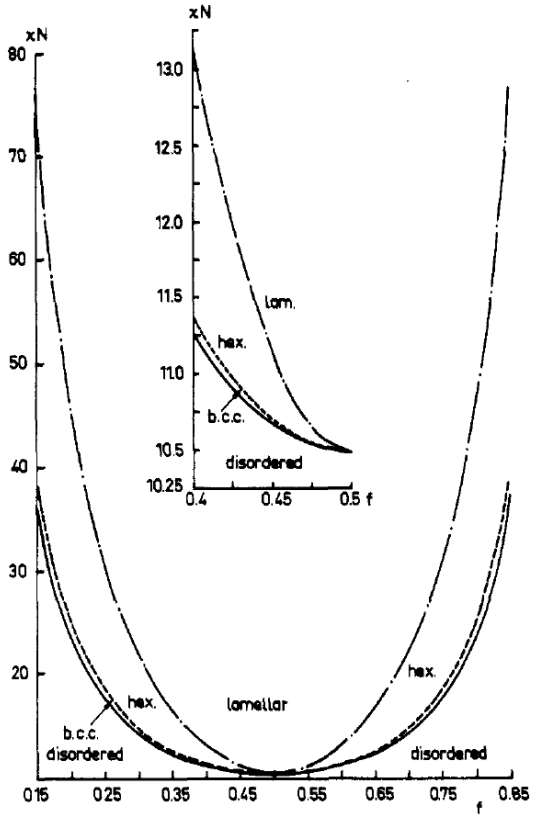

Figure 2-3: Phase diagram for the diblock copolymer: (solid line) transition line from the disordered to the bcc phase ((xNt vs. f); (---) transition line from the bcc phase to the hexagonal mesophase ((xN), vs. f); (·-) transition line from the hexagonal to the lamellar mesophase (xN), vs. f. Reproduced from [4]

Leibler's model, however, did not take into account concentration fluctuations, which can be an important contributor to the ODT. These were first accounted for by Fredrickson and Helfand [6]. The actual T_{ODT} was

found to be reduced by these effects, although the model breaks down at low chain lengths. When studying the phase behavior of star block copolymers, Floudas et al., in addition to measuring overall SAXS intensity, calculated the fluctuation effects obtained by SAXS and obtained deviations from mean field theory at small temperature quenches and q^* was higher than expected. In addition, a predicted intermediate BCC structure did not form. [7]

Helfand and Wasserman [5] developed a self-consistent mean field theory model for determining the various properties of block copolymer microdomains such as interfacial tension, block dimensions, interfacial width. This was done by calculating the free energy associated with these parameters in addition to calculating the probability densities of the blocks in the system. Unlike Leibler's theory, it is assumed that the interfacial region is small when compared with the size of the domains.

2.2.2 Block Copolymers in Solution

2.2.2.1 General

In terms of diblock copolymers, a solvent for block copolymers is classified as either selective or neutral depending on the relative affinities for the different blocks. Specifically, a solvent is referred to as neutral if it is a good solvent ($\chi_{AS} < 0.5$) for the both of the blocks. A slightly selective solvent is one that is either a Θ- or near Θ-solvent ($\chi_{AS} \sim 0.5$) for one of the blocks, and a good solvent for the other, while a selective solvent is a poor solvent $\chi_{AS} > 0.5$ for one block, and is a good solvent for another of the blocks. This can be extended for multiblock polymer systems. A self-consistent mean-field theory for systems that are made up of several different components, including blends, copolymers, and solutions was derived from partition functions by Hong and Noolandi, which allows for the calculation of free energy, the block and solvent concentrations with respect to position, and interfacial tension in phase-separated block copolymer systems in a solvent. This model applies to monodisperse systems with no excess volume. [8] Modeling has shown that solvent distribution in ordered structures in a neutral solvent is relatively even between the two blocks, but solvent tends to accumulate at the interfaces in order to screen unfavorable interactions between the two blocks. [9] Unlike a neutral solvent, a selective solvent will, upon ordering, preferentially partition into one of the blocks [9], and can produce inverted ordered structures [9a]. There have been several phase diagrams produced for block copolymers in both neutral and selective solvents. [9a] It was found in a particular study [10] that the overall melt phase diagram can be described as $\chi_{eff}N$ vs f'_{PS}, where χ_{eff} is the effective χ that describes the interaction between blocks, and is represented by $\chi_{eff} \sim \phi^{\beta}\chi$, while f'_{PS} is the effective PS volume fraction. When β = 1, the dilution approximation results, meaning that an increase in temperature is the same as a decrease in polymer volume fraction. The

dilution approximation was found not to hold for describing the ODT, while the relationship between volume fraction of polymer and χ_{eff} held for describing the OOT. For the case of the T_{ODT}, the relationship found was $\chi_{ODT} \sim \phi^{-1.4}$. [9a, 10] In addition, the phase behavior of block copolymer solutions with solvents of varying selectivities can be approximated qualitatively by differing trajectories across the melt phase diagram, as seen in below

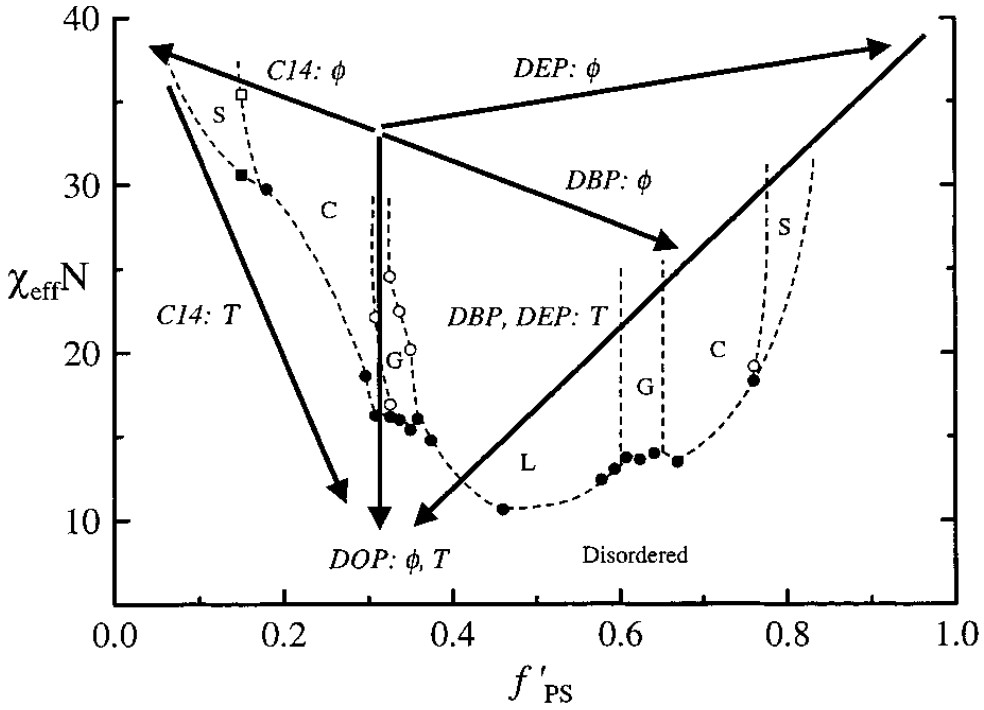

Figure 2-4: Phase trajectories of SI(11-21) in DOP, DBP, DEP, and C14. The open and closed symbols correspond to OOTs and ODTs, respectively, determined by Khandpur et al. (circles) and Ryu et al. (squares) for SI copolymers, with the dashed lines marking the estimated phase boundaries. The trajectories start at the estimated segregation of neat SI(11-21) at 0 °C. Khandpur, A. K.; Forster, S.; Bates, F. S.; Hamley, I. W.; Ryan, A. J.; Bras, W.; Almdal, K.; Mortensen, K. Macromolecules 1995, 28, 8796. Ryu, C. Y.; Lodge, T. P. Macromolecules 1999, 32, 7190. [11 12] Reproduced from [9a]

These trajectories stem from the relationship between f and f', and χ and χ_{eff}, where, in a neutral solvent, $f = f'$, but in highly selective solvents where the solvent partitions completely, $f' = f\phi + (1 - \phi)$, giving a more horizontal trajectory. [9a]. Another study [13] used self-consistent mean field theory that was adapted from that of Matsen, [14,15] who developed a mean-field theory for homopolymer/block copolymer blends. Huang and Lodge[13] studied phase maps of the classical phases as a function of solvent selectivity, temperature, block fraction, volume fraction, and molecular weight in the classical phases. The authors created what they termed as a "phase cube" consisting of f, φ, and $\chi_{AB}N$. In this phase cube, there are planes corresponding to $(\chi_{AB}N)_{melt}$ vs f and pure solvent and A and B homopolymers in solvent.

χ_{AS} was varied and N and χ_{BS} were fixed. In a neutral good solvent, a phase diagram from $(\chi_{AB}\mathrm{N}\phi)_S = F(f)$. The spinodal here corresponded to the ordered phase with $\chi_{AB}\mathrm{N} < 10.495$ corresponding to a disordered phase, with an ordered phase occurring when $\chi_{AB}\mathrm{N} > 10.495$. A schematic of the phase cube that was calculated can be seen in the figure below.

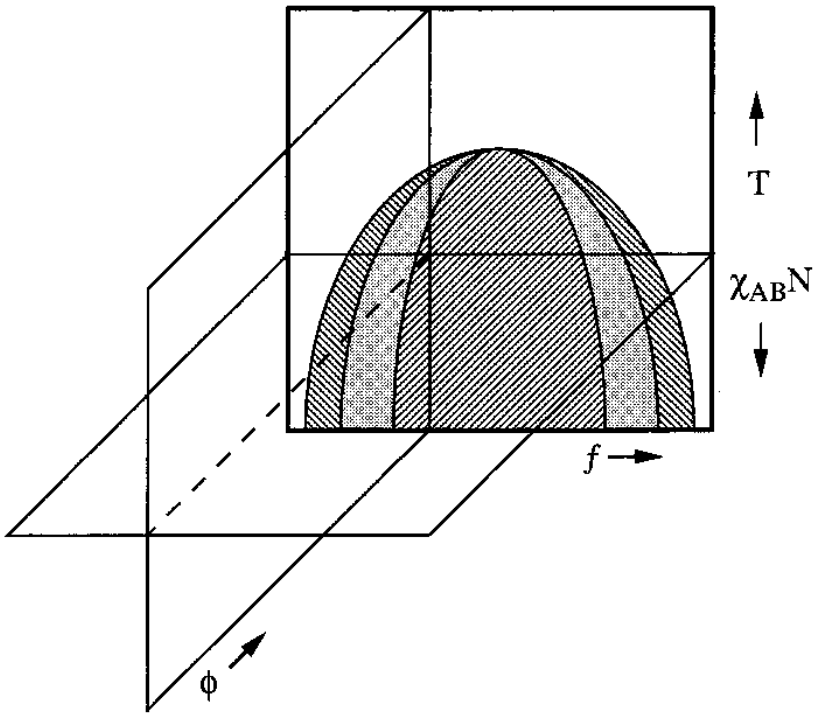

Figure 2-5: Phase cube for diblock copolymer solutions in terms of polymer concentration $\boldsymbol{\phi}$, copolymer composition *f*, and degree of copolymer segregation $\boldsymbol{\phi_{AB}N}$, for a polymer with degree of polymerization *N* in the presence of a solvent with interaction parameters $\boldsymbol{\phi_{AS}}$ and $\boldsymbol{\phi_{BS}}$. The horizontal plane denotes a constant temperature slice ($\boldsymbol{\phi}$ vs *f*), and the vertical planes denote a phase diagram for a particular copolymer ($\boldsymbol{\phi}$ vs *T*) or a phase map for a given concentration (*T* vs *f*). Reproduced from [13].

2.2.2.2 Neutral Solvents

2.2.2.2.1 Ordering

Kim and Libera[16] studied thin (~100nm) SBS films with a HEX morphology that were cast from a 30wt% solution in toluene in order to determine the effects of solvent evaporation on the morphology of microdomains in the film. A competition was found between the thermodynamic and kinetic effects on the overall morphology of the microdomains in the film during solvent evaporation. As the solvent evaporation rate increased, this morphology transitioned from disordered microdomains with no long range ordering to vertical cylinders to a mixture of vertical and horizontal cylinders to fully horizontal

cylinders. The free energy difference between vertical and horizontal HEX cylinder morphology was found to be

$$\Delta G = \frac{2\phi_{PS}\gamma_{PS/PB}}{t} \quad (2\text{-}47)$$

where $\phi_{PS}$is the cylinder (PS) volume fraction, t is the film thickness, and $\gamma_{PS/PB}$is the interfacial tension between the PS and PB blocks. The interfacial tension between the two is small and positive, so the vertical structure was calculated to be metastable when compared to the horizontal structure. It is suggested that because a vertical orientation allows for easier evaporation due to the less tortuous path that the solvent must travel through to exit the film, this morphology forms at a faster evaporation rate. It is argued that the cylinders should grow from the top down due to the higher concentration gradient during faster evaporation. Slower evaporation was found to lead to less significant kinetic effects.[16]

The formation of ordered microstructures in block copolymer solutions in neutral solvents has been found to occur through a nucleation and growth mechanism.[17] A recent study of the effect of solvent concentration on the ordering kinetics of block copolymer microstructures found that a two-step increase in G* obtained from dynamic mechanical response (DMR) occurs near the ODT. This increase was attributed to nucleation and growth. Avrami exponents were extrapolated from the resulting $t_{0.5}$, and exponents of roughly 1.0 were seen with both SAXS and DMR, with the results in DMR being on average slightly lower at around 0.7. Due to the margin of error in the volume fraction of ordered phase obtained with the DMR results, the Avrami exponent was determined to be 1.0. The author tentatively suggested a homogeneous nucleation and 2D growth mechanism with a heterogeneous nucleation and 1D growth at higher concentrations due to a possible mechanism change slowing kinetics. [17]

2.2.2.3 Selective Solvents

2.2.2.3.1 Ordering

In selective solvents, various works[9a, 18] have found that disordered micelles will form from the dissociation of ordered structures. Work by Park, et al.[18] studied disordered micelles in concentrated solutions of symmetric poly(styrene-block-*d*isoprene) in selective solvents and micelles from different ordered structures starting with ordered structure to disordered micelles via small-angle neutron scattering (SANS). The solutions appeared to show a critical micelle transition (cmt) as seen by an increase in the peak width and a decrease in peak height at a given temperature that was roughly the same as the mean-field spinodal temperature, T_s, 20-30% above the T_{ODT}. Above this temperature the aggregation number dropped and the solvent reaches a concentration above 50% in the micelle core, meaning that the micelles

were dissociating. This dissociation increased until the mean-field temperature, at which point all micelles had dissociated into free polymer chains.[18], as seen in the figure below.

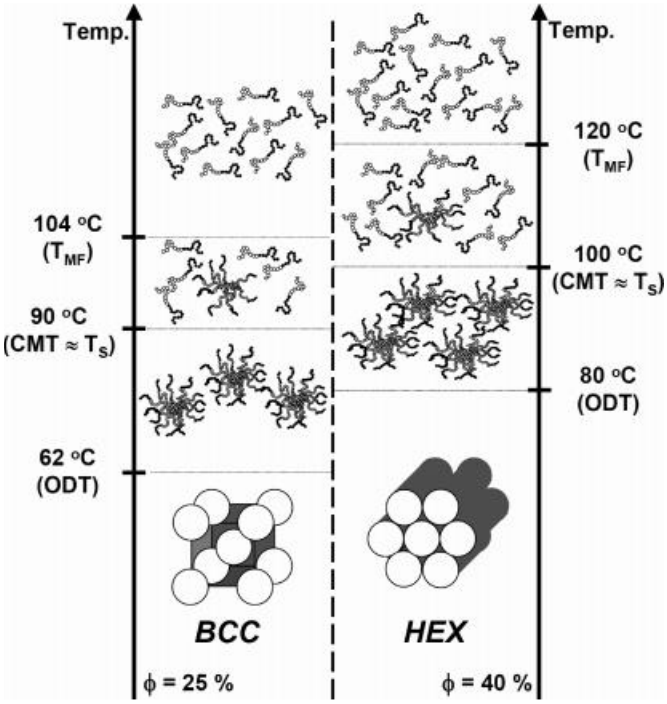

Figure 2-6: Phase behavior for 25% S*d*l(15-14) in DEP/DBP (75/25 vol %) and 40% S*d*l(15-14) in DEP/DBP (75/25 vol %). Bcc and HEX denote the body-centered cubic and the hexagonal cylinder, respectively, and ODT, cmt, *T*S, and *T*MF for the two solutions are shown. A schematic illustrating the regions of the micelles in long-range order, the disordered micelles along with associated transitions is also given. Reproduced from [16]

A study by Hanley, et al.[9a] used SAXS, static birefringence and dynamic light scattering (DLS) to study phase diagrams of SI(11-21) in solvents of differing selectivity, using bis(2-ethylhexyl) phthalate (DOP), di-n-butyl phthalate (DBP), diethyl phthalate (DEP), and tetradecane, where DOP was used as a neutral solvent, DBP and DEP were used as slightly PS-selective and strongly PS-selective solvents respectively, and tetradecan was used as a strongly PI-selective solvent. The study found that increasing the selectivity increased the difference between the T_{ODT}s of the two systems at lower polymer concentrations up to a point where the difference between the two decreased due to the solvent becoming more neutral at higher temperatures as a result of the inverse relationship of χ with temperature. At lower ϕ, the phase behavior became nearly independent of concentration and the ordered phase was more stable at higher temperatures and concentrations than in a neutral solvent. This is due to an increase in segregation in selective solvents,

and the stability of microstructures is improved from that formed out of a solution with a neutral solvent. An increase in cmt was also seen in dilute solvents. In an isoprene selective solvent, reverse "hairy" micelles were observed with shorter PS at the core and the longer PI blocks forming the corona. [9a]

Selective solvents have a tendency to increase the types of phases that can form.

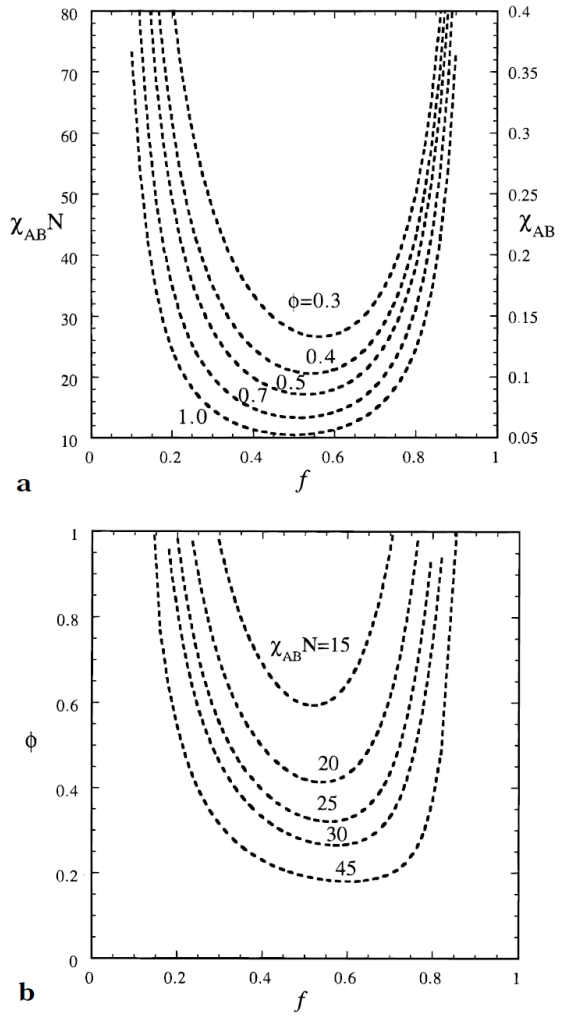

Figure 2-7: Two-dimensional spinodal curves for a disordered block copolymer solution with $N = 200$, $\chi_{AS} = 0.6$, and $\chi_{BS} = 0.4$, for constant ϕ (a) and $\chi_{AB}N$ (b). Reproduced from [13].

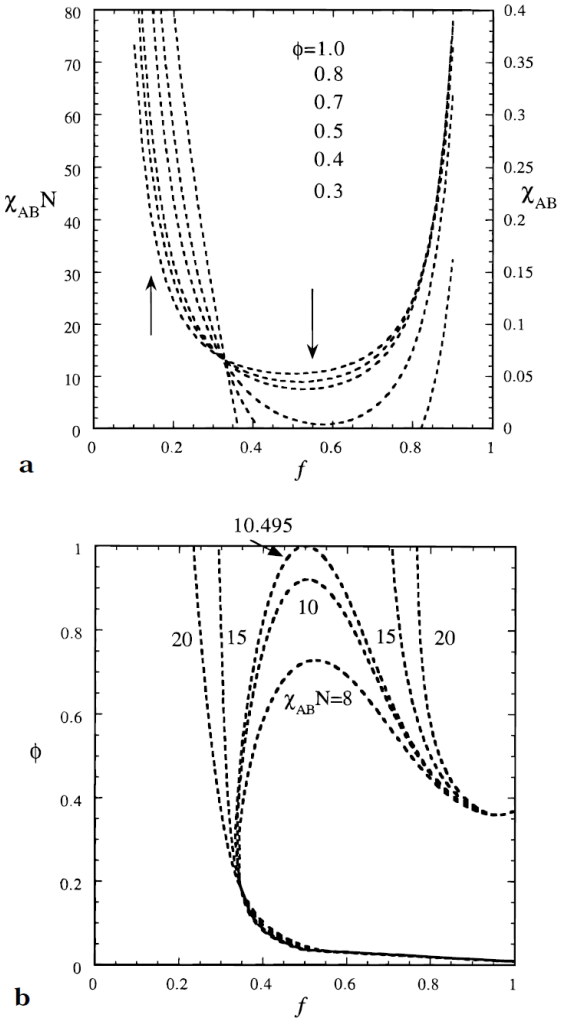

Figure 2-8: Two-dimensional spinodal curves for a disordered block copolymer solution with $\boldsymbol{N = 200}$, $\boldsymbol{\chi_{AS}} = \boldsymbol{0.8}$, and $\boldsymbol{\chi_{BS}} = \boldsymbol{0.4}$, for constant $\boldsymbol{\phi}$ (a) and $\boldsymbol{\chi_{AB}N}$ (b). The arrows in part (a) indicate the order of curves for decreasing $\boldsymbol{\phi}$. Reproduced from [13].

Huang and Lodge [13] calculated spinodal curves and studied the applicability of the dilution approximation as well as the effect that solvent selectivity had on the phase maps. A linear diblock copolymer was again

modeled in solvents with differing selectivity for the A block. It was found that, as the solvent-A interactions became less and less favorable (as modeled by an increase in χ_{AS}, while χ_{BS} remained constant), ordered microdomains were found to be more stable under more conditions. Here, it was found that the dilution approximation didn't describe behavior quantitatively, but there was similar behavior that was seen qualitatively. At $\chi_{AS} = 0.8$, there was an intersection at $f = 1$, meaning that a homopolymer would phase separate. For a constant ϕ in a poor solvent, increasing $\chi_{AB}\mathrm{N}$ causes a transition from a disordered phase to two phases: a solvent rich and a copolymer rich disordered phases. Under a neutral solvent, decreasing ϕ was analagous to increasing temperature, while decreasing ϕ in a selective solvent, much like later results [9a], was analogous to increasing both temperature and f. Under a solvent that is more than slightly selective for the B block, $\chi_{AB}\mathrm{N}$ where ODTs and OOT occur drops because selectivity increases the ordered domain region's size. Inverted phases were also reported under slightly selective and selective solvents because a solvent that is incompatible with the A block can cause A to aggregate. This increase in the number of different morphologies available to block copolymers with the introduction of selective solvents has been seen elsewhere[9a] where phase diagrams of poly(styrene/isoprene) diblocks were produced in differing solvents that had different degrees of selectivity. Ordering in block copolymer solutions in selective solvents has been found to occur through a nucleation and growth mechanism that could be represented by Avrami kinetics, which will be discussed later. [19,20,21]

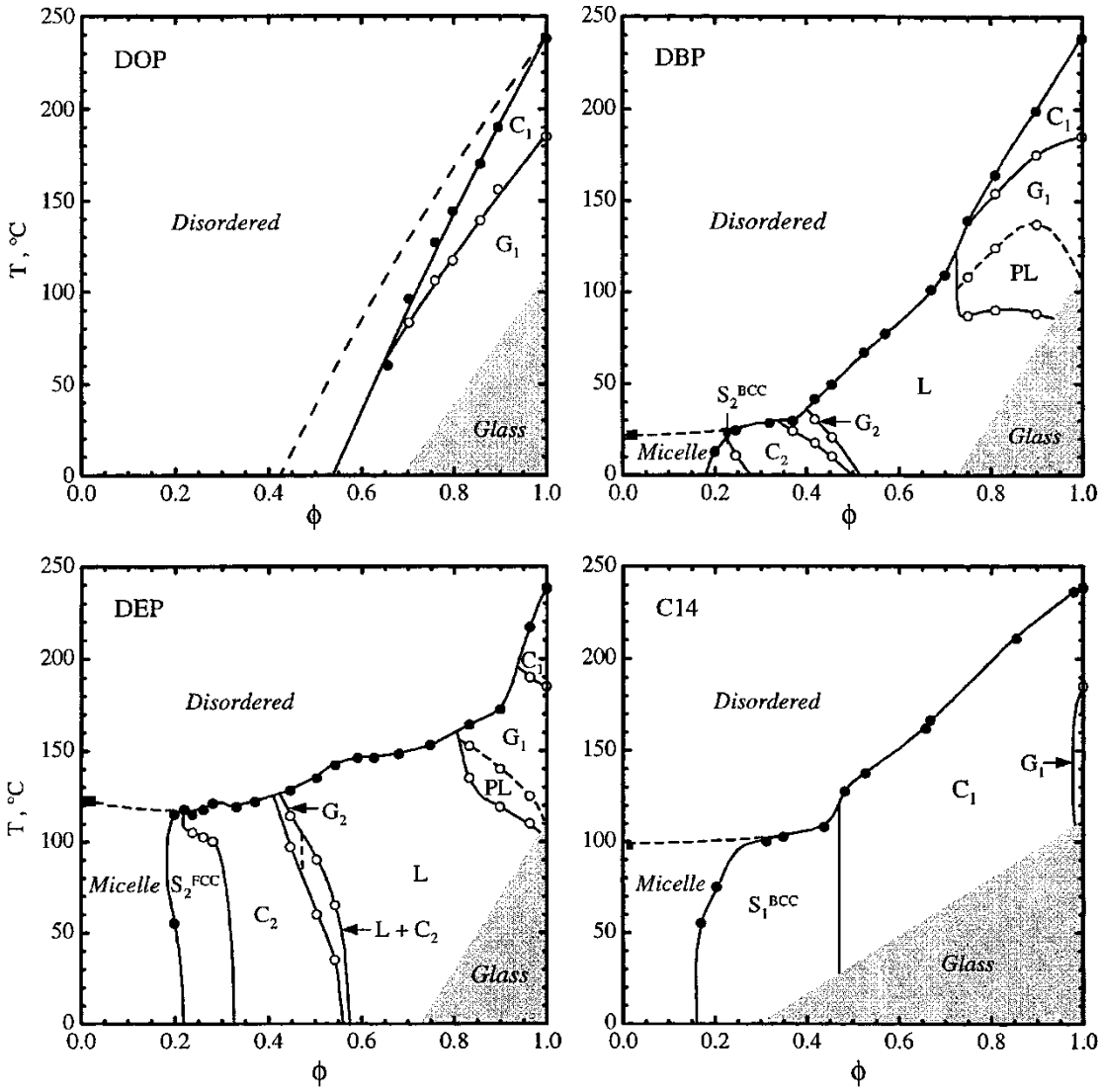

Figure 2-9: Phase diagram for SI(11-21) as a function of temperature (T) and polymer volume fraction (ϕ) for solutions in DOP, DBP, DEP, and C14. Filled and open circles identify ODTs and OOTs, respectively. The dilute solution critical micelle temperature (cmt) is indicated by a filled square. The ordered phases are denoted by: C, hexagonal-packed cylinders; G, gyroid; PL, perforated lamellae; L, lamellae; S, cubic packed spheres. The subscript 1 identifies the phase as "normal" (PS chains reside in the minor domains) or "inverted" (PS chains located in the major domains). The phase boundaries are drawn as a guide to the eye, except for DOP in which the OOT and ODT phase boundaries (solid lines) show the previously determined scaling of the SI interaction parameter ($\chi_{ODT} \sim \phi^{-1.4}$ and $\chi_{OOT} \sim \phi^{-1}$); the dashed line corresponds to the "dilution approximation" ($\chi_{OOT} \sim \phi^{-1}$).

2.3 Kinetics

2.3.1 General

The kinetics of both ODT and OOT transformations have been widely studied in melts, neutral, and selective solvents. Most of these studies have been performed utilizing temperature as a means to control the thermodynamic driving force for ordering.

Ordering kinetics in block copolymer melts have frequently been described via the Avrami model for crystallization kinetics. [22,7,19,20,21] This model was derived for isothermal phase transition kinetics in systems that order via the nucleation and growth mechanism, and can be represented by

$$\phi(t) = \phi_\infty(1 - \exp[-kt^n]) \tag{2-48}$$

where t is time, $\phi(t)$is a volume fraction of ordered phase, $\phi_\infty$is the final volume fraction once ordering is complete, k is a rate constant, and n is the Avrami exponent. Subsequently, the half-time of ordering, which is frequently used to compare ordering kinetics, is given by

$$t_{0.5} = \left(\frac{\ln 2}{k}\right)^{1/n} \tag{2-49}$$

where $t_{0.5}$ is the half-time of ordering. The Avrami exponent is a function of the ordering mechanism that occurs in the system. In addition, the growth front velocity of the grains has been found to be related to block fraction by Goveas and Milner in OOT kinetics in melts. [23] Chastek and Lodge [20] studied ordering kinetics in solutions by tracking the grain growth fronts and the grain volume during temperature quenches from disordered solutions and found correlation between the type of growth observed via POM and the Avrami exponent. This and subsequent papers [19,24] found agreement with Goveas and Milner's model in block copolymer solutions during order-disorder transitions for various morphologies.

G. Floudas, et al. studied phase separation kinetics in star block copolymer melts using both SAXS and isochronal rheology: studying $G'(t)$, $G''(t)$, and $|G^*(t)|$ vs t. It was found that the ordering upon quenching could be described by isothermal Avrami kinetics. In addition, loss modulus results indicated a change from liquid-like to solid-like behavior, as evidenced by a peak in the $G''(t)$ vs t data. The authors used scattering power, given as

$$Q = \frac{1}{2\pi^2}\int_0^\infty q^2 I(q) dq \tag{2-50}$$

where q is the scattering vector, and $I(q)$ is scattering intensity. The authors related Q to the ordered and disordered phases via

$$Q \sim V \Delta\rho^2 \phi(1-\phi) \tag{2-51}$$

where V is the scattering volume. [25] Attempts to correlate the results of the two methods were unsuccessful, as the Avrami exponents obtained under both methods conflicted. However, rheological results suggested that the ordering mechanism was different under shallow quenches $T_{ODT} - T \approx 3$℃, than under a larger quench. [7]

Fredrickson and Binder [26] derived a relationship between nucleation and growth kinetics in block copolymer melts and the thermodynamics of the system, as determined by undercooling and chain length. This was done by taking into account a fluctuation field of a symmetric block copolymer and calculating the free energy density. A dimensionless undercooling of

$$\delta \equiv \frac{\chi N - \chi_T N}{\chi_T N} \tag{2-52}$$

was used to describe the thermodynamic driving force for nucleation. For a supercooled melt, $\delta > 0$. The nucleation free energy differennce was given as

$$\Delta F = 4\pi R^2 \sigma + \frac{4}{3}\pi R^3 \Delta f \tag{2-53}$$

where ΔF is the excess free energy of nucleation for a spherical nucleus of radius R, interfacial tension σ, and free energy difference Δf between the disordered phase, which in this case is metastable, and the lamellae. By using this to obtain the nucleation barrier, a completion time was obtained as

$$\theta_c \sim N^{1/12} \delta^{-3/4} \tau_d \exp\left(\frac{\Delta F^*}{4 k_B T}\right) \tag{2-54}$$

where $\Delta F^* / k_B T \sim \delta^{-2}$.

Avrami kinetics were originally derived for isothermal systems. However, the model has been modified using an Arrhenius relationship to account for the effect of temperature for systems that are undergoing crystallization or phase separation during temperature ramps [27,28,29] using scaling based on the inflection point of $\phi(t)$ vs t [27] or a constant based on temperature, activation energies of nucleation and growth

and ramp rate that is used to modify the rate constant, k. [28] The second model has been shown to apply to order-order transitions in block copolymers. [29]

2.3.2 Phase Separation During Solvent Evaporation

Overall morphology can be controlled by varying the drying rate of polymer films. [30,16] There have been relatively few studies of the effect of solvent concentration on the kinetics of phase transformation in block copolymer solutions. Yamamura, et al. studied the effect of drying rate on the phase separation of polymer blends by varying the drying rate in the film. Yamamura studied the types and sizes of phases that formed in polystyrene/polycarbonate blends in tetrahydrofuran. The drying rate was varied by controlling the flow rate of sweep gas over the film. [30] Heinzer, et al. performed several studies both during film drying and under iso-concentration conditions. However, due to the method that was used to vary the drying rate, a direct comparison between drying rates that was decoupled from the effects of temperature was not able to be obtained. [17, 31]. In polymer blends, it was found that a slower drying rate allowed for better chain mobility for a longer period of time, resulting in larger phase domains in the final film, while at a faster drying rate, smaller domains formed and the final morphology became trapped in a non-equilibrium structure. [30] Non-equilibrium structures have also been seen in block copolymers during film drying, including a loss of long-range order for faster drying rates, while slower drying rates allowed for ordered structures with more long-range character to develop. Long-range ordering was able to be created after the films with slower drying rates were annealed. However, annealing was not able to produce this kind of ordering in films that had been produced with faster drying rates. [16]

In addition, in polymer blends, Yamamura discerned three stages of phase evolution while the blend dried. In the first stage, convection caused patterning of phase-separated domains, which were allowed to fuse together once convection had ceased in the second stage. In the third stage, structure evolution ceased in the film once the solvent content had diminished to the point where the mobility of polymer chains was severely hindered. [30]

In a study by Stegelmeier et al.[32], several PS-P4VP diblock copolymers were cast in a thick film using THF and DMF as solvents. These were cast onto a film conveyor to study the drying film and studied with *in-situ* SAXS and the change the kinetic behavior upon immersion in water. The film was passed beneath a doctor blade to a thickness on the order of 100μm. During the evaporation step, it was found that the characteristic length growth could scale onto an exponential curve at long times, in accordance with a Cahn-Hilliard-Cook model described by Podariu, et al. [33] The characteristic growth time increased with

decreasing molecular weight, while the final characteristic length decreased with decreasing molecular weight. [32]

The first study by Heinzer et al. used small angle x-ray scattering to analyze kinetics of phase separation in thick films while drying.[31] This study tracked solvent concentration during scattering in thick films (~500μm) using a balance. Because the scattering was performed in-situ, a direct study of phase formation during block copolymer film drying was possible. It was determined that the ordering rate during drying was controlled by thermodynamics early on in the drying process and by chain mobility later in the drying process. The drying rate was controlled by changing the temperature of the film. Early on in the ordering process, the thermodynamic driving force controlled the kinetics of phase transformation, and the relationship at small quenches between ordering time, t_c, and dimensionless undercooling should have been $\ln t_c \sim \delta^{-2}$ as predicted by Fredrickson and Binder [26].

Significant skinning was seen at higher temperatures and when a sweep gas was employed.

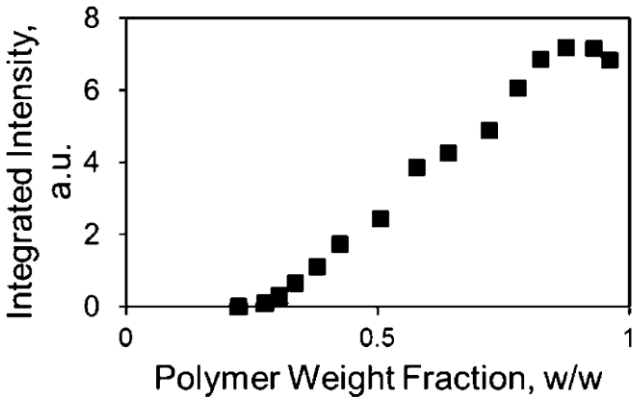

Figure 2-10: Integrated intensity of the primary SAXS peak (n =1) as a function of the polymer weight fraction in a SB/toluene film during solvent removal at 30 °C. (Reproduced from [31])

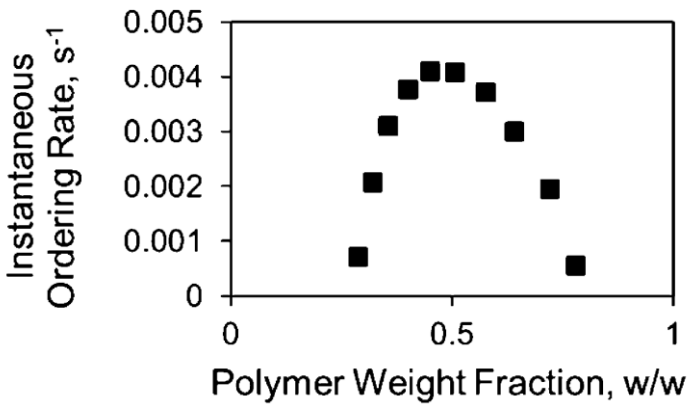

Figure 2-11: Instantaneous rate of ordering of the SB copolymer into hexagonally packed cylinders in a neutral solvent, toluene, during continual solvent removal at 30 °C. (Reproduced from [31])

In another study by Heinzer, et al. [17], the authors studied the phase separation using DMR and SAXS at constant polymer concentrations at different stages during the drying process. Under iso-concentration conditions, ordering of poly(styrene-butadiene) solutions was studied with DMR and SAXS. As can be seen in the figure below, it was found that $t_{0.5}$ vs. ϕ had a trend that was concave up, which was attributed to competition between thermodynamic effects characterized by quench depth, and chain mobility. As concentration moved away from C_{ODT} but still at small quench depths, the rate of phase formation increased, as indicated by a decrease in $t_{0.5}$. This was due to a greater thermodynamic driving force that increased the rate of segregation. As polymer concentration increased further, the polymer chain mobility decreased, slowing kinetics until the chain mobility became the dominant factor controlling the phase separation rate and leading to an increase in $t_{0.5}$. This is similar to previous results that found that under shallow quenches, the kinetics varied with respect to temperature as $\ln t_{0.5} \sim (T_{ODT} - T)^{-2}$, but below a particular temperature, ordering times varied with temperature via the Arrhenius relationship. [34]

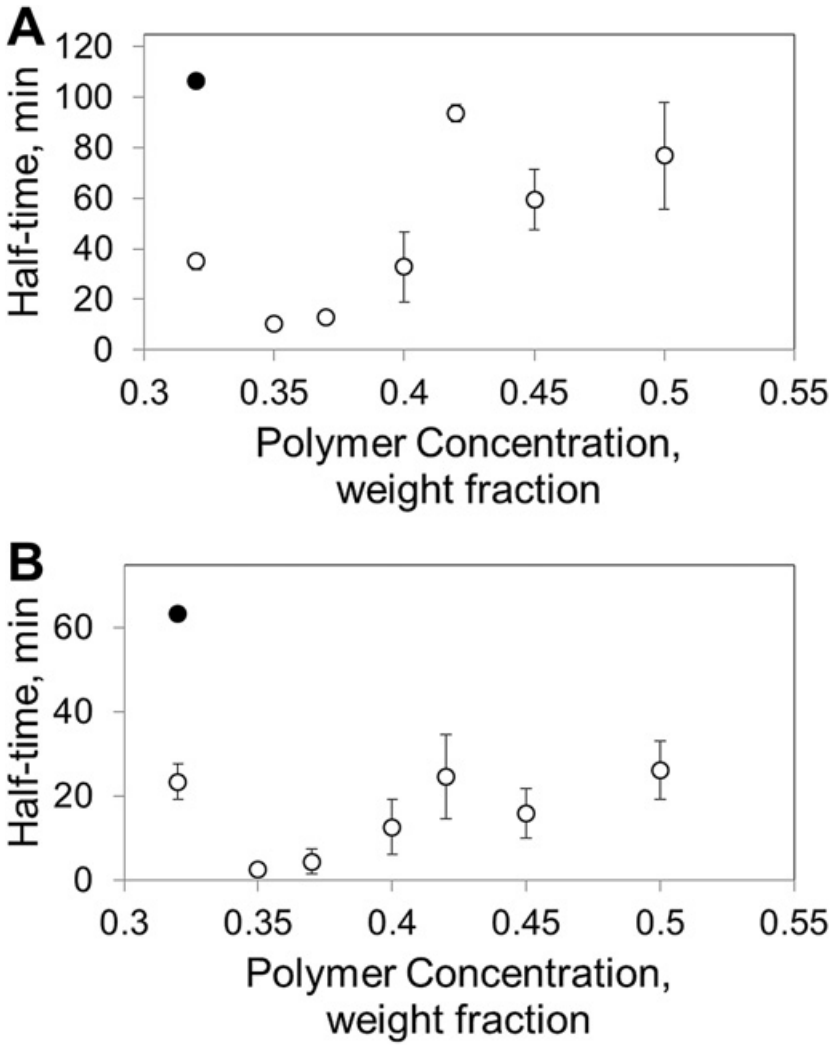

Figure 2-12: Half-times of the ordering of SB in toluene at room temperature following extraction of solvent from a 20 wt% solution as a function of concentration. Half-times were determined using the Avrami equation and calculating f(t) from dynamic mechanical data using the parallel (A) and series (B) approximations for the complex modulus. At 32 wt%, the total half-time (●) and the half-time of the growth period only (○) are shown. At all subsequent concentrations, the half-time corresponds to the single-step growth of G*. (Reproduced from [17])

References

1. Tsige, M.; Grest, G. S., Solvent evaporation and interdiffusion in polymer films. *Journal of Physics: Condensed Matter* **2005,** *17* (49), S4119.
2. Buxton, G. A.; Clarke, N., Ordering polymer blend morphologies via solvent evaporation. *EPL (Europhysics Letters)* **2007,** *78* (5), 56006.
3. Vrentas, J. S.; Vrentas, C. M., Drying of solvent-coated polymer films. *Journal of Polymer Science Part B: Polymer Physics* **1994,** *32* (1), 187-194.
4. Leibler, L., Theory of Microphase Separation in Block Copolymers. *Macromolecules* **1980,** *13* (6), 1602-1617.
5. Helfand, E.; Wasserman, Z. R., Block Copolymer Theory. 4. Narrow Interphase Approximation. *Macromolecules* **1976,** *9* (6), 879-888.
6. Fredrickson, G. H.; Helfand, E., Fluctuation effects in the theory of microphase separation in block copolymers. *The Journal of Chemical Physics* **1987,** *87* (1), 697-705.
7. Floudas, G.; Hadjichristidis, N.; Iatrou, H.; Pakula, T.; Fischer, E. W., Microphase Separation in Model 3-MiktoarmStar Copolymers (Simple Graft and Terpolymers). 1. Statics and Kinetics. *Macromolecules* **1994,** *27* (26), 7735-7746.
8. Hong, K. M.; Noolandi, J., Theory of inhomogeneous multicomponent polymer systems. *Macromolecules* **1981,** *14* (3), 727-736.
9. (a) Hanley, K. J.; Lodge, T. P.; Huang, C.-I., Phase Behavior of a Block Copolymer in Solvents of Varying Selectivity. *Macromolecules* **2000,** *33* (16), 5918-5931; (b) Lodge, T. P.; Hamersky, M. W.; Hanley, K. J.; Huang, C.-I., Solvent Distribution in Weakly-Ordered Block Copolymer Solutions. *Macromolecules* **1997,** *30* (20), 6139-6149.
10. Hanley, K. J.; Lodge, T. P., Effect of dilution on a block copolymer in the complex phase window. *Journal of Polymer Science Part B: Polymer Physics* **1998,** *36* (17), 3101-3113.
11. Khandpur, A. K.; Foerster, S.; Bates, F. S.; Hamley, I. W.; Ryan, A. J.; Bras, W.; Almdal, K.; Mortensen, K., Polyisoprene-Polystyrene Diblock Copolymer Phase Diagram near the Order-Disorder Transition. *Macromolecules* **1995,** *28* (26), 8796-8806.
12. Ryu, C. Y.; Lodge, T. P., Thermodynamic Stability and Anisotropic Fluctuations in the Cylinder-to-Sphere Transition of a Block Copolymer. *Macromolecules* **1999,** *32* (21), 7190-7201.
13. Huang, C.-I.; Lodge, T. P., Self-Consistent Calculations of Block Copolymer Solution Phase Behavior. *Macromolecules* **1998,** *31* (11), 3556-3565.
14. Matsen, M. W., Phase Behavior of Block Copolymer/Homopolymer Blends. *Macromolecules* **1995,** *28* (17), 5765-5773.
15. Matsen, M. W., Stabilizing New Morphologies by Blending Homopolymer with Block Copolymer. *Physical Review Letters* **1995,** *74* (21), 4225-4228.
16. Kim, G.; Libera, M., Morphological Development in Solvent-Cast Polystyrene−Polybutadiene−Polystyrene (SBS) Triblock Copolymer Thin Films. *Macromolecules* **1998,** *31* (8), 2569-2577.
17. Heinzer, M. J.; Han, S.; Pople, J. A.; Martin, S. M.; Baird, D. G., Iso-concentration ordering kinetics of block copolymers in solution during solvent extraction using dynamic oscillatory measurements. *Polymer* **2012,** *53* (15), 3331-3340.
18. Park, M. J.; Char, K.; Bang, J.; Lodge, T. P., Order−Disorder Transition and Critical Micelle Temperature in Concentrated Block Copolymer Solutions. *Macromolecules* **2005,** *38* (6), 2449-2459.
19. Chastek, T. Q.; Lodge, T. P., Measurement of Gyroid Single Grain Growth Rates in Block Copolymer Solutions. *Macromolecules* **2003,** *36* (20), 7672-7680.
20. Chastek, T. Q.; Lodge, T. P., Grain Shapes and Growth Kinetics of the Cylinder Phase in a Block Copolymer Solution. *Macromolecules* **2004,** *37* (13), 4891-4899.

21. Liu, Y.; Nie, H.; Bansil, R.; Steinhart, M.; Bang, J.; Lodge, T. P., Kinetics of disorder-to-fcc phase transition via an intermediate bcc state. *Physical Review E* **2006,** *73* (6), 061803.
22. (a) Avrami, M., Kinetics of Phase Change. I General Theory. *The Journal of Chemical Physics* **1939,** *7* (12), 1103-1112; (b) Avrami, M., Kinetics of Phase Change. II Transformation‐Time Relations for Random Distribution of Nuclei. *The Journal of Chemical Physics* **1940,** *8* (2), 212-224; (c) Avrami, M., Granulation, Phase Change, and Microstructure Kinetics of Phase Change. III. *The Journal of Chemical Physics* **1941,** *9* (2), 177-184.
23. Goveas, J. L.; Milner, S. T., Dynamics of the Lamellar−Cylindrical Transition in Weakly Segregated Diblock Copolymer Melts. *Macromolecules* **1997,** *30* (9), 2605-2612.
24. Chastek, T. Q.; Lodge, T. P., Grain shapes and growth kinetics during self-assembly of block copolymers. *Journal of Polymer Science Part B: Polymer Physics* **2006,** *44* (3), 481-491.
25. Porod, G., *Small angle x-ray scattering*. Academic Press: London; New York, 1982.
26. Fredrickson, G. H.; Binder, K., Kinetics of metastable states in block copolymer melts. *The Journal of Chemical Physics* **1989,** *91* (11), 7265-7275.
27. Lambrigger, M., Non-isothermal polymer crystallization kinetics and avrami master curves. *Polymer Engineering and Science* **1998,** *38* (4), 610.
28. Farjas, J.; Roura, P., Modification of the Kolmogorov–Johnson–Mehl–Avrami rate equation for non-isothermal experiments and its analytical solution. *Acta Materialia* **2006,** *54* (20), 5573-5579.
29. Spring, J. D.; Bansil, R., A Universal Scaling Analysis of Nonisothermal Kinetics in Block Copolymer Phase Transitions. *ACS Macro Letters* **2013,** *2* (8), 745-748.
30. Yamamura, M.; Nishio, T.; Kajiwara, T.; Adachi, K., EFFECT OF STEPWISE CHANGE OF DRYING RATE ON MICROSTRUCTURE EVOLUTION IN POLYMER FILMS. *Drying Technology* **2001,** *19* (7), 1397.
31. Heinzer, M. J.; Han, S.; Pople, J. A.; Baird, D. G.; Martin, S. M., In Situ Measurement of Block Copolymer Ordering Kinetics during the Drying of Solution-Cast Films Using Small-Angle X-ray Scattering. *Macromolecules* **2012,** *45* (8), 3471-3479.
32. Stegelmeier, C.; Exner, A.; Hauschild, S.; Filiz, V.; Perlich, J.; Roth, S. V.; Abetz, V.; Förster, S., Evaporation-Induced Block Copolymer Self-Assembly into Membranes Studied by in Situ Synchrotron SAXS. *Macromolecules* **2015,** *48* (5), 1524-1530.
33. Podariu, I.; Shou, Z.; Chakrabarti, A., Viscous flow and coarsening of microdomains in diblock copolymer thin films. *Physical Review E* **2000,** *62* (3), R3059-R3062.
34. Liu, Z.; Shaw, M.; Hsiao, B. S., Ordering Kinetics of the BCC Morphology in Diblock Copolymer Solutions over a Wide Temperature Range. *Macromolecules* **2004,** *37* (26), 9880-9888.

3 *In-situ* SAXS Analysis of Styrene-Diene Block Copolymer Self-Assembly Kinetics During Solution Casting

3.1 Abstract

In order to determine the effect of the drying process on the phase kinetics of a diblock copolymer, small-angle X-ray scattering was been performed *in-situ* on thick ($\sim 400 \mu m$) solution cast films of poly(styrene-*b*-butadiene) during drying under differing drying rates. To determine the volume fraction of ordered phase with respect to time during these experiments, the concentration profiles of the films were calculated using a drying model. This concentration was then used to calculate the solvent partitioning in the portion of the film above the order-disorder transition concentration (or ordering layer) to extract the volume fraction of ordered phase from the invariant of the scattering profiles. The subsequent ordering curves with respect to time were found to fit the Avrami model for slower drying rates, but not for the faster drying rate, likely due to the more dynamic nature of the system. The ordering layer was found to have a constant concentration until the ordering layer encompassed the entire film. In addition, once the polymer concentration in the entire film passed the order-disorder transition concentration, the relationship between volume fraction ordered phase and polymer concentration was linear.

3.2 Introduction

Block copolymers, when ordered, can form a wide variety of nanodomain structures from simple lamellae to more complex arrangements such as gyroid structures. Because of their ability to form ordered structures on the 10-100nm scale, they have been explored for a wide range of applications such as separation membranes, fuel cell membranes, and lithography. Many applications involve the formation of polymer films or membranes via solution casting. As a production method, solution casting has several advantages over melt processing, as it doesn't require high temperatures and can allow for a wider range of equilibrium structures than is possible in melt cast films. A study by Lodge, et al.[1] mapped out a phase cube base on block fraction, solvent selectivity, and solvent concentration. Order-disorder transition (ODT) transformation kinetics in block copolymers have been widely studied in recent years in both melts and solutions, and with both selective[2,3] and neutral[4] solvents. Because the drying rate of solution cast films can affect both the type of microstructure formed[5,6,7] as well as their rate of formation[8], the effects of solvent removal rate on nanodomain formation need to be well understood. Prior work in our laboratory by Heinzer, et al.[8,9] used both dynamic mechanical rheology (DMR) and in-situ small-angle X-ray scattering (SAXS) to relate the concentration and drying rate to the ordering kinetics in solution cast block copolymer films. However, the effects of drying rate on the kinetics could not be fully understood in these studies

because these studies controlled drying rate with temperature, which also changes the thermodynamic driving force and the kinetics of chain movement.

Phase transformation kinetics in block copolymers are often described using Avrami kinetics, which were originally developed to describe crystallization.[10,11,12,13,14] Avrami kinetics are modeled using the following equation

$$\frac{\phi(t)}{\phi_\infty} = 1 - \exp(-kt^n) \quad \text{(3-1)}$$

where ϕ represents the volume fraction of ordered phase, $\phi_\infty$is the maximum fraction of ordered phase, k is a rate constant, and n is the Avrami exponent. Several modifications to the Avrami equation have been proposed to describe kinetics in general systems during a temperature ramp[15,16] and during monotonic temperature changes[17]. Both of these methods collapse the kinetics onto a master curve for evaluation.

During drying of a cast film, the polymer concentration where the order-disorder transition occurs (C_{ODT}) is reached at progressively lower points in the film while the degree of undercooling in the upper portions of the film increases. An ordering front thus proceeds down through the film, assisting nucleation.[18] This ordering front exists between the boundary of the bulk of the film and the ordering layer, in which the polymer concentration is above the ODT concentration and ordering can proceed. Previous studies have found that drying rate can affect the final morphology of solution cast films.[5,6,7] In all of these prior studies, a calculation of the final ordered volume was not performed. Herein we report on a more detailed experimental and analytical method to determine the ordering kinetics during drying in solution cast films. In addition, we report on the effect of controlling drying rate via sweep gas flow rate to study the effects of solvent removal rate on a film drying using in-situ SAXS.

3.3 Experimental Methods

3.3.1 Materials

Diblock poly(styrene-*b*-butadiene) (SB) was obtained from Sigma-Aldrich® with $f_{styrene} = 0.3$. GPC results for the SB polymer gave a multimodal distribution with M_n values of 15, 81, and 190kDa and M_w/M_n of 1.05, 1.05, and 1.06 with a weight fraction of the total sample of 3wt%, 73wt%, and 22%. The SB copolymer was dissolved in toluene and filtered through a $0.2\mu m$ nylon filter to remove impurities. This solution was then dried for at least 72 hours in a vacuum oven at a temperature of 100°C.

3.3.2 In-situ SAXS

C_{ODT} measurements were performed on a Bruker N8 Horizon on iso-concentration samples in air to prevent drying during measurement. Samples were sealed in a pouch made of polyimide film. The samples were each run for 10min and the resulting profiles checked for ordering. In this case, the C_{ODT} was determined to be 42wt% polymer.

We employed an *in-situ* SAXS drying apparatus to track the morphology changes in thick (~400µm) block copolymer solution-cast films during solvent removal. We used a doctor blade to ensure that the films were of a uniform thickness, and the final film thickness was measured using a caliper. A balance was used to track the solvent concentration of the films during drying. The sweep gas was directed below the stage rather than over the sample to reduce the residence time of solvent vapor in the chamber while reducing the possibility of a "skin" forming on the surface of the sample.

Experiments were performed in-situ with and without a sweep gas flowing beneath the sample stage to control the residence time and amount of solvent vapor in the cell. Sweep gas flow rates were 0 SCFH N_2, 0.1 SCFH N_2, and 0.35 SCFH N_2, hereafter referred to as no sweep, slow sweep and fast sweep respectively. With a calculated chamber volume of 510cm^3, the residence times for the slow sweep and fast sweep systems are 11min and 3.1min respectively. *In-situ* Small Angle X-ray Scattering was performed across

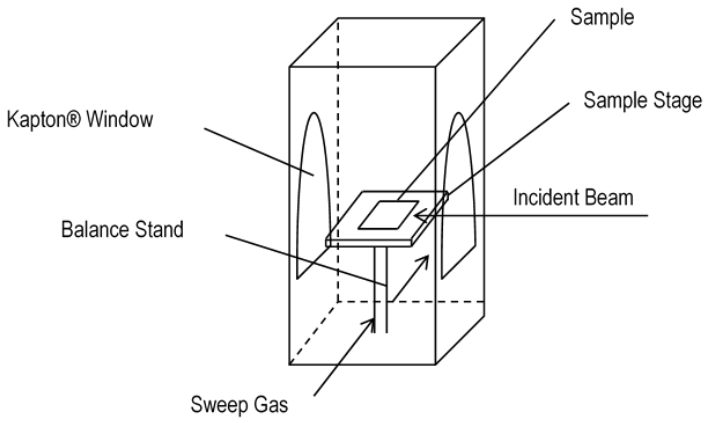

Figure 3-1: Scattering cell used to track the removal of solvent in block copolymer films during small-angle X-ray scattering experiments

the top of the film during drying. In-situ experiments were performed at Beamline 1-4 at the Stanford Synchrotron Radiation Laboratory (SSRL). The beam had an energy range of 7100-9000eV, $\Delta E/E = 4.0 *$

10^{-3}, and the beam diameter was 1.1mm. Data were collected with a Rayonix165 CCD detector. The beamline had a bent crystal Si monochrometer. Figure 3-1 shows a diagram of the drying apparatus.

3.4 Mass Transport

3.4.1 Mass Transport Model for Film Drying

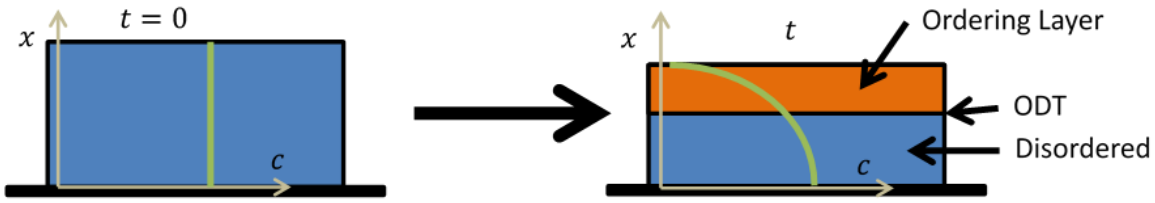

Figure 3-2: Depiction of drying process at t = 0s and t = t ordering layer and concentration profile of the film. Here, ***c*** is defined as the ratio of current solvent mass density to the initial solvent mass density

The films studied in this work are relatively thick (65-400 μm), and thus concentration gradients within the cast films must be accounted for during the experiment in order to correctly analyze the in-situ SAXS results. Initially (at *t = 0*), the solvent concentration in the film is uniform, as depicted in Figure 3-2. During drying, the solvent concentration decreases due to solvent evaporation from the surface of the film, resulting in a concentration profile that drives diffusive solvent transport within the polymer film. Once the concentration at the film surface reaches the order-disorder transition (ODT) concentration in solution, the film surface is then capable of ordering. As time increases, the position of the ODT in the film (the ordering front) moves downwards in the film until it reaches the solid substrate. The ordering layer, the portion of the film that is above the ODT and is thus capable of ordering, therefore increases in volume with increasing time until the ordering front reaches the substrate. At later times, the volume of the ordering layer decreases as solvent is removed and the overall film thickness decreases.

As shown in Figure 3-3, the ordering layer concentration was calculated from the ODT data, weight tracking data, and initial diffusivity. The initial diffusivity was put into the Vrentas and Vrentas model[19] to calculate the concentration profile. This was integrated to calculate the bulk concentration and compared with the weight tracking data. The diffusivity at this time point was then altered slightly, and the concentration profile was calculated again. This was repeated several hundred times recursively. The concentration profile was then integrated where polymer concentration was greater than the C_{ODT} to

determine the ordering layer concentration. The volume of each individual segment of the profile were then calculated, assuming that each contains the same amount of polymer. This volume was used to determine the total thickness of the ordering layer.

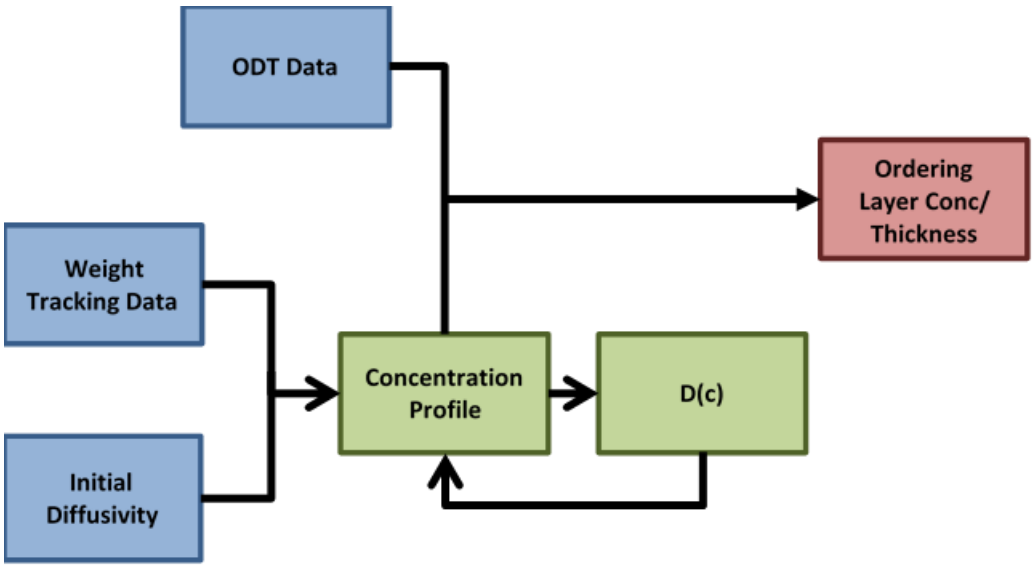

Figure 3-3: Depiction of drying process at t = 0s and t = t ordering layer and concentration profile of the film. Here, c is defined as the ratio of current solvent mass density to the initial solvent mass density

The fraction of the film thickness taken up by the ordering layer is related to the solvent concentration profile in the film. Thus, a model of the drying process based on that developed by J.S. Vrentas and C.M. Vrentas[19] was created in MATLAB (see Supplemental Information) to calculate the solvent concentration at different levels in the film. This model uses a jump mass balance at the air-solution interface to calculate the solvent concentration profile in the film as a function of time. The resulting dimensionless partial differential equation becomes

$$\frac{\partial c}{\partial t^*} - \frac{\eta}{X^*}\frac{dX^*}{dt^*}\frac{\partial c}{\partial \eta} = \frac{1}{(X^*)^2}\frac{\partial}{\partial \eta}\frac{D^P}{D_0^P}\frac{\partial c}{\partial \eta} \qquad \textbf{(3-2)}$$

Where $c = \rho_1^P/\rho_{10}^P$, $\eta = x/X(t)$, and $X^* = X(t)/L$. Here, $X(t)$ is defined as the location of the upper boundary of the film as measured from the substrate, L is the initial film thickness, x is the vertical position in the film as defined by distance from the film substrate, D_0^P and D^P are the initial and current diffusivity of the solvent in the film, and ρ_{10}^P and ρ_1^P are the initial and current mass densities. At $\eta = 0$, $\partial c/\partial \eta = 0$. In addition $c(0,\eta) = 1$, with the location of the upper interface of the film as

$$X^* = \frac{1 - \hat{V}_1^P \rho_{10}^P}{1 - \hat{V}_1^P \rho_{10}^P \left(\int_0^1 c d\eta \right)} \quad \text{(3-3)}$$

Here, $\hat{V}_1^P$ is the solvent specific volume in the film. The dimensionless time is defined as

$$t^* = \frac{D_0^P t}{L^2} \quad \text{(3-4)}$$

Assuming a negligible volume change upon mixing, the thickness was calculated based on the known film mass, the dimensions of the substrate, and the height of the doctor blade. Using the upper film location as well as Equation (3-2) and (3-3), a MATLAB model was created. The diffusivity was calculated recursively and concentration profiles were found throughout the film thickness given known bulk concentrations. The diffusivity could not be assumed to be equal to the measured diffusivity at a given concentration because the ordering rate and the drying rate were on the same time scale; any ordering in the system could affect the value of the overall diffusivity. However, calculating a known diffusivity at the initial concentration where the system was disordered allowed for the approximation of diffusivity profiles throughout the film.

Concentrations obtained from the film drying model were used in the Flory-Huggins model to calculate the partitioning of solvent between phases, shown in Equation (3-5) below.

$$\ln(a_s) = \ln\left(1 - \Phi_p^*\right) + \left(1 - \frac{1}{r}\right)\Phi_p^* + \chi {\Phi_p^*}^2 \quad \text{(3-5)}$$

Here, a_s is the solvent activity, Φ_p^* is the fraction of lattice sites occupied by polymer, r is the number of segments in the polymer molecule that are equal in size to the solvent, and χ is the polymer-solvent interaction parameter. The boundaries between the phases were assumed to be sharp, the excess volume in the solution and the ordered phase was assumed to be negligible, and the long-range solvent concentration was assumed to be uniform between the ordered phase and the bulk with uniform local concentration within the blocks. The thickness of the ordering layer was estimated based on the C_{ODT} found using iso-concentration SAXS measurements. The ordering layer is defined as the region in the film where polymer concentration is above C_{ODT}, meaning that ordering is thermodynamically favored.

Once the ODT was determined, the solvent concentration in the film at different levels as a function of time was calculated using the Vrentas and Vrentas model[19]. Using volume rather than mass in the jump mass balance simplifies the mass, energy, and momentum balances.

We solved for c as a function of η, and for $D^P(\eta)/D_0^P$, as X^* was known from the film thickness. Diffusivity and concentration were solved iteratively. Diffusivity at the surface was assumed to be lower than that in the rest of the film, as this is the region of lowest solvent concentration. The diffusivity at $t = 0$ was determined experimentally at the initial solution concentration. Toluene sorption experiments were used to determine the diffusivities at the initial solution concentrations in the in-situ X-ray diffraction experiments. A schematic of the method used can be seen below.

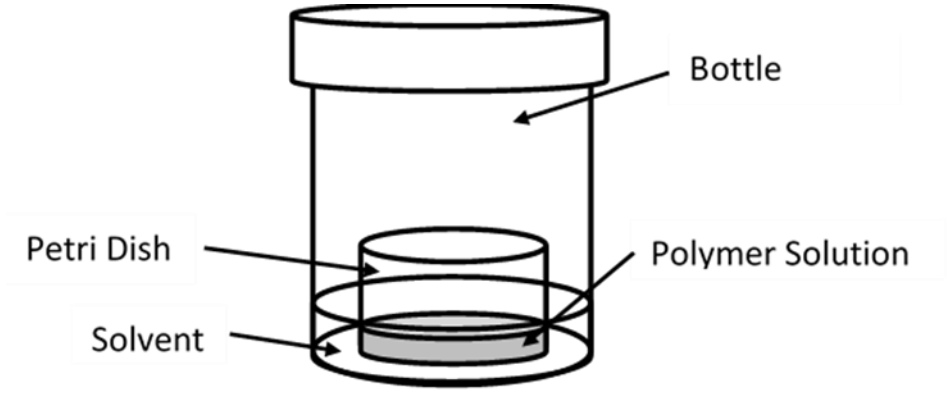

Figure 3-4: Weight fraction poly(styrene-b-butadiene) in toluene during *in-situ* SAXS drying experiments

The neat polymer samples were placed in a petri dish in a bottle with solvent vapor, and mass was measured as a function of time. As the concentrations of the solution at infinite time in the experiment encompassed that of the initial cast solution, the final calculated diffusivities in the sorption experiments could be used to obtain the initial diffusivities during drying. Final diffusion coefficients in a plane sheet during solvent sorption were calculated used the following equation:

$$\frac{d}{dt}(\ln(M_\infty - M_t)) = -\frac{D^P \pi^2}{L^2} \tag{3-6}$$

derived by J. Crank.[20] M_∞ and M_t are the masses of solvent taken up by the film at time $t = \infty$ and t, and L is the initial thickness of the sample. The toluene diffusivities at polymer weight fractions of 0.2 were found to be $2.5 \pm 0.3 * 10^{-11} m^2/s$ for SB.

3.4.2 Mass Transport Modeling Results

Using the Vrentas and Vrentas[19] drying model, we calculated the concentration profiles of solvent in all polymer systems during solution casting. The bulk weight fractions during the *in-situ* experiments for the styrene/butadiene copolymer are depicted in Figure 3-5. All of the drying curves were initially exponential

before beginning to level off at later times. The trials with slow sweep gas and no sweep gas had similar initial drying rates, but the curves eventually diverged, with the slow sweep gas providing more rapid solvent removal before both curves leveled off. The fast sweep gas of 0.35 SCFH N_2 produced a faster initial and overall drying rate than the other two cases. The initial thicknesses of the SB films were within 5% of each other.

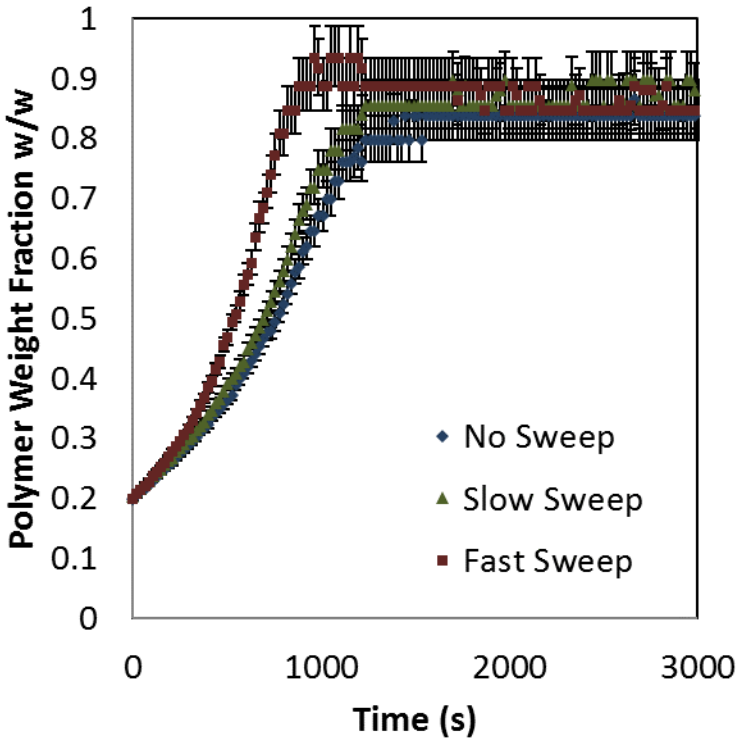

Figure 3-5: Weight fraction poly(styrene-b-butadiene) in toluene during *in-situ* SAXS drying experiments

The solvent concentration profiles for no sweep gas are shown Figure 3-6**.** Due to the slow drying rate and the high solvent diffusivity ($\sim 2 \cdot 10^{-11} m^2/s$), the concentration profile widens at initial times without forming a skin before flattening out at later times in the experiment. The concentration increases quickly at the surface early in the experiment and then more gradually as the solvent diffusivity drops in the upper portion of the film.

The solvent partitioning at different positions in the film, η, where $c(\eta) \geq C_{ODT}$, was determined based on the calculated concentration profile for a particular time. The thickness of the ordering layer was calculated from the thickness of all positions where $c(\eta) \geq C_{ODT}$. To allow calculation of the total volume

available for ordering, a second-order polynomial was fit to the calculated concentration to determine the ordering layer thickness. The calculated location of the ordering front for all three trials is plotted in Figure 3-7. The system with no sweep gas and the system with a slow sweep gas have similar times needed for the ordering front to reach the bottom of the film, due to the similar drying rates. Whereas, the quicker drying rate of the trial with a fast sweep gas allowed the ordering front to reach the substrate more quickly and subsequently for the ordering layer to encompass the entire film more quickly than in the other two trials.

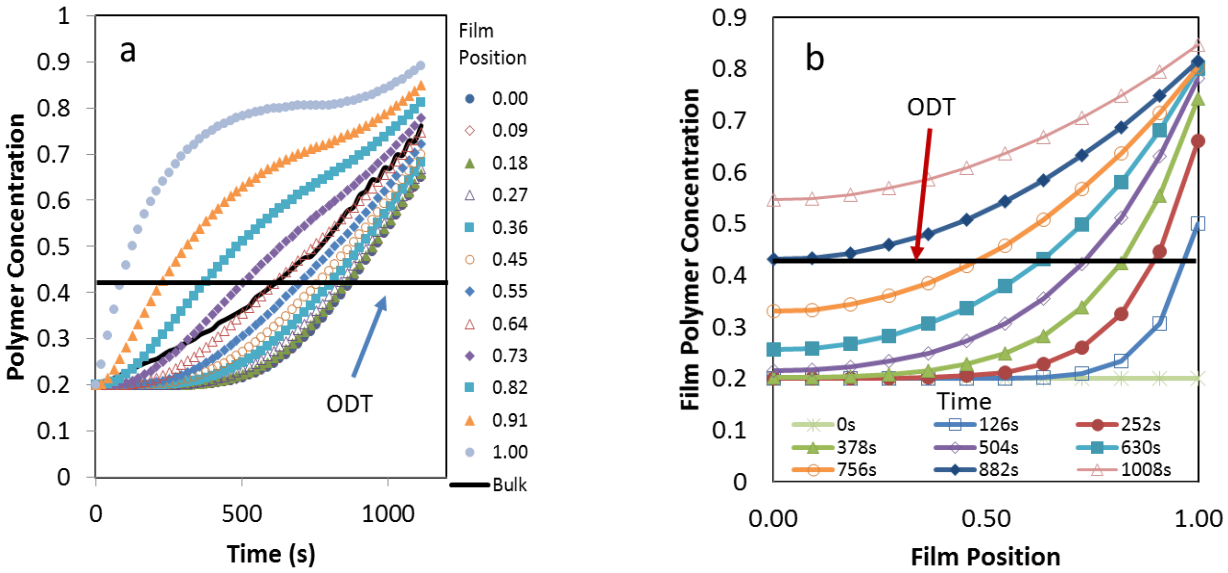

Figure 3-6: a) Polymer concentration as a function of time for different positions in the film from the substrate (0) to film surface (1.0) in a styrene-butadiene diblock in toluene with no sweep gas; **b)** Polymer concentration as a function of position in the film at different times.

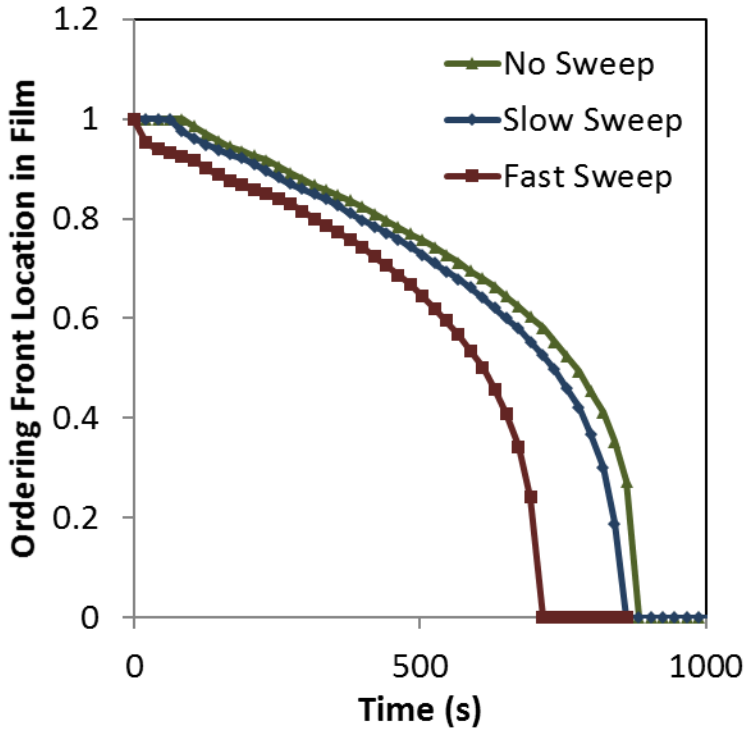

Figure 3-7: Ordering front position as a function of time for poly(styrene-*block*-butadiene) in toluene at various sweep gas flow rates.

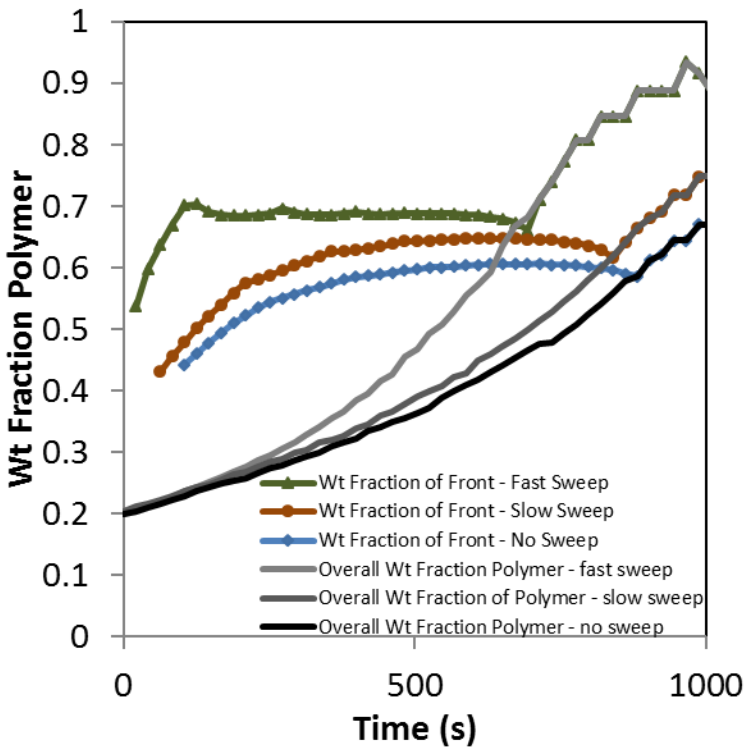

Figure 3-8: Calculated weight fraction of poly(styrene-*block*-butadiene) in toluene in ordering layer and bulk film during in-situ SAXS experiments under various drying conditions.

Comparing the various systems, as seen in Figure 3-6, the system without a sweep gas had a similar drying rate to that of the system with a slow sweep gas, especially at low times. The faster sweep gas allowed for a quicker drying time with ordering beginning early. The duration of time over which the ordering front existed was shorter in the faster sweep gas system (650s to 780s with a slow sweep gas). This was due to the more rapid drying in the film during these trials. In the faster drying system, the concentration profile increases rapidly at the surface of the film before flattening at the substrate. This skinning means that there is a higher concentration gradient between the bottom and the top of the film. The profile also flattens out with time as the solvent has a chance to migrate to the surface. This results from the solvent concentration gradient throughout the film and the higher diffusivity in the lower portion of the film, leading to the ordering layer concentration remaining level throughout much of its progress.

3.5 Kinetics of Ordering via In-situ SAXS

Time-resolved *in-situ* small-angle X-ray scattering (SAXS) was used to track the growth of ordered block copolymer microstructures during solvent removal. The scattering invariant, Q, can be used to calculate the total relative ordered volume using Equation (3-7).

$$Q \equiv \int_0^\infty I(q)q^2dq = 2\pi^2 V\varphi_1\varphi_2(\rho_1^e - \rho_2^e)^2 \quad \textbf{(3-7)}$$

where $I(q)$ is the scattering intensity, and q is the scattering vector that is defined as $q = 4\pi \sin\theta/\lambda$. θ is the scattering angle and λ is the distance from the sample to the detector, V is the total relative ordered volume, φ_n is the volume fraction in ordered phase of nanodomain n, and ρ_n^e is the electron density of nanodomain n.[21]

The invariant of the system as a function of time could not be accurately calculated due to the shifting background scattering resulting from the decreasing thickness of the film. Therefore, the trend of the invariant as a function of time was calculated using the area of $I(q)q^2$ under the primary peak, as given in Equation (3-8).

$$Q{\sim}A \equiv \int_{Peak} I(q)q^2dq \quad \textbf{(3-8)}$$

A diagram of the area that was integrated in the $q^2I(q)$ vs. q plot is shown below in Figure 3-9.

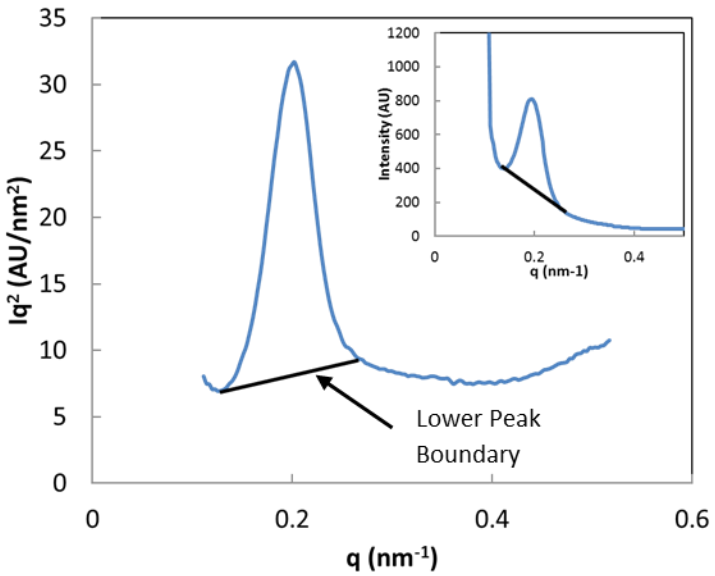

Figure 3-9: Diagram of the area under the $q^2I(q)$ vs. q primary peak that was used to estimate the overall trend of the invariant. Inset shows primary peak in $I(q)$ vs. q

Here, the boundaries of the peak were taken from the peak boundaries in the $I(q)$ vs. q data, and the lower boundary of this peak was assumed to be linear. The integrated area, A, was calculated from the portion of the peak between the peak and the lower peak boundary. Equation (3-7) requires sharp

interfaces. The interfaces between the phases do have a non-zero thickness that decreases with time. However, as the area under the primary $q^2I(q)$ vs. q peak was used to perform background subtraction, interfacial effects do not change the calculated A value. In addition, the high and flat ordering layer concentration insulates the system from the effects of changing interfacial thickness. However, it should be noted that interfacial and solvent effects will change the total overall invariant, and A is being used as an approximation.

Data were then normalized for volume using the ordering layer thickness and values for A at long times to calculate the maximum volume fraction of the ordered phase. The relative volumes of the styrene and diene blocks were calculated using the Flory-Huggins model with χ values calculated from solubility parameters. This included the differential solvent partitioning between the blocks in an approach similar to that taken by Gallot and Sadron[23].

Using the initial diffusivity at $t = 0$, an exponential function of diffusivity with respect to c was assumed. This diffusivity allowed for the iterative solution of the solvent content.

Solvent partitioning was calculated for the entire film based on the mean bulk concentration in the ordering layer. Solvent partitioning between the two blocks was calculated by minimizing the difference in the solvent activities of the two blocks in Equation (3-5), allowing the solvent concentration of each to be calculated. The multimodal nature of both the diblock and triblock copolymers was taken into account by adding both solvent activities resulting from a given polymer block for both copolymers. Styrene-butadiene was assumed to be bimodal rather than trimodal due to the small fraction of the low MW species. M_w/M_n was assumed to be 1 in all cases.

3.5.1 Solvent Partitioning

The variation in the solvent content of the system during solution casting presents several challenges for the analysis of the SAXS data. In addition to the time sensitive nature of the measurements, the nanodomains that form exhibit changing mass and electron densities due to deswelling of the microstructure upon solvent removal. Both the volume and electron density of each nanodomain must be calculated in order to track the total volume of the ordered phase throughout the process, because the scattering invariant, Q, is dependent on the electron density of the nanodomains. The electron density was calculated using the following equation:

$$\rho^e = \frac{\sum b_i}{V} = \frac{l_e N_A n_e}{M} \qquad \textbf{(3-9)}$$

where ρ^e is the electron density, in cm^{-2} of a species, b_i is the scattering length of an electron, N_A is Avogadro's number, n_e is the number of electrons in a molecule, M is the molecular weight of a molecule, and l_e is the scattering length of an electron, or $0.28 * 10^{-12}$ cm. [22] The total mass of a given nanodomain is taken as:

$$m_1 = f_1\left(\frac{w_S X}{\phi_{1,0}} + w_P\right) \tag{3-10}$$

where f_1 is the weight fraction of block 1, $\phi_{1,0}$ is the volume fraction of block 1 in a lattice consisting of pure block copolymer, and w_i is the bulk weight fraction of solvent, S, or polymer, P. Here, $X/\phi_{1,0}$ is a quantity that represents the actual number of solvent molecules in a nanodomain with respect to the theoretical number of solvent molecules in that nanodomain. This mass was used to calculate the total volume fraction of the phase, which was then used to calculate the electron density of a particular domain, using

$$\rho_A^e = \sum_{i=1}^{n} \rho_i^e \phi_i \tag{3-11}$$

Here, ϕ_i is the volume fraction of species i. The specific volume of a domain is calculated using the equation

$$v_A = \frac{w_1}{\rho_1} + \frac{X w_S v_1}{\rho_S v_P} \tag{3-12}$$

where v_i is the specific volume of species i in a nanodomain, and v_P is the specific volume of the polymer, and ρ_i is the mass density of species i. The specific volumes were used to calculate the volume fraction of each nanodomain.

3.5.2 In-situ SAXS Results

The volume fraction of the ordered phase is plotted in Figure 3-10 as a function of time from the onset of ordering during the solution casting of SB in toluene at 24°C. Given that the ordered volumes are calculated with respect to the overall ordered volume in each system, a comparison cannot be made between total ordered volumes, and so volume fraction ordered phase has been used. The data exhibits the expected sigmoidal shape. In addition, the ordering rate increases with drying rate as controlled via the sweep gas flow rate. The drying rates of the trials with a 0.1 SCFH nitrogen sweep and without sweep gas were similar as seen in Figure 3-5. However, the trials with both slower and faster sweep gas showed similar growth rates with respect to time. This may be due to additional kinetic entrapment occurring in the faster drying system that does not occur to the same extent in the slower drying system. However, in

general, sweep gas and increased drying rate appear give rise to an increase in the ordering rate of nanostructure. The volume fractions of ordered phase are similar at initial times, but as the weight fraction difference between the trials becomes larger, the curves diverge and the faster drying samples show a greater ordering rate. The half-times of ordering are shown in Table 3-1. The decreasing half-time with respect to sweep gas flow rate is indicative of the increased ordering rate at faster drying rates.

Table 3-1: Half-times from start of ordering for SB diblock copolymer trials at different sweep gas flow rates

Sweep Gas Flow Rate	$t_{1/2}$ from start of ordering (min)	Calculated $t_{1/2}$ from Avrami Equation
None	10.9	11.0
0.1 SCFH	9.0	9.0
0.35 SCFH	9.2	8.6

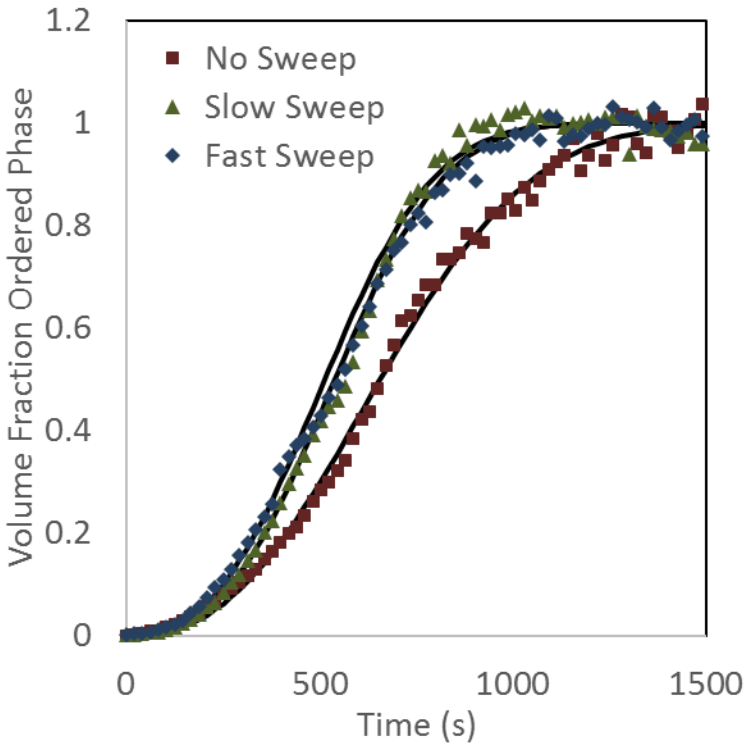

Figure 3-10: Calculated relative ordered volume fraction of SB in toluene with respect to time since start of ordering. Lines indicate Avrami fit.

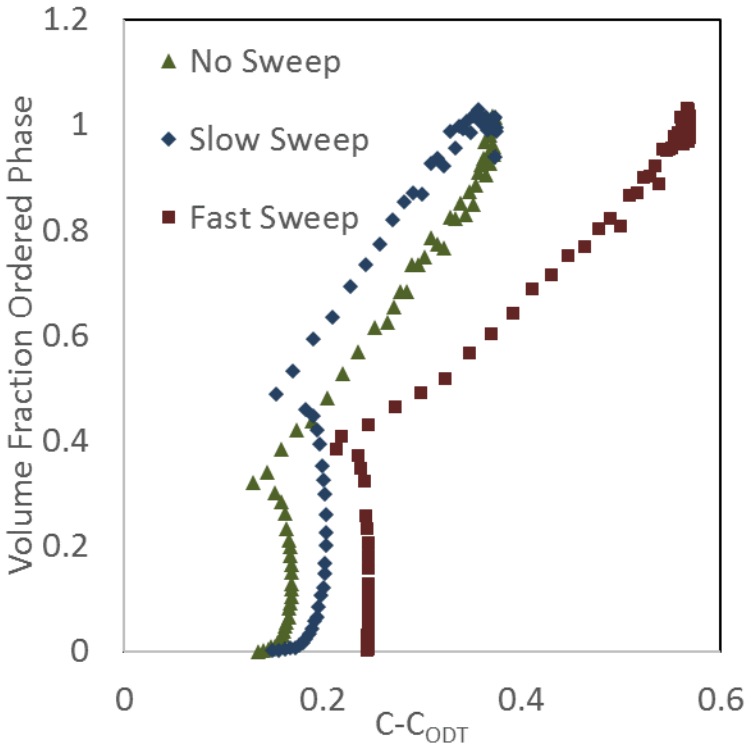

Figure 3-11: Calculated polymer ordered volume fraction of SB in toluene with respect to weight fraction of ordering layer

The volume fraction curves in Figure 3-10 and the half-time results in Table 3-1 suggest that an Avrami fit will not be able to describe the ordering behavior for faster drying rates. There is significant deviation between the theoretical half-time calculated from the Avrami model and the actual half-time calculated from the data. This is not surprising given the dynamic nature of the quench depth of the system with respect to time and position in the film and given the reduction in chain mobility that results. The Avrami model does describe the ordering of slower drying systems, which was unexpected, as the system is not isotropic with respect to time.

The volume fraction curves with respect to concentration difference from the C_{ODT} in the ordering layer are shown in Figure 3-11. Due to the lack of significant change in the ordering layer concentration before the ordering front reaches the bottom of the film, the curves have two distinct regions; ordering that occurs before and after the ordering front reaches the substrate. Before the ordering front reaches the substrate, the average ordering layer concentration remains constant, resulting in a vertical rise in ordered volume fraction. The concentration of the ordering layer increases once the ordering front

reaches the bottom of the film. This allows the volume fraction to increase with concentration. Despite the similar amount of time over which the slow and no sweep ordering fronts exist, the slow sweep gas system was able to undergo a more complete ordering process over that time period relative to total ordering. This is likely due to greater driving force caused by increased quench depth and greater polymer concentration. This is also true for the fast sweep gas system, as it is able to undergo greater relative ordering over a shorter period of time than a system without sweep gas. Because the faster sweep gas system is at a higher polymer concentration at a given volume fraction ordered phase, it is reasonable to suggest that it experiences a greater degree of kinetic entrapment. Once the ordering layer has reached the substrate, all three curves have a linear relationship with volume fraction ordered phase. The reasons for this are not entirely known at this time.

3.6 Conclusions

We were able to use the calculated diffusivities of toluene in solution and the weight tracking to calculate the concentration profiles of the solvent in drying films. These profiles were used to calculate the solvent partitioning between the two blocks to obtain the volume fraction of ordered phase in the films. The ordering curve produced by the faster drying system could not described using Avrami kinetics, likely due to the dynamic concentration profile in the film. When the volume fraction of the ordered nanostructure was calculated with respect to ordering layer concentration quench depth, two distinct regions were seen: ordering that occurs before the ordering front reaches the substrate and ordering that occurs throughout the entire film. It was found that the slow drying rate used in the SB diblock experiments caused the system to order more quickly with respect to concentration than either the faster or slower drying systems, likely due to kinetic entrapment.

References

1. Lodge, T. P.; Pudil, B.; Hanley, K. J., The Full Phase Behavior for Block Copolymers in Solvents of Varying Selectivity. *Macromolecules* **2002,** *35* (12), 4707-4717.
2. Chastek, T. Q.; Lodge, T. P., Measurement of Gyroid Single Grain Growth Rates in Block Copolymer Solutions. *Macromolecules* **2003,** *36* (20), 7672-7680.
3. Chastek, T. Q.; Lodge, T. P., Grain Shapes and Growth Kinetics of the Cylinder Phase in a Block Copolymer Solution. *Macromolecules* **2004,** *37* (13), 4891-4899.
4. Chastek, T. Q.; Lodge, T. P., Twinning and growth kinetics of lamellar grains in a diblock copolymer solution. *Journal of Polymer Science Part B: Polymer Physics* **2005,** *43* (4), 405-412.
5. Yamamura, M.; Nishio, T.; Kajiwara, T.; Adachi, K., EFFECT OF STEPWISE CHANGE OF DRYING RATE ON MICROSTRUCTURE EVOLUTION IN POLYMER FILMS. *Drying Technology* **2001,** *19* (7), 1397.
6. Kim, G.; Libera, M., Morphological Development in Solvent-Cast Polystyrene−Polybutadiene−Polystyrene (SBS) Triblock Copolymer Thin Films. *Macromolecules* **1998,** *31* (8), 2569-2577.
7. Huang, H.; Zhang, F.; Hu, Z.; Du, B.; He, T.; Lee, F. K.; Wang, Y.; Tsui, O. K. C., Study on the Origin of Inverted Phase in Drying Solution-Cast Block Copolymer Films. *Macromolecules* **2003,** *36* (11), 4084-4092.
8. Heinzer, M. J.; Han, S.; Pople, J. A.; Baird, D. G.; Martin, S. M., In Situ Measurement of Block Copolymer Ordering Kinetics during the Drying of Solution-Cast Films Using Small-Angle X-ray Scattering. *Macromolecules* **2012,** *45* (8), 3471-3479.
9. Heinzer, M. J.; Han, S.; Pople, J. A.; Martin, S. M.; Baird, D. G., Iso-concentration ordering kinetics of block copolymers in solution during solvent extraction using dynamic oscillatory measurements. *Polymer* **2012,** *53* (15), 3331-3340.
10. Avrami, M., Kinetics of Phase Change. I General Theory. *The Journal of Chemical Physics* **1939,** *7* (12), 1103-1112.
11. Avrami, M., Kinetics of Phase Change. II Transformation‐Time Relations for Random Distribution of Nuclei. *The Journal of Chemical Physics* **1940,** *8* (2), 212-224.
12. Avrami, M., Granulation, Phase Change, and Microstructure Kinetics of Phase Change. III. *The Journal of Chemical Physics* **1941,** *9* (2), 177-184.
13. Floudas, G.; Hadjichristidis, N.; Iatrou, H.; Pakula, T.; Fischer, E. W., Microphase Separation in Model 3-MiktoarmStar Copolymers (Simple Graft and Terpolymers). 1. Statics and Kinetics. *Macromolecules* **1994,** *27* (26), 7735-7746.
14. Liu, Y.; Nie, H.; Bansil, R.; Steinhart, M.; Bang, J.; Lodge, T. P., Kinetics of disorder-to-fcc phase transition via an intermediate bcc state. *Physical Review E* **2006,** *73* (6), 061803.
15. Farjas, J.; Roura, P., Modification of the Kolmogorov–Johnson–Mehl–Avrami rate equation for non-isothermal experiments and its analytical solution. *Acta Materialia* **2006,** *54* (20), 5573-5579.
16. Farjas, J.; Roura, P., Solid-phase crystallization under continuous heating: Kinetic and microstructure scaling laws. *Journal of Materials Research* **2008,** *23* (02), 418-426.
17. Lambrigger, M., Non-isothermal polymer crystallization kinetics and avrami master curves. *Polymer Engineering and Science* **1998,** *38* (4), 610.
18. Buxton, G. A.; Clarke, N., Ordering polymer blend morphologies via solvent evaporation. *EPL (Europhysics Letters)* **2007,** *78* (5), 56006.
19. Vrentas, J. S.; Vrentas, C. M., Drying of solvent-coated polymer films. *Journal of Polymer Science Part B: Polymer Physics* **1994,** *32* (1), 187-194.
20. Crank, J., *The Mathematics of Diffusion*. 2nd ed.; Clarendon Press: Oxford, 1975; p 410.
21. Porod, G., *Small angle x-ray scattering*. Academic Press: London; New York, 1982.
22. Stuhrmann, H. B., *Small angle x-ray scattering*. Academic Press: London; New York, 1982.

23. Sadron, C.; Gallot, B., Heterophases in block-copolymer/solvent systems in the liquid and in the solid state. *Die Makromolekulare Chemie* **1973,** *164* (1), 301-332.

4 Calculation of Volume Fraction Ordered Phase of Styrene-Diene Triblock Copolymer Solutions by *In-Situ* Small-Angle X-ray Scattering

4.1 Introduction

To ensure that the method for determining the extent of ordering as described in Chapter 3 was viable for triblock copolymers and for copolymers whose solvent diffusivity was lower than that of SB diblock, two additional block copolymers polymers were analyzed using this method. The two polymers also possessed lower block fractions of styrene than the diblock. In addition, polyisoprene has a lowered affinity for toluene than polybutadiene ($\chi_{IT} \cong 0.46$ vs. $\chi_{BT} \cong 0.40$)[1], although toluene is still a good solvent for both polymers.

4.2 Materials

A Sigma-Aldrich® triblock poly(styrene-*b*-butadiene-*b*-styrene) (SBS) $f_{styrene} = 0.2$. GPC results for the SBS polymer gave a multimodal distribution with M_n values of 18, 80, and 170kDa at weight fractions of 0.018, 0.123, and 0.839 and M_w/M_n of 1.06, 1.02, and 1.06. For analysis, the polymer was assumed to be bimodal due to the small fraction of 18kDa species. A Kraton® poly(styrene-*b*-isoprene-*b*-styrene) (SIS) triblock copolymer $f_{styrene} = 0.15$ was used as purchased. The SIS polymer had a bimodal distribution with $M_n$values of 144kDa and 79kDa with M_w/M_n of 1.02 and 1.01 and weight fractions of diblock and triblock of 0.81 and 0.19 respectively.

4.3 Methods

The experimental methods used are similar to those used in Chapter 3. The SIS experiments used the same sweep gas flow rates as the diblock experiments described previously in Chapter 3. The SBS experiments used 0 SCFH N_2, 0.1 SCFH N_2, and 0.2 SCFH N_2 referred to as no sweep, slow sweep, and medium sweep respectively. Both triblock copolymers were used as purchased.

4.3.1 Mass Transport Model

The model used for mass transport was identical to that used in Chapter 3. The diffusivities calculate from sorption experiments were found to be $6.5 \pm 0.3 * 10^{-12} m^2/s$ for SIS, and $2.2 \pm 0.3 * 10^{-12} m^2/s$ for SBS at a polymer weight fraction of 0.2, significantly slower than those of the SB diblock copolymer, or $2.5 \pm 0.3 * 10^{-11} m^2/s$.

4.4 Results and discussion

SIS drying curves, as seen in Figure 4-1, have similar drying rates for slow and no sweep experiments, with divergence of the two occurring later in the experiment. The initial thicknesses of the SIS films were within 7% of each other. The fast sweep system displays a faster drying rate than either of the two. The SBS drying curves, shown below in Figure 4-2, behaved differently. The no sweep and medium sweep systems had similar initial drying rates before diverging. The slow sweep system dried more slowly than either of the other two trials and had a lower weight fraction of polymer than the no sweep trial until late in the process, at $\sim$1100s, when a crossover occurred. This may be due to the greater initial thickness in the slow sweep system as compared to the other two trials (500μm vs. 450μm and 460μm for the slow, no, and medium sweep trials respectively), which would have caused slower drying and increased the effect of the low diffusivity in the slow sweep trial.

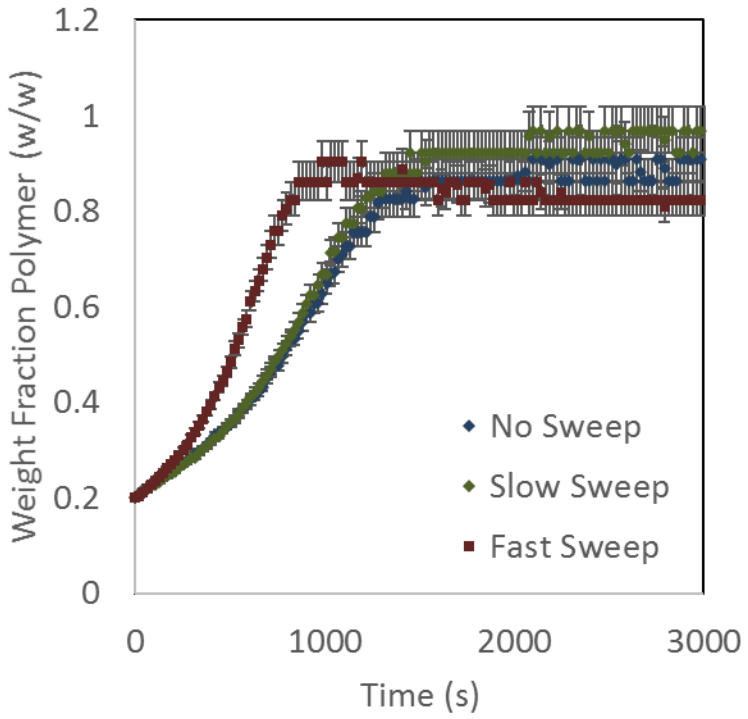

Figure 4-1: Weight fraction poly(styrene-*b*-isoprene-*b*-styrene) in toluene during *in-situ* SAXS drying experiments

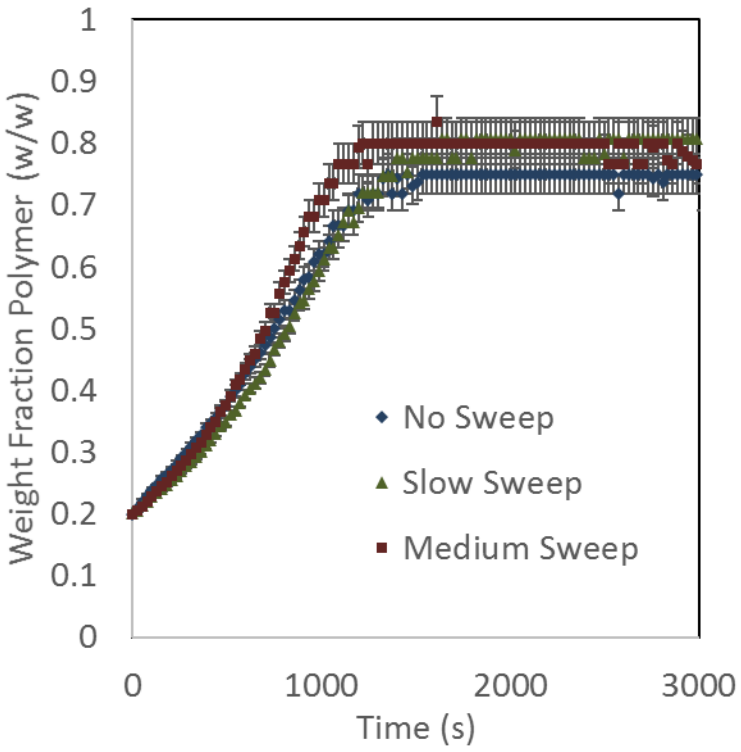

Figure 4-2: Weight fraction poly(styrene-*b*-butadiene-*b*-styrene) in toluene during *in-situ* SAXS drying experiments

The calculated concentration profiles for SBS are pictured below in Figure 4-3. A skin formed on the surface of the film soon after the initiation of drying. This skin was thin, initially less than 2% of the thickness of the film, and would have slowed evaporation of the solvent significantly. Discontinuities in the concentration curves are an artifact of the different sections of fitted film thickness used in the model.

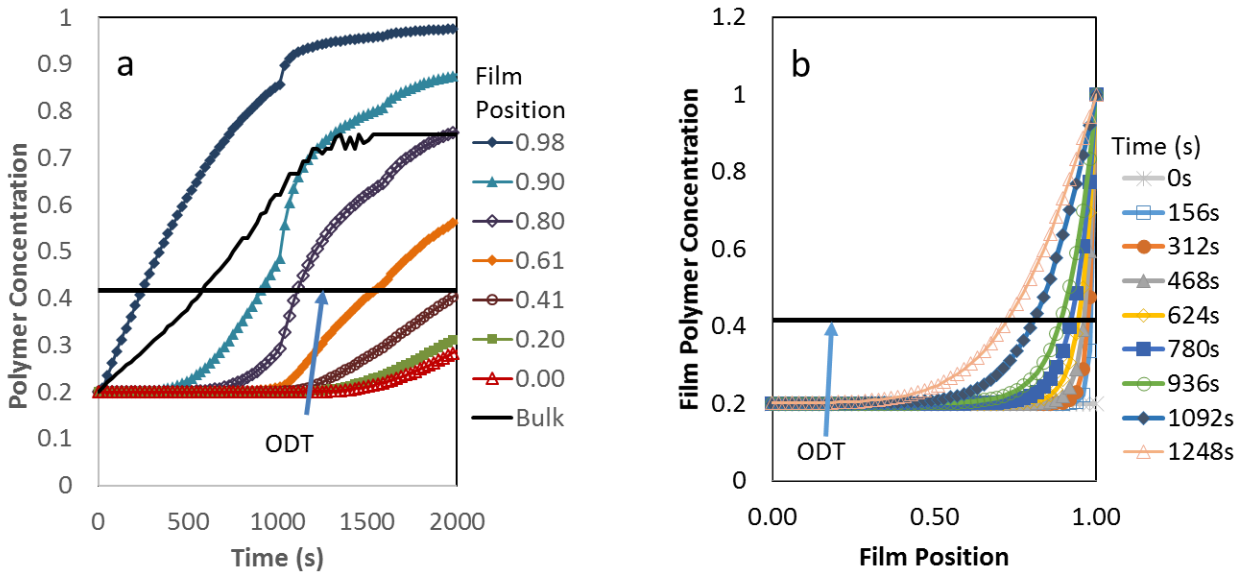

Figure 4-3: a) Calculated polymer concentration as a function of time for different positions in the film from the substrate (0) to film surface (1.0) in a styrene-butadiene-styrene triblock in toluene with no sweep gas; **b)** Polymer concentration as a function of position in the film at different times.

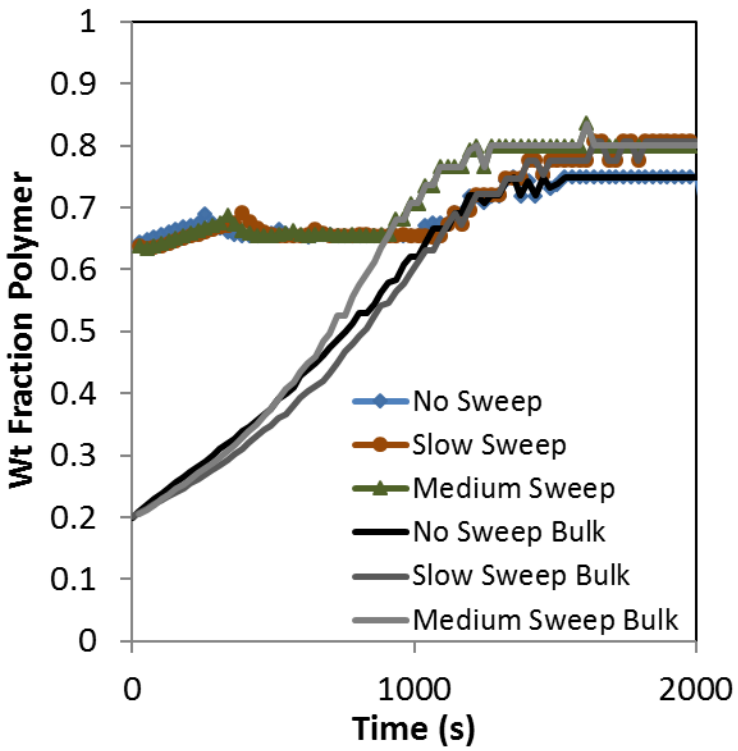

Figure 4-4: Calculated weight fraction of poly(styrene-*b*-butadiene-*b*-styrene) in toluene in ordering layer and bulk film during in-situ SAXS experiments under various drying conditions.

Constant ordering layer concentration occurred in both triblock copolymers. The ordering front concentrations for SBS can be seen in Figure 4-4. The front lasted longer in the slow and no sweep systems than in the medium sweep system (1070s and 1090s vs. 880s), likely due to the faster drying rate. Because of the low diffusivity ($10^{-12} m^2/s$) and the skinning that occurred at the surface of the film, the drying model did not accurately predict the latter stages of drying. It is also possible that the calculated diffusivity at the initial concentration was lower than the actual diffusivity. The concentration of the ordering layer showed a lower concentration than in the bulk of the film, which should not have been possible. Thus, the ordering front was assumed to reach the bottom of the film when this crossover occurred, meaning that the bulk concentration would be assumed to be the average ordering layer concentration at this time. At early times, the shape of the concentration vs. position curve varied little with time, merely broadening, as can be seen in Figure 4-3b. The similar shape of these curves and the skinning that occurred at the top of the film would have contributed to the average concentration of the ordering layer remaining consistent over time.

The concentrations profiles can be seen in Figure 4-5. As in the SBS films, the SIS films exhibit skinning on the surface. However, the drying rates were more rapid and the concentration profiles more narrow with respect to position, in part due to the higher initial diffusivity. The profiles smoothed with respect to concentration much more rapidly

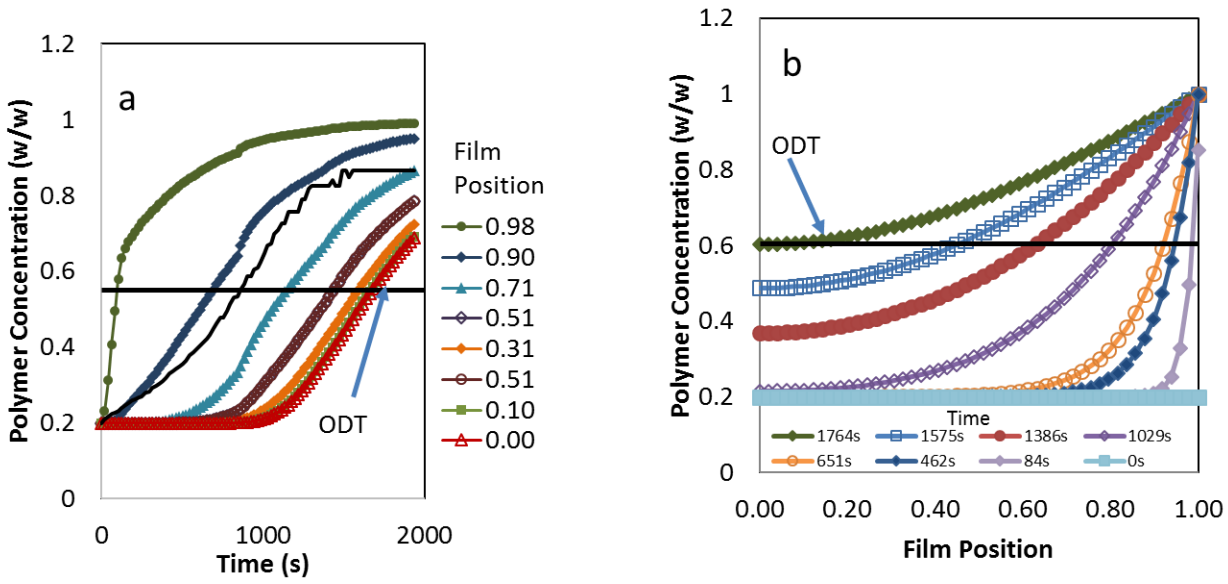

Figure 4-5: a) Calculated polymer concentration as a function of time for different positions in the film from the substrate (0) to film surface (1.0) in a styrene-isoprene-styrene triblock in toluene with no sweep gas. The solid line represents bulk concentration in the film **b)** Polymer concentration as a function of position in the film at different times.

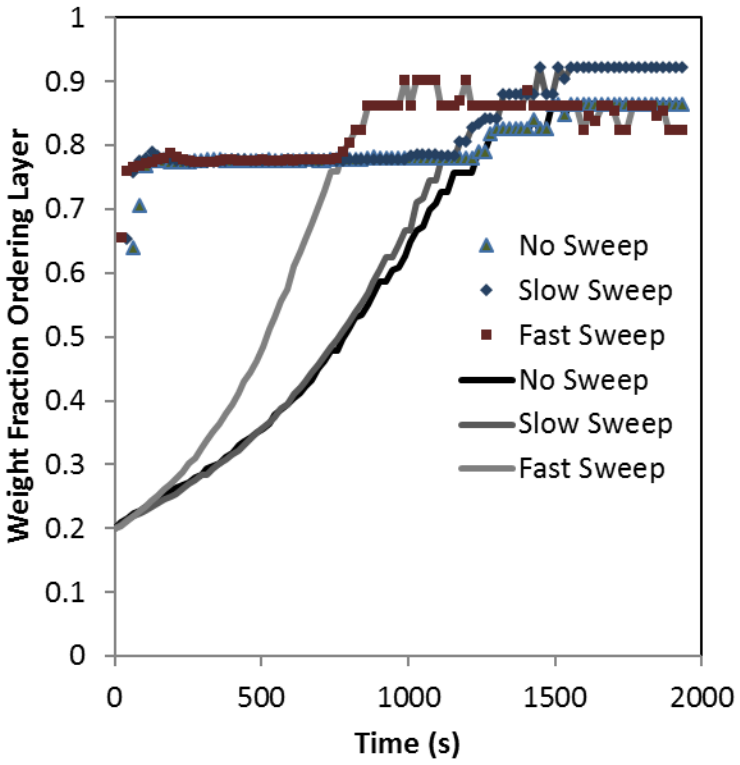

Figure 4-6: Calculated weight fraction of poly(styrene-*b*-isoprene-*b*-styrene) in toluene in ordering layer and bulk film during in-situ SAXS experiments under various drying conditions.

The diffusivity of toluene was also low in the SIS system ($6.5 \pm 0.3 * 10^{-12} m^2/s$), and therefore, the calculated ordering layer concentration was lower than that of the bulk for several minutes during the ordering. Thus, the ordering layer concentration was assumed to equal that of the bulk, once the bulk concentration was reached by the ordering layer.

As in the SBS trials, the ordering layer concentration, shown in Figure 4-6, shows constant concentration in the layer until it reaches the bottom of the film, at which point it has the same concentration as the bulk. Similar to the SBS trials, the skinning and consistent shape of the ordering layer concentration profile promoted constant average concentration in the ordering layer. Once again, the fast sweep gas produced an ordering front that reached the bottom of the film more rapidly than in the slow and no sweep systems (740s vs. 1110s and 1180s). The ordering front reached the substrate in a similar amount of time in the slow and no sweep systems due to the similar drying rates throughout the process.

For the SIS solutions, as seen in Figure 4-7, the difference between the kinetics of the slow and fast sweep systems with respect to time are much more pronounced. The drying curves of the slow and no sweep

systems were quite similar, and thus the two had similar kinetics with much more rapid ordering occurring in the faster sweep system. The difference between the slow and no sweep drying rates does not appear to have been significant enough to produce any change in the kinetics. Thus, for this system, more data are needed to determine the conditions where the system's ordering response would change from being dominated by the quench depth to being dominated by the slowed chain mobility. The half-times for all systems are similar to that calculated by the Avrami model, as shown in Table 4-1. However, the slow sweep system diverges from the Avrami model later in the ordering process.

Table 4-1: Avrami and actual half-times of ordering for cast SIS films in toluene

Sweep Gas Flow Rate	$t_{1/2}$ from start of ordering (min)	Calculated $t_{1/2}$ from Avrami Equation
None	8.25	8.4
0.1 SCFH	10.2	10.6
0.35 SCFH	6.1	6.4

This is surprising, as the Avrami model describes kinetics under iso-concentration and isothermal conditions. Thus, the faster drying system, with more rapidly changing concentration in the film, should show more of a deviation from the model. This did not appear to be the case, and the reasons for this are unknown at this time. It is possible that the fit is coincidental.

The ordered volume with respect to ordering layer concentration is shown below in Figure 4-8. As before, there are two different regions to the curves, with a region before and after the ordering front reaches the substrate. All three trials have the same slope once the bottom of the film has been reached. In addition, the fast and no sweep systems reached the same relative ordered volume before the bottom of the film was reached. This could either be due to the ordering rate being driven by quench depth or due to a different total ordering volume being reached, meaning that there is a different total ordering, ϕ_∞, with respect to concentration, but the relative ordering rate with respect to total ordering, $\phi(t)/\phi_\infty$, is similar. The ordered volume of the slow sweep system reached $\sim 65\%$ of the ordering volume of the other two trials by the time the ordering front reached the bottom of the film. Given the similarities between the drying rates of the slow and fast systems, this is unexpected. It is possible that the total ordered volume of the slow sweep system was different from that of the no sweep trial, meaning that the similar slopes in fraction ordered phase were coincidental. However, the slow sweep film was 10% thicker than that of the other two drying systems. This means that if ordering proceeded at a similar rate to that of the slow system, which must have been the case given that the bulk concentrations were so similar, then

there would have been more total volume to be ordered. This would be especially true near the ordering front, which had high specific and total volumes. With more volume at low concentrations with low segregation power, growth likely would have been slower in the lower portion of the film than in the other two trials. This is also reflected in the ordering with respect to time, as the slow sweep film orders more slowly than the no sweep film when the ordering front reaches the bottom of the film around 500s after ordering begins.

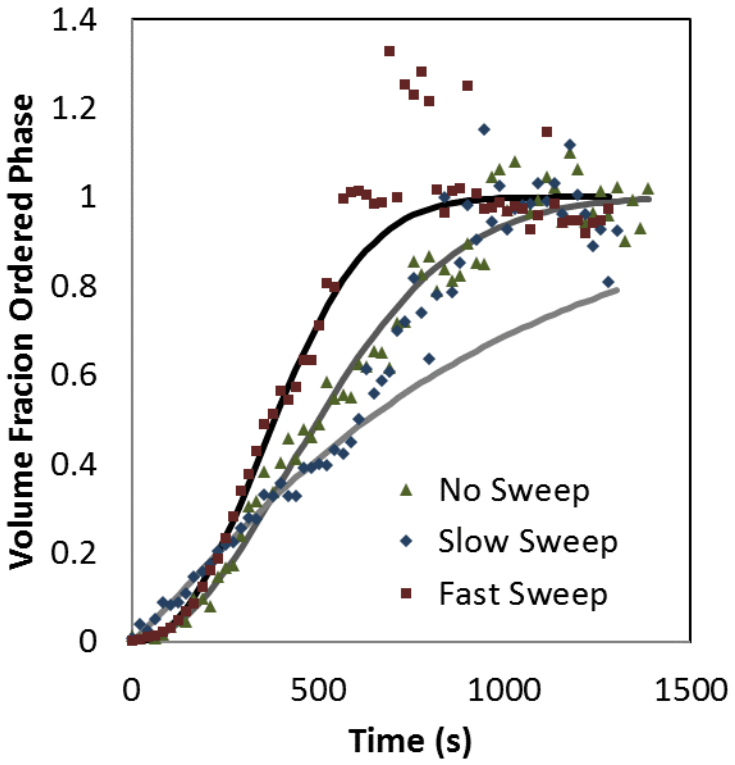

Figure 4-7: Calculated relative ordered volume fraction of SIS in toluene with respect to time from start of ordering. Lines indicate Avrami fit.

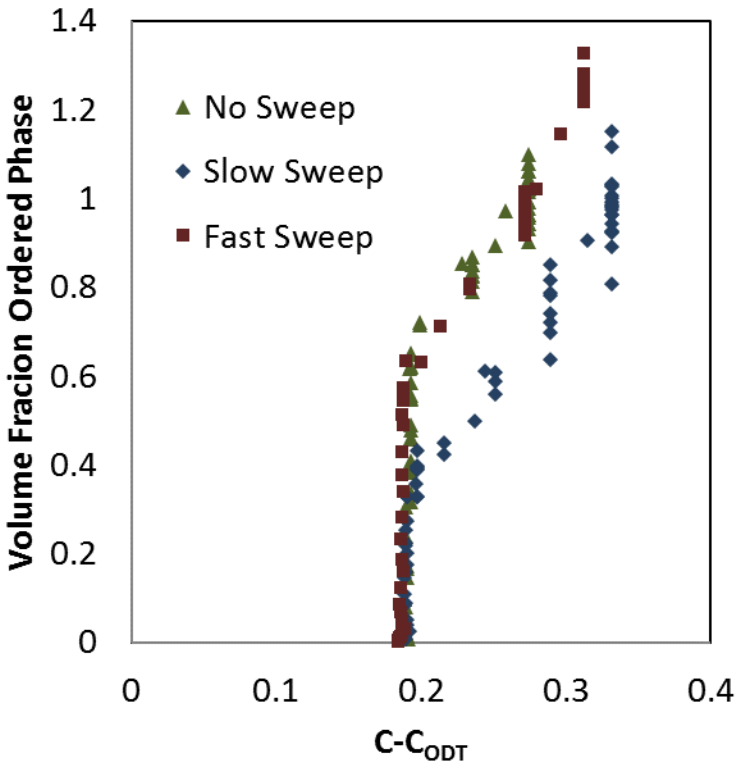

Figure 4-8: Calculated relative ordered volume fraction of SIS in toluene with respect to ordering layer concentration difference from ODT.

In the SBS triblock, the Avrami equation only fits the data for the faster drying conditions, in this case the medium sweep system and slow sweep systems, shown in Figure 4-9, half-times of which are displayed in Table 4-2.

Table 4-2: Avrami and actual half-times of ordering for cast SBS films in toluene

Sweep Gas Flow Rate	$t_{1/2}$ from start of ordering (min)	Calculated $t_{1/2}$ from Avrami Equation
None	5.8	5.5
0.1 SCFH	6.3	6.6
0.2 SCFH	5.5	5.6

The reason for the lack of fit in the no sweep system, with a fit possible in a faster drying system may be that the no sweep system has fast initial drying that slows later. The slow and no sweep systems had similar kinetics at later times, with the no sweep system having similar kinetics to the medium sweep system at early times. This is not surprising given that the no sweep system's drying rate is greater than

that of the slow sweep system until late in the ordering process, and the small difference between the no and medium sweep trials' bulk concentration early in the process.

When compared to the average ordering layer concentration, seen below in Figure 4-10, the slow and the medium sweep films had overlapping data throughout the ordering process. Once again, there was a two-step process to the ordering, with ordering occurring in an ordering layer with more or less constant bulk concentration until the ordering front reached the bottom of the film. However, the no sweep film was able to achieve more complete ordering before the ordering front reached the bottom of the film. This may be due to the ordering initially occurring at a similar rate to that of the medium sweep film and the longer lasting ordering front. Nevertheless, all three trials have overlapping ordered volume with respect to concentration, and all three curves have the same slope during the second phase of ordering, when the ordering layer encompasses the entire film. Here, given that the same extent of ordering exists at the same bulk concentration, and grows with the same rate, this may be due to the ordering rate being driven primarily by quench depth as in the SIS trials, rather than being hindered by a large degree of kinetic entrapment. If difference in chain mobility had been the dominant factor contributing to the rate of growth of ordered phase, then increasing drying rate, which would have reduced chain mobility, would cause a drop in ordering rate with respect to concentration under conditions of faster sweep gas. All trials experienced skinning on the surface of the film. Thus, phase separation would be proceeding largely in the lower sections of the film with greater chain mobility, enabling thermodynamic driving force to play a larger role than chain diffusion.

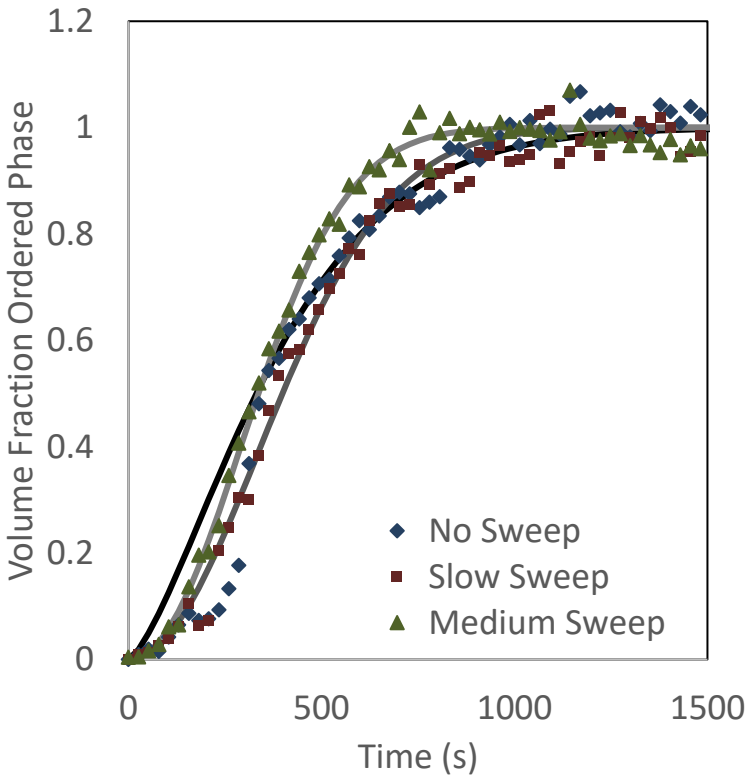

Figure 4-9: Calculated relative ordered volume fraction of SBS in toluene with respect to time from start of ordering. Lines indicate Avrami fit.

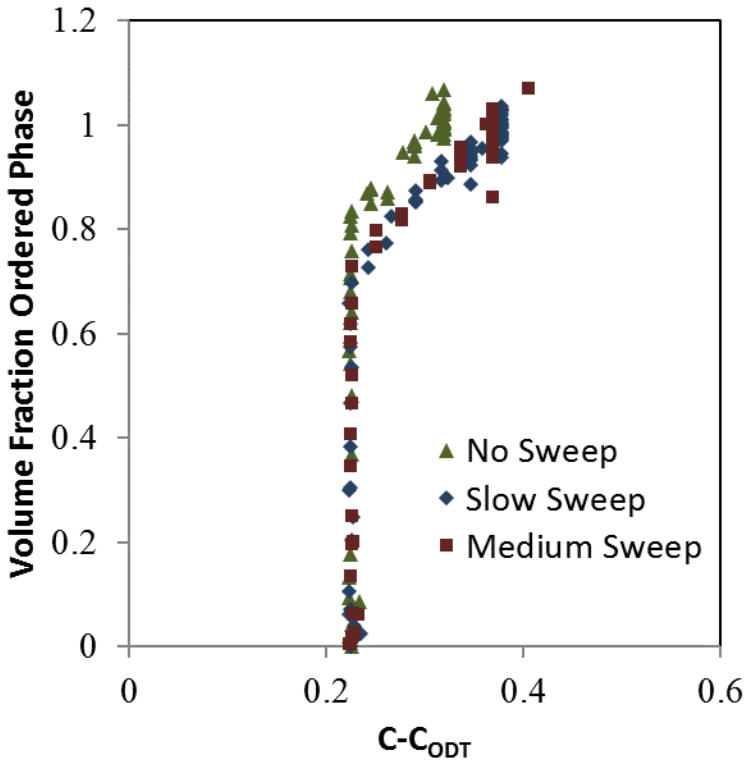

Figure 4-10: Calculated relative ordered volume fraction of SBS in toluene with respect to concentration difference from ODT

4.5 Conclusions

We were able to use a modified Vrentas and Vrentas model[2] along with calculated solvent partitioning parameters to calculate the volume fraction of ordered phase in two triblock copolymers during film drying at different drying rates. The low diffusivity of toluene in both polymers caused skinning on the surface that occurred soon after drying began. As in the case of the diblock copolymers in last chapter, two regions of growth were seen in the volume fraction ordered phase. The slope of the volume fraction ordered phase with respect to concentration was the same regardless of drying rate in both sets once the ordering front reached the bottom of the film. This was attributed to ordering at this stage largely taking place in the bottom of the film where the polymer concentration was lower, enabling the driving force produced by the quench depth to dominate the ordering kinetics.

References

1. *Polymer Handbook, Solubility Parameter Tables*. 4 ed.
2. Vrentas, J. S.; Vrentas, C. M., Drying of solvent-coated polymer films. *Journal of Polymer Science Part B: Polymer Physics* **1994,** *32* (1), 187-194.

5 d-Spacing and Ordered Volume Reduction due to Compression in Thick Solution-cast Acrylate Copolymer Films

5.1 Abstract

Utilizing three different poly(methyl methacrylate-*b*-butyl acrylate-*b*-methyl methacrylate) triblock copolymers of varying PMMA block fractions under solution casting conditions, we observed both a primary peak shift and a peak height reduction in the small-angle X-ray scattering (SAXS) profile in the vertical direction, and a peak height reduction in the horizontal direction. The d-spacing reduced by 20% across all samples. Relative volume fraction ordered phase was calculated, and the ordered volume was seen to reduce by several orders of magnitude in all samples. These effects indicate the presence of compressive forces in the samples during drying, which are disruptive to the ordering and indeed cause the sample to disorder.

5.2 Intro

Block copolymers phase separation has in recent years been explored for use in various applications, such as gas separation membranes[1], and proton exchange membranes (PEMs) for fuel cells[2]. Extent of ordering, orientation of blocks, domain size and processing conditions of these membranes can have an effect on transport properties in PEMs. This makes domain size and ordering extent important variables to study to improve the properties of these membranes.

Recently, Heinzer, et al.[3] studied the compression of domains the occurs during the film drying process, and found a significant directionality of domain spacing. That is, it was found that the spacing was reduced in the vertical direction due to compression in the film as the sample dried.

The application of shear forces on ordering systems changes the ultimate morphology. For example, Wang, et al.[4] found that the application of shear forces on ordering block copolymer micelles can lead to either formation of vesicles or cylinders due to clustering of individual micelles, or can break up large cylinders to form spheres depending on the amount of shear stress and the equilibrium state. In addition, Tomita, et al.[5] utilized compressional flow to produce an order-order transition from spherical to cylindrical morphology and subsequently orient the cylinders in a single direction upon annealing.

5.3 Materials

Three separate poly(methyl methacrylate-*b*-butyl acrylate-*b*-methyl methacrylate) (PMMA/PBA/PMMA) triblock copolymers were used as received from Kuraray®. These had PMMA fractions of f = 0.2, 0.33, and 0.51 with M_n values of 66.8, 64.0, and 59.2kDa respectively, henceforth referred to as PMMA/PBA-20, PMMA/PBA-33, and PMMA/PBA-51. M_w/M_n values were 1.12, 1.03, and 1.10 respectively. The polymers were dissolved in toluene via sonication to produce 20 wt% solutions. A Bruker N8 Horizon was used to determine C_{ODT} for the polymers. This was done using iso-concentration samples in air. These samples were allowed to equilibrate for at least 24 hours before being sealed in a polyimide pouch and exposed for 10 minutes, after which, the profiles were checked for a primary peak to determine whether ordering is present.

We performed in-situ SAXS experiments during on solution casting on Beamline 1-4 at Stanford Synchrotron Radiation Laboratory (SSRL). The samples were cast onto a silicon wafer with a doctor blade set to 400μm and placed on a balance in a drying chamber as described previously in Chapter 3. The beam was transmitted through the sample and scattering profiles were collected with a Rayonix165 CCD detector.

5.4 Methods

The in-situ SAXS experimental and data analysis methods were presented in detail in Chapter 3, and the experimental methods were similar to those used by Heinzer, et al.[6] A drying model was used to model the average concentration of the ordering layer, or the layer in the film where concentration is at or above the ODT and ordering can proceed. The ordering layer solvent concentration was used to determine the concentration of solvent in each phase (i.e. PMMA, PBA) using the Flory-Huggins solution model to determine the solvent activity in each block. The equilibrium solvent concentration in each block was determined by minimizing the difference in the calculated solvent activities. Scattering profiles taken during solution casting were numerically integrated to determine the scattering power, and then corrected for total ordered phase volume and relative volume of the two blocks in the ordered phase.

5.5 Results and Discussion

5.5.1 Drying and Initial Morphology

Diffusivities of toluene in the polymer solutions were calculated for each of the polymers using sorption experiments, as mentioned previously in Chapter 4, and it was found that the polymers had diffusivities of $9.1 \pm 0.6 * 10^{-11} m^2/s$, $3.2 \pm 0.7 * 10^{-12} m^2/s$, and $2.4 \pm 0.8 * 10^{-11} m^2/s$ for PMMA/PBA-20, 33, and 51 respectively. A plot of weight fraction over time during the *in-situ* trials can be seen in Figure 5-1.

Here, PMMA/PBA-20 had a faster drying time than either PMMA/PBA-33 or PMMA/PBA-51. The apparent faster drying rate was likely caused by the higher solvent diffusivity in PMMA/PBA-20, and the lower initial film thickness in the film compared to the other two ($290\mu m$ for PMMA/PBA-20 compared to $360\mu m$ and $390\mu m$ for PMMA/PBA-33 and 51 respectively).

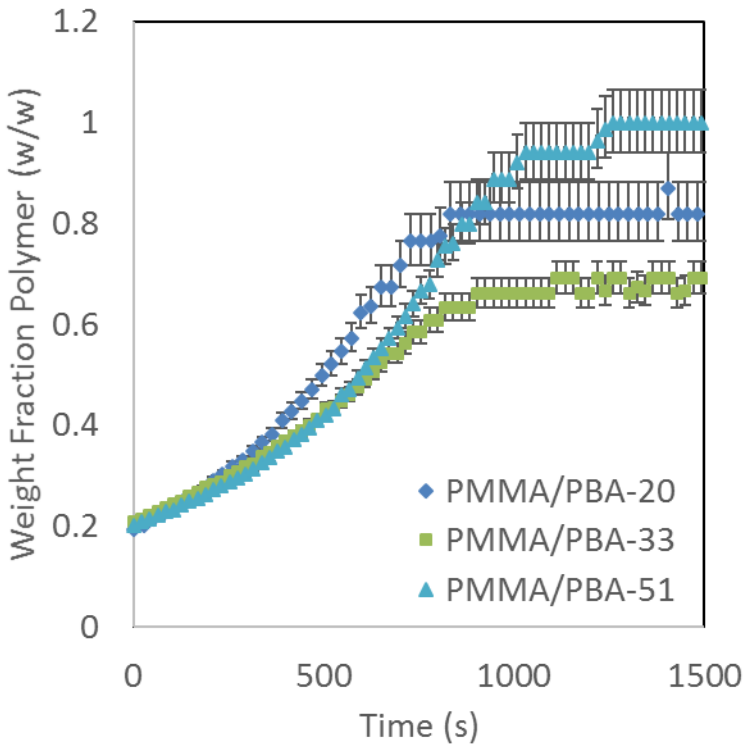

Figure 5-1: Calculated weight fraction of poly(methyl methacrylate-b-butyl acrylate) in toluene during in-situ SAXS experiments

The polymer was dried in the in-situ SAXS drying rig at room temperature to determine the final morphology of the samples. The samples were then allowed to dry completely for 24hrs before being imaged using atomic force microscopy (AFM). AFM images of the film surfaces are shown in in Figure 5-2.

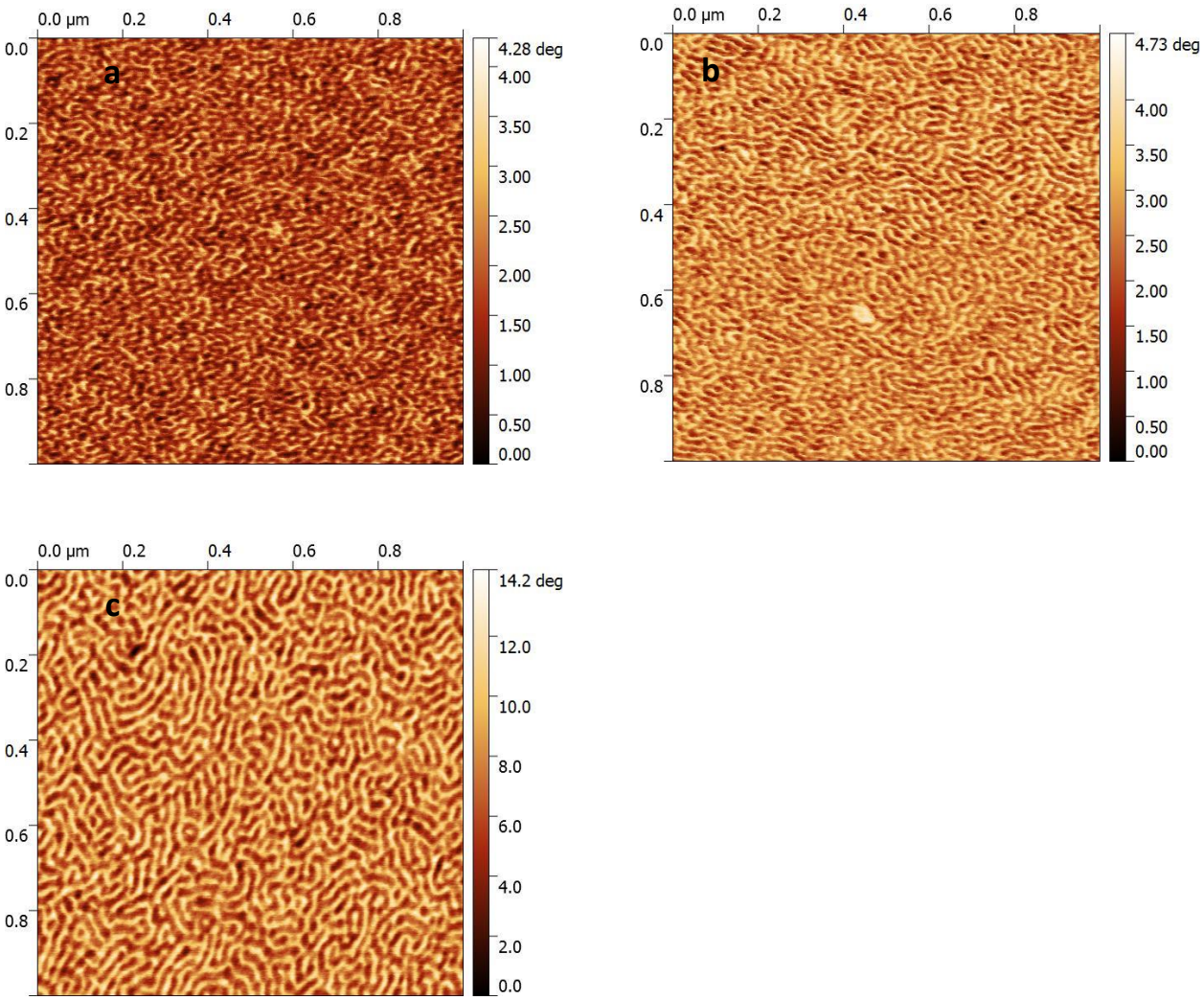

Figure 5-2*:* AFM images of a) PMMA/PBA-20, b) PMMA/PBA-33, and c) PMMA/PBA-51 taken after solution-casting and drying

PMMA/PBA-20 exhibits a cylindrical (C) morphology, while PMMA/PBA-51 appears lamellar (L) at the surface. The morphology of PMMA/PBA-33 appears to have either a lamellar or short cylindrical structure at the surface (SC).

5.5.2 SAXS Results

Integration occurred over various angle ranges to determine directionality of compression and ordering. A schematic of these ranges can be seen below. These ranges were used because most images were elliptical in shape.

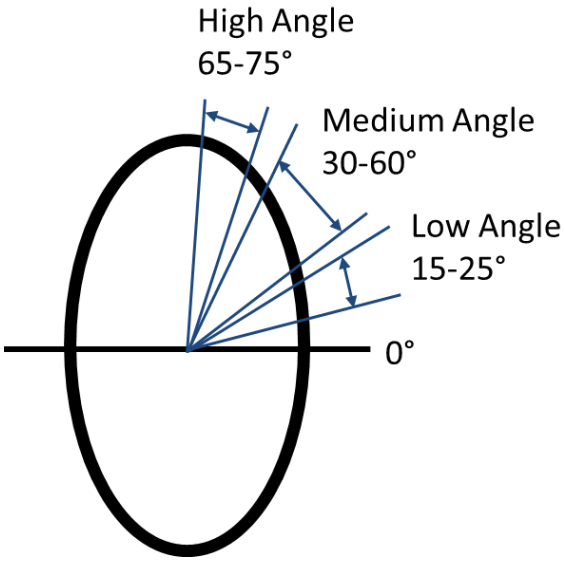

Figure 5-3: Schematic of arcs used for integration of images.

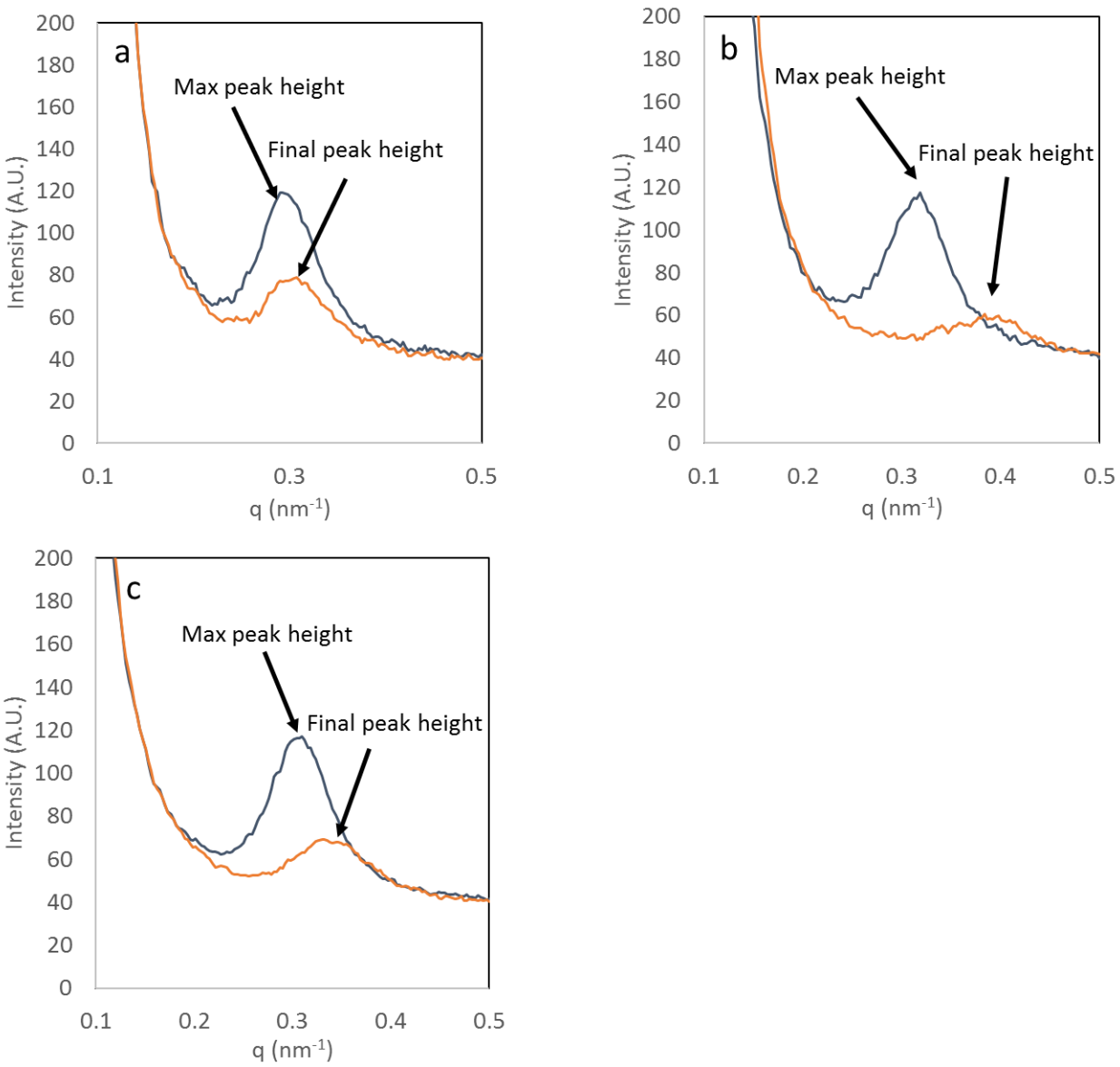

Figure 5-4: SAXS image data for PMMA/PBA-20 integrated over different angle ranges measured from the horizontal a) 15-25deg b) 65-75deg c) 30-60deg

The SAXS patterns taken during film drying were integrated over low, medium and high angular ranges to determine the extent of anisotropy development during the drying process. Low angles are defined as being 15-25 degrees from the horizontal, medium angles are defined as being 30-60 degrees from the horizontal, and high angles are defined as being 65-75 degrees from the horizontal. For all three samples, the peak location shifted by a larger amount at high angles than at low angles. After the initial period of growth, the peak height decreased significantly over time. The peak shifts were smooth and did not

appear to be the result of order-order transitions, which would have caused a second primary peak to grow in as the initial primary peak shrank. This is similar to the result seen by Heinzer, et al., where peaks produced by block copolymer ordering during film drying were observed to shift to higher scattering angle, q, values when integrated at high angles.[3] However, unlike the results obtained by Heinzer, et al., the primary peaks in this instance were seen to shrink. There was no corresponding reduction in background scattering, indicating that the beam intensity remained constant. The overall peak shifts are recorded in Table 5-1.

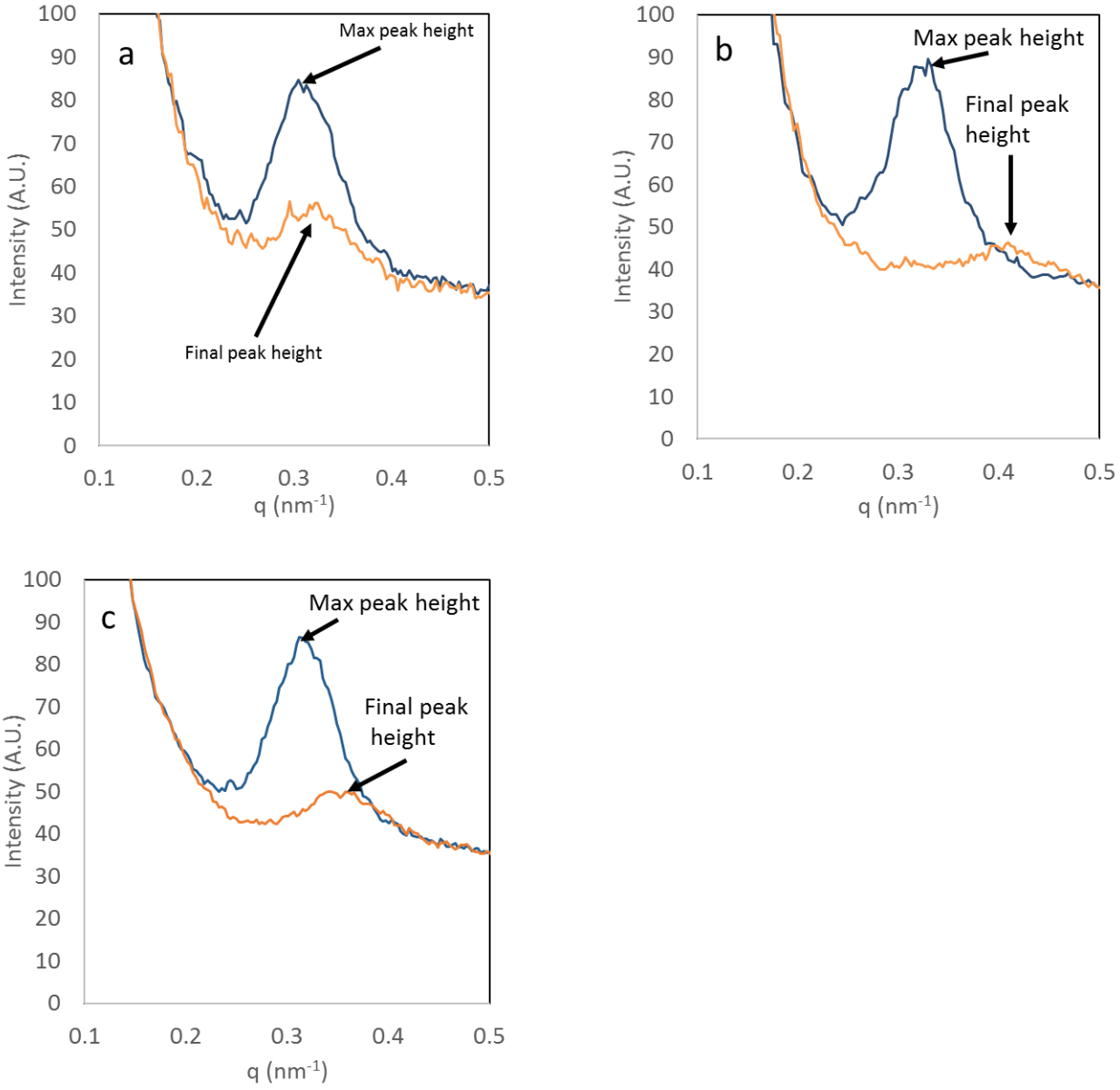

Figure 5-5: SAXS image data for PMMA/PBA-33 integrated over different angle ranges measured from the horizontal a) 15-25deg b) 65-75deg c) 30-60deg

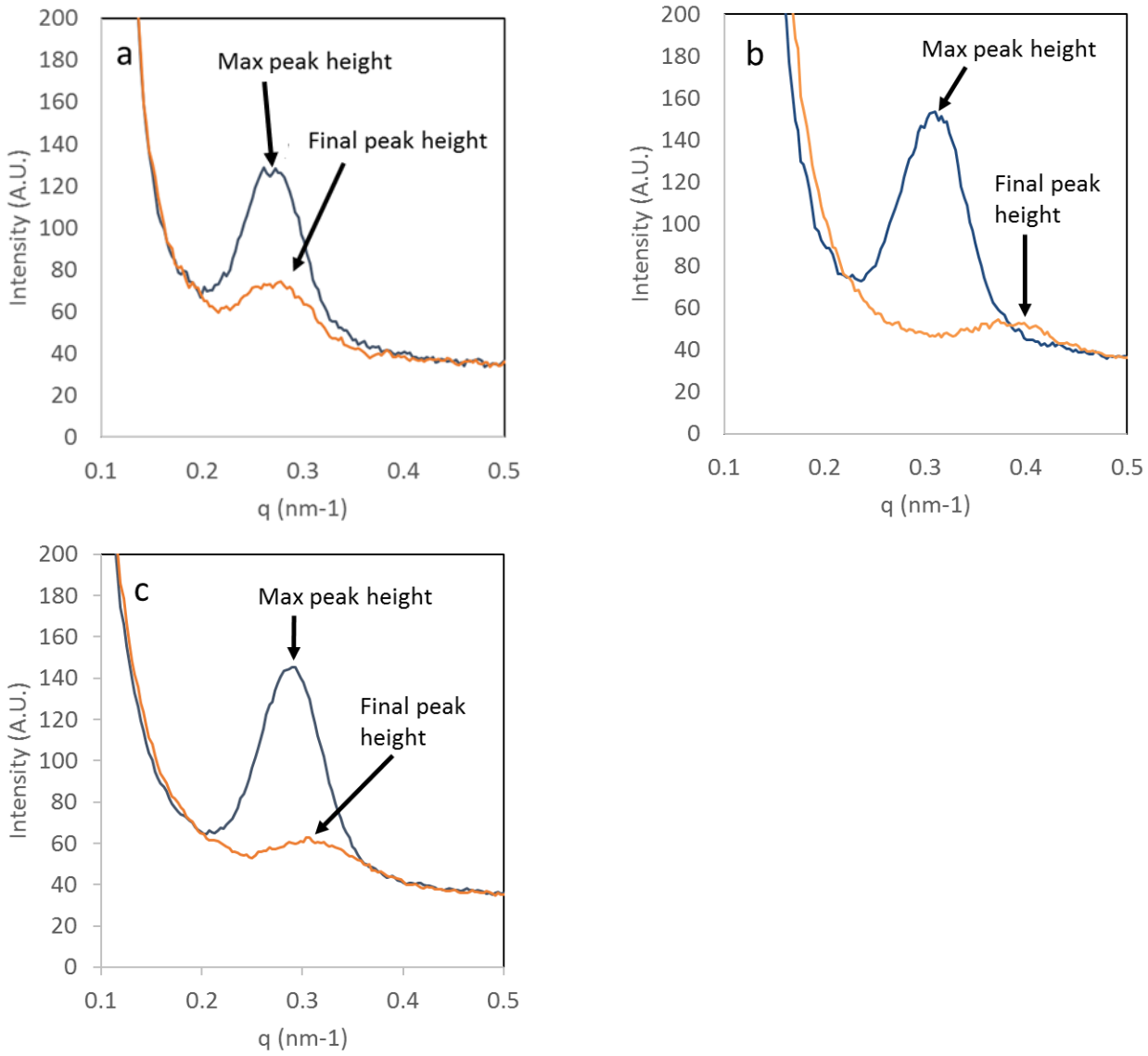

Figure 5-6: SAXS image data for PMMA/PBA-51 integrated over different angle ranges measured from the horizontal a) 15-25deg b) 65-75deg c) 30-60deg

5.5.3 d-Spacing Shift

Table 5-1: Shift in q and d-spacing over the course of the three drying trials at both low and high angles

	$15-25°$		$65-75°$	
	q Shift	d-Spacing Shift	q Shift	d-Spacing Shift
PMMA/PBA-20 (C)	$0.04 \pm 0.01 nm^{-1}$	$-2.9 \pm 0.9 nm$	$0.092 \pm 0.003 nm^{-1}$	$-4.9 \pm 0.2 nm$
PMMA/PBA-33 (SC)	$0.013 \pm 0.005 nm^{-1}$	$-0.9 \pm 0.3 nm$	$0.090 \pm 0.005 nm^{-1}$	$-4.4 \pm 0.3 nm$
PMMA/PBA-51 (L)	$0.004 \pm 0.003 nm^{-1}$	$-0.3 \pm 0.3 nm$	$0.083 \pm 0.005 nm^{-1}$	$-5.1 \pm 0.3 nm$

At high angles, the d-spacing shift was consistent over all three sample sets. The spacing shifted by $4.5 - 5 nm$ over the course of the experiments, after starting at a spacing of $20 nm$, $20 nm$, and $24 nm$ for

PMMA/PBA-20, PMMA/PBA-33, and PMMA/PBA-51 respectively. The horizontal shift observed in PMMA/PBA-20 was significantly greater than that of PMMA/PBA-33 and PMMA/PBA-51. However, the shift observed was still lower than that at high angles. It is possible that the low angle d-spacing shifts were due to deswelling in the nanodomains as solvent was removed. All three samples experienced a significant decrease in the peak height with respect to time at all three sample angle ranges. This greater shift at higher angles appears to indicate a size reduction in the individual nanodomains in the vertical direction, and to a much lesser extent the horizontal direction occurring in all three different block fractions. This is likely due to the compressive forces in the sample as it dries, as the change would be independent of direction if it were the result of deswelling because the sample is pinned to the substrate and cannot compress in the horizontal direction. The correspondence between peak shifts at high and low angles is clearly demonstrated when plotted with respect to total film thickness (Figure 5-7.)

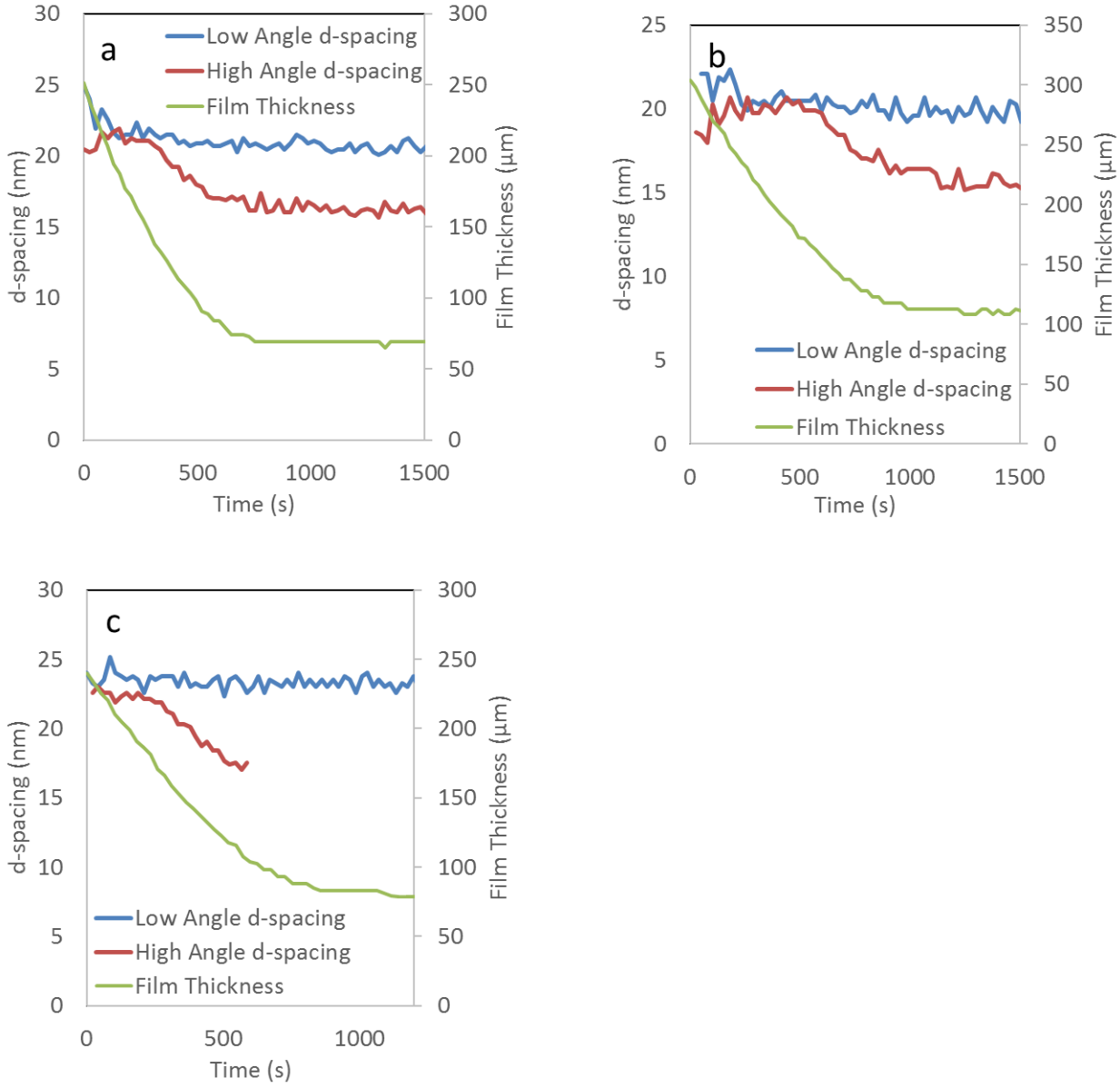

Figure 5-7: Calculated d-spacing at low and high angles along with film thickness after the start of ordering for all three block fractions a) PMMA/PBA-20 b) PMMA/PBA-33 c) PMMA/PBA-51. The d-spacing for PMMA/PBA-51 does not extend beyond 600s and high angles because the broadness of the peaks at these angles prevented the calculation of peak boundaries

After the initiation of ordering during drying, the sample thickness decreases significantly, and divergence between the vertical and horizontal d-spacing occurs. The vertical d-spacing does not change significantly once the final thickness of the sample has been reached, due to either confinement caused by increased modulus preventing further change or cessation of compression. There is a delay in the initiation of the

d-spacing decrease that likely occurs due to a lack of compressive force or to polymer concentrations that are low enough to allow chain reorganization up until this point.

The volume of ordered phase was calculated relative to the final average calculated ordered volume in each trial. In order to account for the solvent partitioning between phases and deswelling, the SAXS data were analyzed according to methods previously described in Chapter 4. and dividing by the total ordered phase volume (i.e. ordered phase thickness) to normalize the data. To summarize, a drying model was used to determine the average polymer concentration in the upper part of the film undergoing ordering, that is, the part of the film whose polymer concentration was above the order-disorder transition. This concentration was used to determine the solvent partitioning between the phases to find the electron density and the volume of each phase to determine the volume of ordered phase. The data were then normalized to the maximum average volume for both high and low angle ranges.

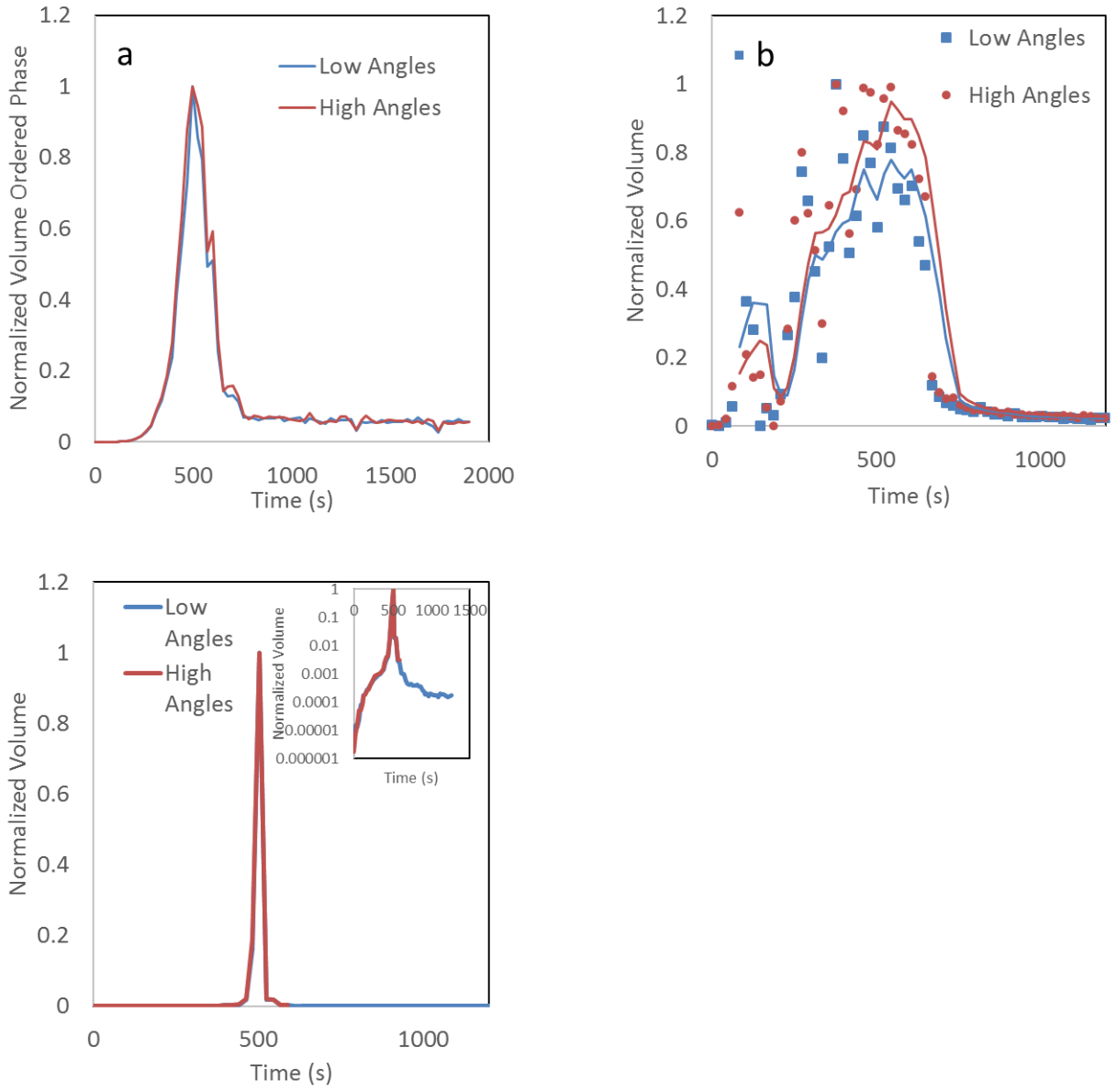

Figure 5-8: Calculated volume ordered phase relative to final volume at low and high angles a) PMMA/PBA-20 b) PMMA/PBA-33 (average indicated by lines) and c) PMMA/PBA-51

The volumes obtained in both the horizontal and vertical directions are consistent with each other, indicating that the resulting drop in total ordered volume occurs in both directions. This must therefore be an isotropic effect in the sample. Due to the inconsistency of the data at the tail end of the high angles of PMMA/PBA-51, the datasets of PMMA/PBA-51 were normalized to the peak rather than the final values

for volume. PMMA/PBA-51 experienced a large drop in volume of four orders of magnitude, rather than two orders as in the other two samples. It is unclear whether this is a real effect or the result of the system reaching the limits of the drying model. Nevertheless, all three samples show a large drop in ordering regardless of direction. Given that there are compressive forces in the sample, it is likely that these forces are causing the ordered structure to disorder. The effect of this is the significant reduction in ordering as the thickness is further reduced. This may be caused by deformation of the nanostructures themselves. This deformation would result in an increase in the interfacial curvature in some areas and a decrease in others, increasing interfacial tension and disrupting the interface. This may lead to the dissolution of a portion of the microstructure.

5.6 Conclusions

Ordering of acrylate copolymers with three different block fractions of PMMA were examined under solution casting conditions. A three-phase process is observed under solution casting conditions that occurs after initiation of drying which includes: initiation of ordering, initiation of domain compression, and termination of domain compression as the thickness no longer decreases. It was determined that no order-order transition was occurring, and that the nanodomains were growing and then dissociating as the film further dried. Compression was seen to only occur in the vertical direction, indicating that this was not due to deswelling of the domains. This compression resulted in an isotropic two-order of magnitude decrease in the volume fraction of ordered phase during drying, as the stress would have disrupted the ordered microstructure.

References

1. Buonomenna, M. G.; Yave, W.; Golemme, G., Some approaches for high performance polymer based membranes for gas separation: block copolymers, carbon molecular sieves and mixed matrix membranes. *RSC Advances* **2012,** *2* (29), 10745-10773.
2. Lee, M.; Park, J. K.; Lee, H.-S.; Lane, O.; Moore, R. B.; McGrath, J. E.; Baird, D. G., Effects of block length and solution-casting conditions on the final morphology and properties of disulfonated poly(arylene ether sulfone) multiblock copolymer films for proton exchange membranes. *Polymer* **2009,** *50* (25), 6129-6138.
3. Heinzer, M. J.; Han, S.; Pople, J. A.; Baird, D. G.; Martin, S. M., In Situ Tracking of Microstructure Spacing and Ordered Domain Compression during the Drying of Solution-Cast Block Copolymer Films Using Small-Angle X-ray Scattering. *Macromolecules* **2012,** *45* (8), 3480-3486.
4. Wang, C.-W.; Sinton, D.; Moffitt, M. G., Morphological Control via Chemical and Shear Forces in Block Copolymer Self-Assembly in the Lab-on-Chip. *ACS Nano* **2013,** *7* (2), 1424-1436.
5. Tomita, S.; Urakawa, H.; Wataoka, I.; Sasaki, S.; Sakurai, S., Complete and comprehensive orientation of cylindrical microdomains in a block copolymer sheet. *Polym J* **2016,** *48* (12), 1123-1131.
6. Heinzer, M. J.; Han, S.; Pople, J. A.; Baird, D. G.; Martin, S. M., In Situ Measurement of Block Copolymer Ordering Kinetics during the Drying of Solution-Cast Films Using Small-Angle X-ray Scattering. *Macromolecules* **2012,** *45* (8), 3471-3479.
7. Helfand, E.; Wasserman, Z. R., Block Copolymer Theory. 4. Narrow Interphase Approximation. *Macromolecules* **1976,** *9* (6), 879-888.

6 Ordering Kinetics with Respect to Concentration in Styrene-Diene Copolymers

6.1 Introduction

The Avrami model[1,2,3] is often used to characterize the growth of microstructure in block copolymers[4,5,6,7,8] based on the nucleation and growth mechanism proposed by Frederickson and Binder:[9,10]

$$\frac{\phi(t)}{\phi_\infty} = 1 - \exp(-kt^n) \tag{6-1}$$

Here, ϕ is the volume fraction of ordered phase at time t, ϕ_∞ is the total volume fraction of ordered phase, k is a rate constant, and n is the Avrami constant. The half-time of ordering can then be calculated from the Avrami parameters:

$$t_{1/2} = \left(\frac{\ln 2}{k}\right)^{\frac{1}{n}} \tag{6-2}$$

Spring and Bansil[4a] developed a method based on work by Farjas and Roura[11,12] to scale the kinetic data of block copolymers undergoing order-order transitions to a master Avrami curve during temperature ramp experiments.

Liu, et al.[13] performed several kinetic studies with respect to temperature at different concentrations of polymer. At all of these concentrations at large quenches, the half-times were related to temperature according to the relationship predicted by Frederickson and Binder: $\ln(t_{1/2}) \sim (T_{ODT} - T)^{-2}$, with $t_{1/2}$ being the half-time of ordering, T_{ODT} being the order-disorder transition temperature, and T being the temperature of the polymer solution. For small quenches, the half-time was shown to vary with temperature by $\ln t_{1/2} \sim (T_{ODT} - T)$, which was determined to be the result of nucleation or thermodynamic effects dominating for small quenches, and diffusion or kinetic effects dominating for large quenches.

As an increase in solvent concentration will also improve chain mobility and affect the T_{ODT}[14], Heinzer, et al.[15] studied the effect that concentration had on the ordering kinetics during film drying and found a U-shaped curve of half-time vs. solvent concentration similar to that found by Liu, et al for half-time vs. temperature[13]. However, these samples were taken at various times during the drying process, and the samples were thus not homogeneous.

6.2 Materials and Methods

The triblock copolymer SIS used was the same as that described in Chapter 4, section 2. The C_{ODT} was found to be 59wt% polymer via SAXS at room temperature. 20wt% solutions of SIS in toluene were prepared in 20mL vials and allowed to dry slowly over the course of several weeks to each desired concentration. These solutions were then sealed with PTFE tape and placed in an oil bath at varying temperatures. The SIS solutions were placed in a bath heated by a 300°C element for two hours to induce disordering. The bath was only run for a short time to prevent decomposition. A N_2 sweep gas was run perpendicular to the top of the vial to prevent softening of the cap. Because of the sweep gas and the fact that the bath was in room temperature air, the oil would remain at a temperature lower than 300°C. The final surface temperature of the bath was found to be $190 \pm 5°C$, via infrared thermometer.

The vials were then quenched in a room temperature water bath. A sample of the polymer solution was removed and sandwiched in 2mil Kapton® film and sealed with tape. The sample was then placed in a Bruker® N8 Horizon SAXS instrument in an air atmosphere, and SAXS patterns were obtained every X minutes for X minutes (hours.) SAXS patterns were obtained using a wavelength of λ = 1.54185 Å. The time from the beginning of the quench to the initiation of SAXS data acquisition was 3 minutes.

The invariants of the resulting scattering patterns were estimated by integrating the primary peak as described in Chapter 4, section 3. The volumes of each block did not need to be estimated because there was no change in concentration over the course of the experiment, and the relative volumes of ordered phase were determined from the invariant directly. The Avrami model was fit to the data to determine the half-times of ordering.

6.2.1 Results and Discussion

6.2.1.1 Model

In order to compare the half-times to each other and further understand their relation, the concentration of polymer needs to be taken into account. To find the Avrami model as applied to concentration during various processes in which concentration changes, the half-time and its derivative with respect to concentration can be used to determine the different constants, as shown below in Equations (6-3 and (6-4.

$$\ln t_{1/2} = \frac{1}{n}\ln(ln\,2) - \frac{1}{n}\ln k \qquad (6\text{-}3)$$

$$\frac{d \ln t_{1/2}}{dc} = \left(\frac{\ln k - \ln(\ln 2)}{n^2}\right)\frac{dn}{dc} - \left(\frac{1}{nk}\right)\frac{dk}{dc} \tag{6-4}$$

Here, c is polymer concentration in solution.

6.2.1.2 Results

Integrated SAXS profiles for a 63.1 wt% sample of SIS in toluene are shown in Figure 6-1a, following the initial quench and after ordering is complete. It is clear that heating the samples above the ODT does not fully disorder the SIS systems. In addition, none of the systems had clear secondary peaks. The partial disordering, and the 3 minute delay in data acquisition following the initial quench meant that the early stages of ordered phase nucleation and growth could not be observed. However, given that the concentration and temperature were constant throughout the experiment, and the parameters k and n are assumed to be constant, Avrami curves could be fitted to the data at longer times. In order to fit curves for the ordering process already underway, the Avrami equation had to be modified:

$$\frac{\phi(t)}{\phi_\infty} = 1 - \exp(k(t + t_0)^n) \tag{6-5}$$

where t_0, a fitted parameter, is the theoretical time for the nucleation and growth process to reach the initial state of the SAXS experiment if the system was completely disordered prior to quenching.

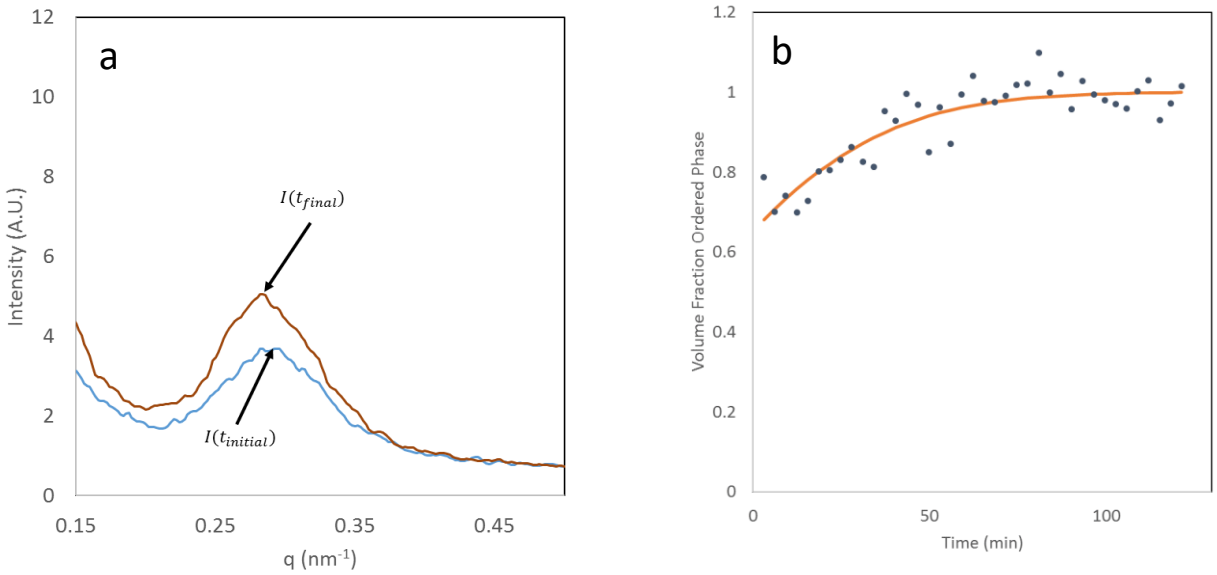

Figure 6-1: a) Scattering profiles from samples of 63.1 wt% SIS in toluene at initial and final times b) Fitted Avrami curve to normalized volume fractions calculated from the area under the Iq^2 peak

The half-times calculated using the Avrami fits are given in Table 6-1, and plotted in Figure 6-2. The half-

times given are those starting from $t = -t_0$, as none of the curves were fit to data with an ordered volume fraction of less than 0.7.

Table 6-1: Avrami parameters calculated for SIS solutions in toluene phase growth after quenches

wt%	d (nm)	t_0 (min)	n	$t_{1/2}$ (min)
61.3%	23	120	1.60	77
63.1%	21	80	2.03	65
67.7%	22	85	1.88	31
69.2%	23	190	2.75	131
69.3%	25	100	1.77	58
70.0%	24	210	2.71	151
76.4%	24	150	2.14	94
80.7%	23	230	2.01	128

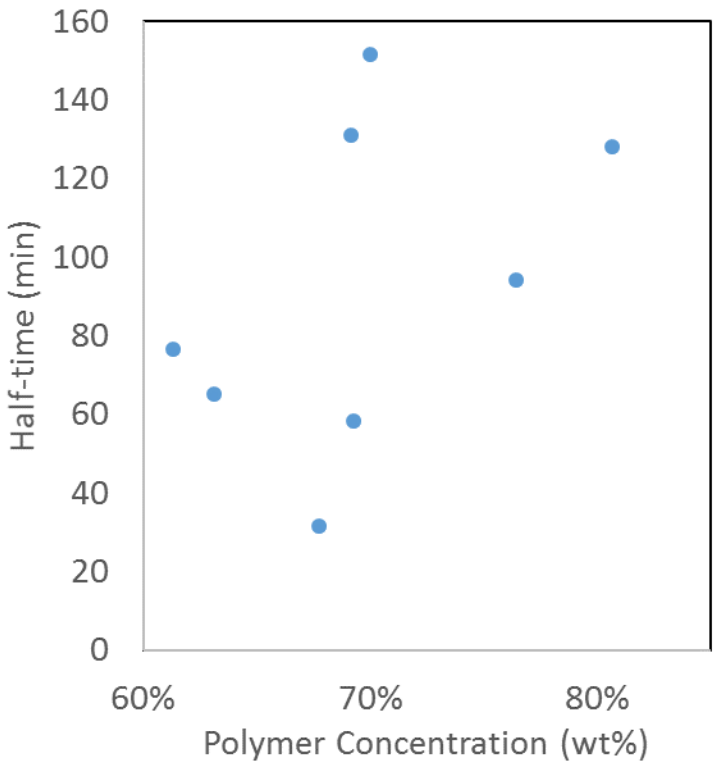

Figure 6-2: Calculated half-times from temperature quenches of SIS solution in toluene

Outside of two of the values near 69wt% polymer, the plot has a consistent U-shaped curve of half-time with respect to concentration. In addition, all of the values of n in this set are similar to one another, averaging 1.90 ± 0.08. The shape of the curve is influenced by a combination of two distinct factors. At a smaller degrees of undercooling, the distance from the C_{ODT} produces greater driving force for ordering, increasing the ordering rate and producing a lower half-time. At large degrees of undercooling, chain mobility is further reduced and becomes a larger factor in the rate of ordering. As in the case of the temperature dependence of half-time, the reduced mobility causes a slowed ordering rate at greater quench depths.

The fits of $t_{1/2}$ vs. c for each half of the V-curve, assuming $n = 1.9$, are shown below.

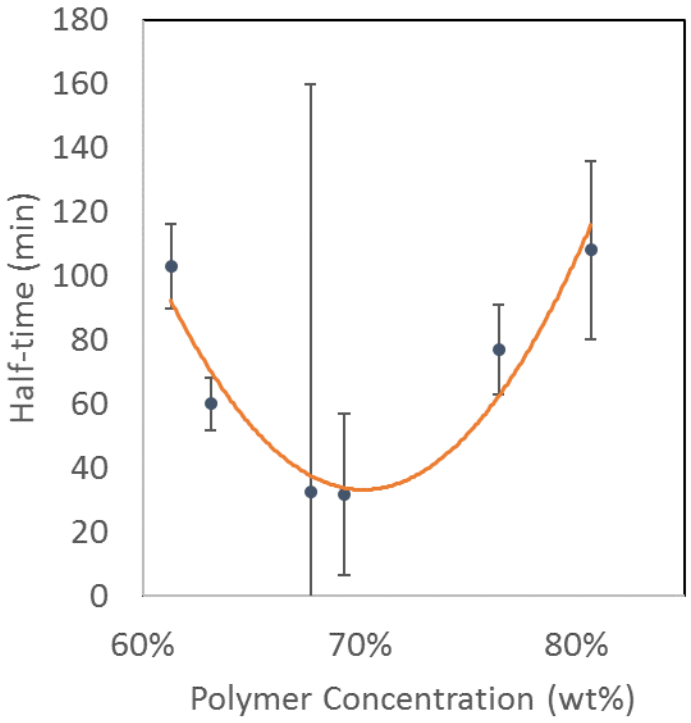

Figure 6-3: Curve fits of half-time vs concentration for temperature quenches of SIS triblock in toluene

Unlike the half-time vs. temperature relationship seen by Liu, et al,[13] the relationship between half-time and concentration does not appear to be exponential. Rather, the relationship appears to be a second order polynomial at concentrations giving

$$t_{1/2} = ac^2 + bc + d \tag{6-6}$$

With a, b, and d being fitted parameters. Since n is unaffected by concentration in this case, k becomes

$$k = \frac{\ln 2}{(ac^2 + bc + d)^n} \tag{6-7}$$

Thus, a final relationship between $\phi(t)/\phi_\infty$ and c for this polymer/solvent system, would be

$$\frac{\phi(t)}{\phi_\infty} = 1 - \exp\left(\frac{t^n \, ln\, 2}{(ac^2 + bc + d)^n}\right) \tag{6-8}$$

6.3 Conclusions

Kinetics of self-assembly of poly(styrene-*b*-isoprene-*b*-styrene) triblock copolymers in solution were studied by means of small-angle X-ray scattering using temperature quenches at differing weight fractions of polymer, ranging from 60-80wt%. After performing temperature quenches of iso-concentration solutions, Avrami curves were able to be fit to the resulting ordered volumes calculated from the SAXS results. The half-times were found to follow a U-shaped curve with a quadratic relationship with concentration, resulting from competition between thermodynamic and kinetic effects in the system. There was little change in the Avrami exponent across all polymer concentrations, thus a modified Avrami model was derived by determining the concentration dependence of the rate constant.

References

1. Avrami, M., Kinetics of Phase Change. I General Theory. *The Journal of Chemical Physics* **1939,** *7* (12), 1103-1112.
2. Avrami, M., Kinetics of Phase Change. II Transformation‐Time Relations for Random Distribution of Nuclei. *The Journal of Chemical Physics* **1940,** *8* (2), 212-224.
3. Avrami, M., Granulation, Phase Change, and Microstructure Kinetics of Phase Change. III. *The Journal of Chemical Physics* **1941,** *9* (2), 177-184.
4. (a) Spring, J. D.; Bansil, R., A Universal Scaling Analysis of Nonisothermal Kinetics in Block Copolymer Phase Transitions. *ACS Macro Letters* **2013,** *2* (8), 745-748; (b) Floudas, G.; Hadjichristidis, N.; Iatrou, H.; Pakula, T.; Fischer, E. W., Microphase Separation in Model 3-MiktoarmStar Copolymers (Simple Graft and Terpolymers). 1. Statics and Kinetics. *Macromolecules* **1994,** *27* (26), 7735-7746.
5. Liu, Y.; Nie, H.; Bansil, R.; Steinhart, M.; Bang, J.; Lodge, T. P., Kinetics of disorder-to-fcc phase transition via an intermediate bcc state. *Physical Review E* **2006,** *73* (6), 061803.
6. Chastek, T. Q.; Lodge, T. P., Grain Shapes and Growth Kinetics of the Cylinder Phase in a Block Copolymer Solution. *Macromolecules* **2004,** *37* (13), 4891-4899.
7. Chastek, T. Q.; Lodge, T. P., Twinning and growth kinetics of lamellar grains in a diblock copolymer solution. *Journal of Polymer Science Part B: Polymer Physics* **2005,** *43* (4), 405-412.
8. Chastek, T. Q.; Lodge, T. P., Grain shapes and growth kinetics during self-assembly of block copolymers. *Journal of Polymer Science Part B: Polymer Physics* **2006,** *44* (3), 481-491.
9. Fredrickson, G. H.; Binder, K., Kinetics of metastable states in block copolymer melts. *The Journal of Chemical Physics* **1989,** *91* (11), 7265-7275.
10. Binder, K., Nucleation phenomena in polymeric systems. *Physica A: Statistical Mechanics and its Applications* **1995,** *213* (1–2), 118-129.
11. Farjas, J.; Roura, P., Modification of the Kolmogorov–Johnson–Mehl–Avrami rate equation for non-isothermal experiments and its analytical solution. *Acta Materialia* **2006,** *54* (20), 5573-5579.
12. Farjas, J.; Roura, P., Solid-phase crystallization under continuous heating: Kinetic and microstructure scaling laws. *Journal of Materials Research* **2008,** *23* (02), 418-426.
13. Liu, Z.; Shaw, M.; Hsiao, B. S., Ordering Kinetics of the BCC Morphology in Diblock Copolymer Solutions over a Wide Temperature Range. *Macromolecules* **2004,** *37* (26), 9880-9888.
14. Lodge, T. P.; Pudil, B.; Hanley, K. J., The Full Phase Behavior for Block Copolymers in Solvents of Varying Selectivity. *Macromolecules* **2002,** *35* (12), 4707-4717.
15. Heinzer, M. J.; Han, S.; Pople, J. A.; Martin, S. M.; Baird, D. G., Iso-concentration ordering kinetics of block copolymers in solution during solvent extraction using dynamic oscillatory measurements. *Polymer* **2012,** *53* (15), 3331-3340.

7 Conclusions and Future Work

7.1 Conclusions

Initially, the purpose of this work was to better describe the kinetics of the ordering process during the solution-casting process, as the drying rate can have a significant effect on the final film.[1] The work done previously by our group[2,3,4] provided some insight, but the method used controlled drying using temperature which partially altered the characteristics of the system. A method was developed to study the effect of drying rate *in-situ* by controlling the solvent content of the drying chamber. This was done by running a sweep gas beneath the stage of the balance in the drying chamber.

A method to directly determine the volume fraction of ordered microstructure in a polymer/solvent system was developed, which has never been done before. This was accomplished by creating a drying model based on work by Vrentas and Vrentas[5]. The solvent concentration was then used in the Flory-Huggins model to calculate the solvent partitioning in the system. The electron density was then calculated to find the volume fraction of ordered phase. It was found that the most rapid ordering occurred in the system that dried at a medium rate, likely because kinetic entrapment occurred in the fast drying system. This kinetic entrapment reduced the speed at which ordering could occur in these systems.

It was found that there was a two-step process to the ordering. The first occurred during the initial drying phase as the ordering front progressed down the film. The second phase occurred once the ordering front reached the bottom of the film. It was found that, under all styrene-diene systems, the drying rate was not rapid enough to cause a significant reduction in the ordering rate, as the skinning on the surface caused much of the ordering to take place near the bottom of the film.

The compression of PMMA/PBA triblock copolymers was tracked over the course of drying. It was found that this compression resulted in partial disordering of the ordered phase of the system, which was attributed to disruption of the interface.

In addition, iso-concentration temperature quenches were also performed and Avrami curves were fit to these data. The Avrami exponent did not change significantly over a wide concentration range. This produced a V-shaped curve when half-time of ordering was compared to temperature. This curve was caused by competition of thermodynamic driving force as the concentration moved away from the C_{ODT}, and kinetic entrapment as the solvent content was lowered and the chain mobility was reduced.

The sum of these chapters produces a picture of different phenomena that occur in ordering block copolymer films during drying. Calculating the volume fraction of ordered phase directly allowed for clarification and greater accuracy. A medium drying rate discourages some of the kinetic entrapment that occurs in a faster drying system. In addition, it is important to select a solvent that can rapidly diffuse through the block copolymer to prevent skinning on the surface. Compression can have an effect on the final ordered structure, as it can ultimately cause a system to partially disorder upon further drying. Finally, the actual ordering rate that occurs at various concentrations throughout the film is able to be calculated based on the Avrami model developed in this work.

There are still several unanswered questions that this work has not addressed. The volume fractions were normalized to the final volume fraction of ordered phase. Thus, a direct comparison between the kinetics of different drying rates and between the different concentrations during the iso-concentration temperature quenches was unable to be obtained. In addition, the work does not directly relate the iso-concentration data with the drying data to obtain a more generalized model. Finally, only the final portion of the growth phase in the iso-concentration work presented in Chapter 7 was able to be obtained during the experiment. This leaves large errors in the Avrami fits to these data, preventing a more comprehensive analysis. These questions would provide interesting topics for future work.

7.2 Future Work

7.2.1 Kinetic Model

There are several questions that remain as yet unanswered. A comprehensive kinetic model has not yet been fully explored. The reasons that this has not been done are two-fold. The iso-concentration data was not complete enough to obtain an accurate representation of the trends in the data. Specifically, it was difficult to fit a complete model of the behaviors of thermodynamic driving force and chain mobility and their sum. Thus, more information of the effect of drying and concentration on half-times and overall kinetics are needed.

7.2.1.1 Drying Data

The drying curves obtained had changing solvent concentrations that were exponential in nature. It might be possible to perform scaling analysis on the Avrami model that uses fitted exponential drying curves to produce a dimensionless time. This dimensionless time could potentially be used to obtain master kinetic curves with respect to drying rate that could better describe the kinetics in these systems. This work is currently being explored at the writing of this document. Furthermore, additional drying rates using the same experimental setup would enhance the ability of this model to predict the kinetics of block

copolymers in solution during film drying. A potential set of experiments would include sweep gas flow rates of 0.15, 0.3, 0.45, 0.5, 1.0, and 2.0 SCFH N_2. This would enable the Avrami equation to be analyzed to include the effect concentration change, via the equation shown below.

$$\frac{d\phi}{dt} = t^{n-1}\left(k(c) + \frac{dk(c)}{dt}t\right)\exp(-k(c)t^n) \tag{7-1}$$

Here, n is the Avrami exponent, $\phi(t)$ is the volume fraction of ordered phase with respect to a completely ordered system, and $K(c)$ is the rate constant, which is a function of polymer concentration, c.

7.2.1.2 Iso-concentration Data

The iso-concentration data were fit to the end of the growth stage of ordering, and thus the fitted data had a degree of precision that was too low for a more comprehensive kinetic model. It was difficult to produce sufficient disordering in these systems without introducing decomposition. When the samples were placed in an oil bath that reached approximately 210°C, the sample would yellow after two hours. And when the same sample was run multiple times at 195°C, it would also yellow. To enhance the degree of disordering obtained during the temperature rise, it is proposed to introduce shear into the system. This would be done halfway through oil bath at 195°C. This would be done using an impeller, with the following set-up.

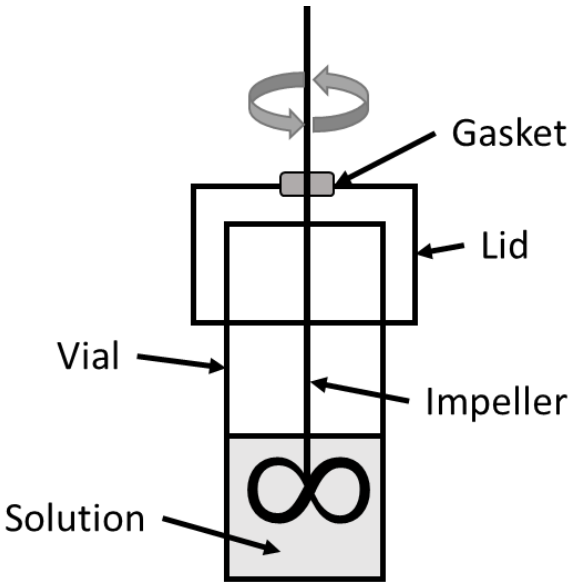

Figure 7-1: Curve fits of half-time vs concentration for temperature quenches of SIS triblock in toluene

Here, a silicone gasket would be adhered inside an opening in the lid to prevent solvent vapor from escaping. A metal impeller would be placed inside and rotated to provide shear which would help to disorder the microstructure of the solution. This would allow for a more precise fit to the Avrami model, as more of the ordering would be able to be observed. More conclusions would be able to be drawn from the resulting kinetic data. Better data would enable a more accurate overall kinetic model with respect to concentration than was possible in the current work.

7.2.2 Solvents

A selective solvent that preferentially partitions to one block or another will change the domain size by swelling one block, and may ultimately cause a change in behavior in the system. In a styrene/diene system, cyclohexane will be selective for the diene block. A solvent such as benzene will be selective for the styrene block. Both of these solvents have similar boiling points (81°C vs 80°C), and could be used to study the difference that selectivity has on the ordering behavior of solution-cast block copolymer films. Differing sweep gas flow rates could be used to evaluate the effect of drying rate. As the two solvents have low boiling points, it may be necessary to saturate the drying chamber with solvent to slow the drying process during experimentation. Iso-concentration experiments similar to those performed previously could be conducted, and the kinetic behavior of a diene-selective solvent, a neutral solvent, and a styrene-selective solvent could be compared.

References

1. Huang, H.; Zhang, F.; Hu, Z.; Du, B.; He, T.; Lee, F. K.; Wang, Y.; Tsui, O. K. C., Study on the Origin of Inverted Phase in Drying Solution-Cast Block Copolymer Films. *Macromolecules* **2003,** *36* (11), 4084-4092.
2. Heinzer, M. J.; Han, S.; Pople, J. A.; Baird, D. G.; Martin, S. M., In Situ Measurement of Block Copolymer Ordering Kinetics during the Drying of Solution-Cast Films Using Small-Angle X-ray Scattering. *Macromolecules* **2012,** *45* (8), 3471-3479.
3. Heinzer, M. J.; Han, S.; Pople, J. A.; Baird, D. G.; Martin, S. M., In Situ Tracking of Microstructure Spacing and Ordered Domain Compression during the Drying of Solution-Cast Block Copolymer Films Using Small-Angle X-ray Scattering. *Macromolecules* **2012,** *45* (8), 3480-3486.
4. Heinzer, M. J.; Han, S.; Pople, J. A.; Martin, S. M.; Baird, D. G., Iso-concentration ordering kinetics of block copolymers in solution during solvent extraction using dynamic oscillatory measurements. *Polymer* **2012,** *53* (15), 3331-3340.
5. Vrentas, J. S.; Vrentas, C. M., Drying of solvent-coated polymer films. *Journal of Polymer Science Part B: Polymer Physics* **1994,** *32* (1), 187-194.

Appendix

A1. Chapter 4 Appendix

A1.1 Data

A1.1.1 Solvent Diffusivity

Diffusivity was calculated by putting a petri dish in a bottle with solvent in the bottom and weighing the petri dish every few days as the polymer absorbed the solvent vapor. A schematic is represented below.

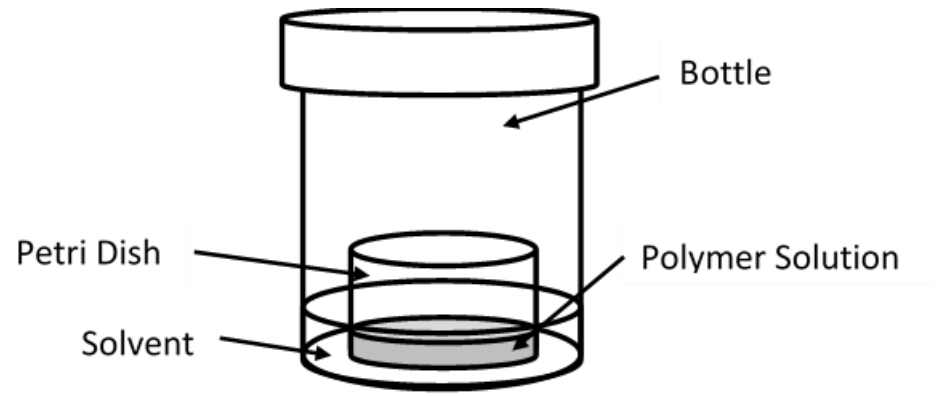

Figure A1: Schematic of the sorption experiment used to determine the duffusivity of toluene in each solution

Diffusivity is calculated using the equation:

$$\frac{d}{dt}(\ln(M_\infty - M_t)) = -\frac{D^P \pi^2}{L^2}$$

Weight data were then taken periodically during the sorption experiment. The final mass of solvent was calculated via allowing the system to equilibrate and taking the final mass. The mass taken during the equilibration is represented in the figure below.

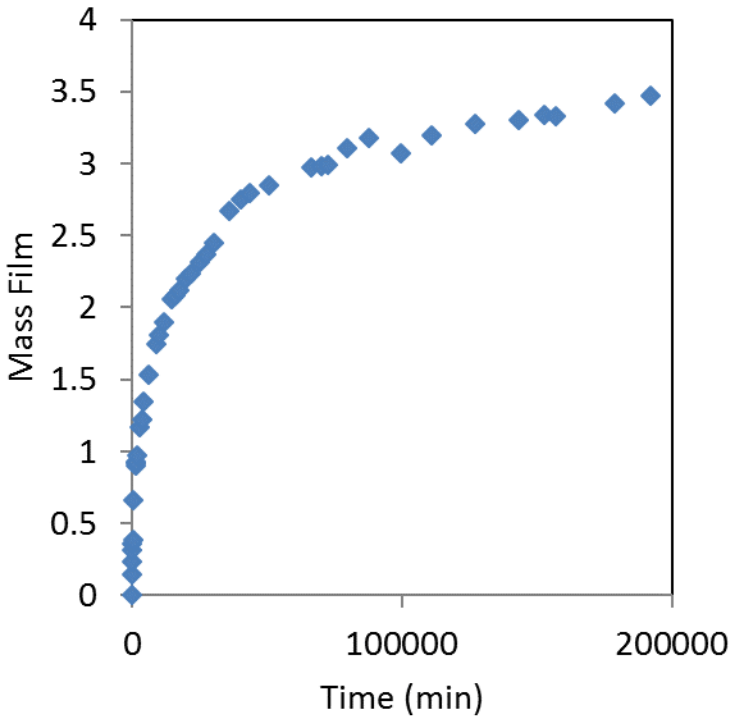

Figure A2: Mass of the polymer film during sorption to determine equilibrium total mass solution

The sample was then dried down to a solvent concentration near 0.75wt%, and tracked as the solvent was sorbed. The results are listed in the table below.

Table A1: Diffusivity calculation data for toluene in styrene/butadiene diblock copolymer

Mass	Mass Solvent	Time (min)	Thickness (m)	Solvent Concentration	M/Minf	Thickness Error	Calculated Diffusivity (m^2/s)	Error (m^2/s)
3.15	2.39	4296	2.22E-03	0.756	0.69	1.97E-07		
3.40	2.63	5758	2.40E-03	0.774	0.76	2.12E-07	1.1765E-11	2.4282E-13
3.49	2.73	15928	2.47E-03	0.780	0.79	2.18E-07	1.58892E-11	8.24505E-13
3.64	2.87	24585	2.57E-03	0.789	0.83	2.28E-07	1.9129E-11	1.47632E-12
3.75	2.98	31628	2.65E-03	0.795	0.86	2.35E-07	2.15809E-11	2.11289E-12
3.79	3.03	36085	2.68E-03	0.798	0.87	2.38E-07	2.30473E-11	2.565E-12
3.86	3.09	41777	2.73E-03	0.801	0.89	2.41E-07	2.48241E-11	3.19792E-12
4.00	3.24	54830	2.83E-03	0.808	0.93	2.51E-07	2.84917E-11	4.88452E-12
4.08	3.31	63250	2.89E-03	0.812	0.96	2.56E-07	3.0557E-11	6.14627E-12

To calculate the diffusivity, a 3rd degree polynomial was fit to $\ln(M_\infty - M)$ data and the derivative taken. The results for this polymer are shown in the figure below.

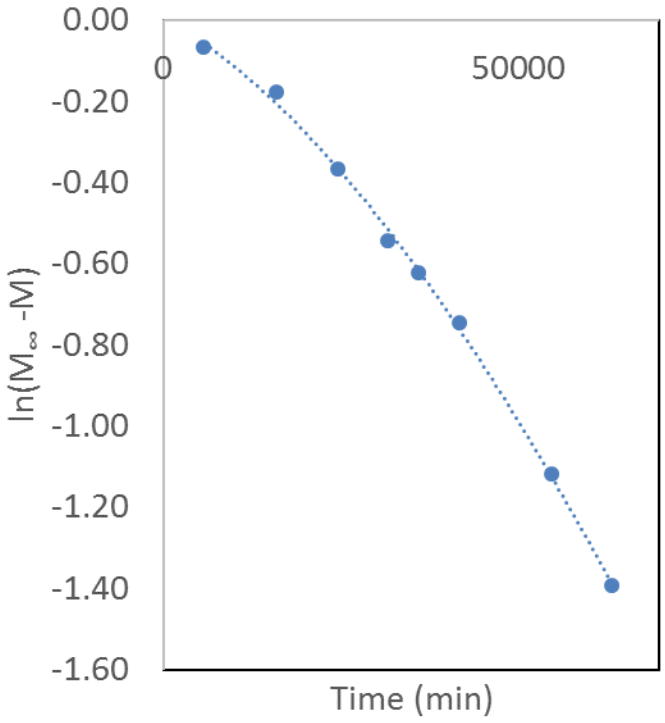

Figure A3: Fit of natural log of mass difference with respect to time for diffusivity calculation

1) *A1.1.2 Integrated Data*

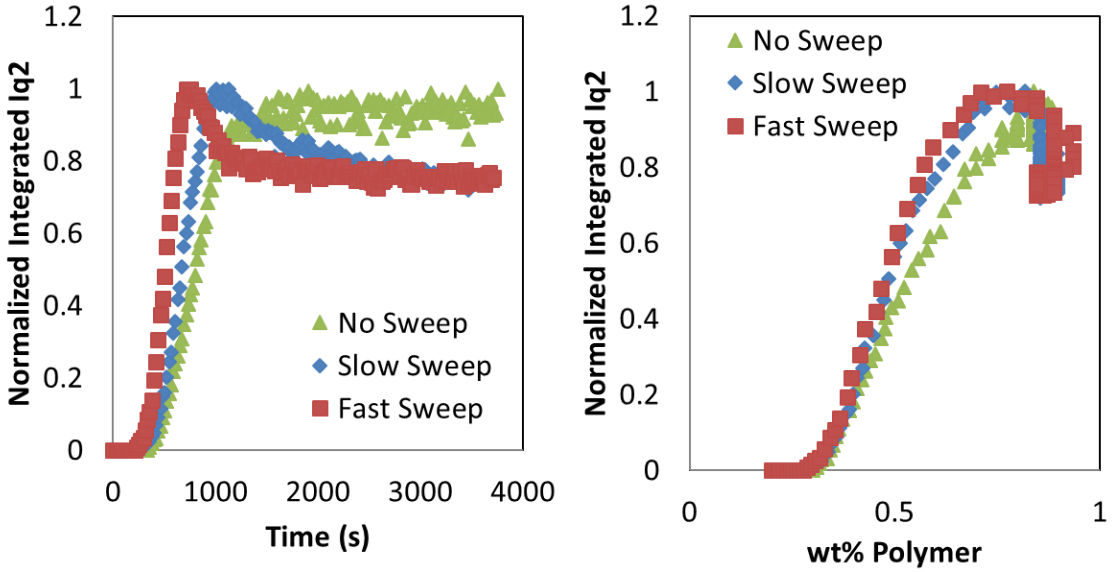

Figure A4: SB in toluene data with respect to total concentration and time

A1.2 Code

MATLAB Code

Diffusivity Fit

```
function [time, p, mdl] = DiffFit(filein, range, sheet)
%Calculates the Avrami parameters for quench kinetic data, plus the initial
%time


data1 = xlsread(filein, sheet, range);


%time in minutes and integrated Iq2dq data
time = data1(:,1);
lnM = data1(:,11);
thickness = data1(:,4);

L = length(time);



%tInit is theoretical time from the BEGINNING of the experiment from which
%the kinetics should have begun if all ordering were removed.
tInit = 0;


%inital guesses for initial time (in minutes), k, and n

[p,S] = polyfit(time,lnM,3);
[y, delta] = polyval(p,time,S);

p
y
delta

%displays final values

%beta = coeffvalues(mdl);


a = p(1);
b = p(2);
c = p(3);
d = p(4);

beta = [0.00001; 0.01; 1; d]

mdl = fitnlm(time,lnM,@Equation,beta);
```

```
plot(time,lnM,'-o')
hold on
plot(time,a*(time(:).^3) + b*(time(:).^2) + c*time(:) + d)
mdl

xlswrite(filein,p',sheet,'R29:R32');
end

function yhat = Equation(beta,time)

a = beta(1);
b = beta(2);
c = beta(3);
d = beta(4);

L = length(time);

%38 is used here because that is the length of the run
for i = 1:1:L
   yhat(i,1) = a*((time(i))^3) + b*((time(i))^2) + c*(time(i)) + d;
end

end
```

Integration of peak data

```
function fileout = SAXSIntIq2LS(filein, fnum, fcol, MinLimit)

%Check handles on trapezoidal rule
%data1 is the I data, and data2 is the Iq2 data

data1 = xlsread(filein, 'Sheet1', 'A4:IG200');
data2 = xlsread(filein, 'Sheet2', 'A4:IG200');


    %Initialize
    Min2 = 0;

    %Initialize print matrix
    fileout = zeros(2,fcol);
    test = zeros(10, fcol);

    %Step through columns (files)
    for Z = 2:fcol

        i = 1021;
        %Initialize integrated areas to 0
        Simpson = 0;
```

```
        Triangle = 0;
        Rectangle = 0;

        %Initialize minimum intensity values so that the first point must be
taken as your initial minimum intensity
        Min1 = 100000;
        Min2 = 100000;
        Min1out = 0;

 %~~~~~~~Initialize peak local and height to zero?
        qPeak = 0;
        PeakHeight = 0;

        %Step through rows for a given column (file)
        for x1 = 30:MinLimit
            %Find the first minimum intensity value (initial integration
point)
            %If the intensity is less than the previous minimum intensity, it
becomes the new minimum
            if data1(x1, Z) < Min1
                Min1 = data1(x1, Z);
                Min1out = data2(x1, Z);
                q_min1 = data1(x1, 1); %Wave vector of the first minimum
intensity
                test(1, Z) = q_min1;
                test(2, Z) = Min1;
                %Base1 is the lower bound of a triangle and a rectangle that
will be subtracted from Simpson Rule integration
                Base1 = data1(x1, 1);
                Base1out = data2(x1, 1);
                %Cell from which integration will be started
                Min1x = x1;
            end


        end

        Minx2 = Min1x;
        Min2out = Min1out;
        Base2 = Base1;
        Base2out = Base1out;

        %Search for the second minimum on the other side of the Bragg peak
        %This will be the upper bound for integration
        for x2 = MinLimit + 1: 197

            if data1(x2, Z) < Min2
                Number = 0;

                    %Height of a rectangle occupying the area under the peak
to be integrated
                    Height = Min1 - data1(x2, Z);
                    %Length of a rectangle occupying the area under the peak
to be integrated
                    Base = Base1 - data1(x2, 1);
```

```
                    %Slope of a line running from the first minimum wave
vector and the second minimum wave vector
                    Slope = Height / Base;
                    %Intercept of line
                    b = Min1 - (data1(Min1x, 1) * Slope);

                    %We know the second minimum wave vector must be at an
intensity lower than that of the first minimum
                    %I(q) naturally slopes down
                    %Therefore, if minimums were correctly found, the slope
of the line is negative
                    if Slope <= 0

                    for j = Min1x: x2
                        %Calculate the value of the line at different wave
vectors
                        LineValue = Slope * data1(j, 1) + b;

                        %Set a criteria that the line cannot be grater than
the measured intensity more than twice between the two minimum
                        %This ensures the line is not intersecting the Bragg
peak
                        if LineValue > data1(j, Z)
                            Number = Number + 1;
                        end
                    end
                        %If the criteria is met, we define a triangle and
rectangle occupying the area under the baseline of the scattering curves
                        if Number < 2
                            Min2 = data1(x2, Z);
                            Min2out = data2(x2, Z);
                            Base2 = data1(x2, 1);
                            Base2out = data2(x2, 1);
                            Minx2 = x2;
                        end
                    end


            end

        end
        test(3, Z) = data1(Minx2, 1);
        test(4, Z) = Min2;
        %Use Simpson's rule to calculate the area between the first and
second minimum intensities (i.e. over the Bragg peak)

        Lower1 = Min1x;
        Upper1 = Minx2;

        %Numerical Integration Boundary and index
        Q = zeros(1, Upper1 - Lower1 + 1);
        j = 1;

        %Numerical Integration Intensity
        I = zeros(1, Upper1 - Lower1 + 1);
```

```
        for x = Lower1: Upper1
            Q(j) = data2(x, 1);
            I(j) = data2(x, Z);
            j = j + 1;
        end



        %Integral via the trapezoidal rule
        if Min1x ~= Minx2
        Trapezoidal = trapz(Q, I);

        else
            Trapezoidal = 0;
        end

        test(5, Z) = Trapezoidal;
        test(9, Z) = 0;

        %Define triangle and rectangle to be substracted from Simpson Sum
        Height = Min1out - Min2out;

        Base = Base1out - Base2out;
        Triangle = abs(Base) * Height / 2;
        Rectangle = abs(Base) * Min2out;

        test(6, Z) = Triangle;
        test(7, Z) = Rectangle;

        if (Trapezoidal - Triangle - Rectangle) < 0
            fileout(1, Z) = 0;
        else
            fileout(1, Z) = Trapezoidal - Triangle - Rectangle;
        end

        test(8, Z) = fileout(1, Z);

        for x = Min1x: Minx2
            if data2(x, Z) > PeakHeight
                qPeak = data2(x, 1);
                PeakHeight = data2(x, Z);
            end
        end


        if q_min1 ~= qPeak
            fileout(2, Z) = qPeak;
            test(10, Z) = qPeak;
        end

    end

end
```

Code that implements the integration code and writes it to Excel files

```
function DataWriteIq2LSLarge

%If the program can't find anything with the Iq2 data, find the min/max
%with the I data and integrate over that

file1 = 'SBch-15-RT-DB-1_195-205.xlsx';
file2 = 'SBch-15-RT-DB-1_200-250.xlsx';
file3 = 'SBch-15-RT-DB-1_210-240.xlsx';
file4 = 'SBch-15-RT-DB-1_245-255.xlsx';

fileout = 'SBch-15-RT-DB-1.xlsx';

LowMin = 58;
HighMin = 78;
NumCol = 134;
TimeGap = 16;
Range = 'A4:JQ200';


%Initializes the files data1 - data6
data1 = zeros(197,NumCol);
data2 = zeros(197,NumCol);
data3 = zeros(197,NumCol);
data4 = zeros(197,NumCol);


%Initializes the output data files
DataOut1 = zeros(197,NumCol);
DataOut2 = zeros(197,NumCol);
DataOut3 = zeros(197,NumCol);
DataOut4 = zeros(197,NumCol);

%Imports the data from the Excel files for analysis
data1 = xlsread(file1, 'Sheet1', Range);
data2 = xlsread(file2, 'Sheet1', Range);
data3 = xlsread(file3, 'Sheet1', Range);
data4 = xlsread(file4, 'Sheet1', Range);

%Puts q into the first column of DataOut1 - DataOut6
for row = 1:197
    DataOut1(row, 1) = data1(row, 1);
    DataOut2(row, 1) = data2(row, 1);
    DataOut3(row, 1) = data3(row, 1);
    DataOut4(row, 1) = data4(row, 1);
end

%Modifies the data to Iq^2
for col = 2:NumCol
    for row = 1:197
        DataOut1(row,col) = (data1(row, 1)^2) * data1(row, col);
```

```
        DataOut2(row,col) = (data2(row, 1)^2) * data2(row, col);
        DataOut3(row,col) = (data3(row, 1)^2) * data3(row, col);
        DataOut4(row,col) = (data4(row, 1)^2) * data4(row, col);

    end
end


%Writes Iq^2 data to the various files
xlswrite(file1,DataOut1,'Sheet2',Range);
xlswrite(file2,DataOut2,'Sheet2',Range);
xlswrite(file3,DataOut3,'Sheet2',Range);
xlswrite(file4,DataOut4,'Sheet2',Range);


a1 = 1;
a2 = 1;
a3 = 1;
a4 = 1;
a5 = 1;
a6 = 1;
Length = HighMin - LowMin + 1;

%Initializes output matrices
out1 = zeros(2*Length, NumCol);
out2 = zeros(2*Length, NumCol);
out3 = zeros(2*Length, NumCol);
out4 = zeros(2*Length, NumCol);

%Calls SAXSInt for various limits and puts them into an array
for x = LowMin:HighMin
   fout1 = SAXSIntIq2LSLarge(file1, 1, NumCol, x);
   out1(2*a1-1,:) = fout1(1, :);
   out1(2*a1,:) = fout1(2, :);

   a1 = a1 + 1;

end



for x = LowMin:HighMin
   fout2 = SAXSIntIq2LSLarge(file2, 1, NumCol, x);
   out2(2*a2-1,:) = fout2(1, :);
   out2(2*a2,:) = fout2(2, :);

   a2 = a2 + 1;
end

for x = LowMin:HighMin
   fout3 = SAXSIntIq2LSLarge(file3, 1, NumCol, x);
   out3(2*a3-1,:) = fout3(1, :);
   out3(2*a3,:) = fout3(2, :);
```

```
   a3 = a3 + 1;
end

for x = LowMin:HighMin
   fout4 = SAXSIntIq2LSLarge(file4, 1, NumCol, x);
   out4(2*a4-1,:) = fout4(1, :);
   out4(2*a4,:) = fout4(2, :);

   a4 = a4 + 1;
end

%Creates the time array and writes it to Sheet2 of the Excel file
Time = zeros(NumCol - 1);
Time = 0:TimeGap:(TimeGap*(NumCol - 2));

xlswrite(fileout,Time,'Sheet2','B2:JQ2');
xlswrite(fileout,Time,'Sheet2','B51:JQ51');
xlswrite(fileout,Time,'Sheet2','B101:JQ101');
xlswrite(fileout,Time,'Sheet2','B151:JQ151');

%Writes tho low and high minimum to the Excel file
xlswrite(fileout,LowMin,'Sheet2','B1:B1');
xlswrite(fileout,HighMin,'Sheet2','C1:C1');

%Writes to the Excel file for analysis
xlswrite(fileout,out1,'Sheet2','A3:JQ42');
xlswrite(fileout,out2,'Sheet2','A52:JQ91');
xlswrite(fileout,out3,'Sheet2','A102:JQ141');
xlswrite(fileout,out4,'Sheet2','A152:JQ191');



end
```

Code that calculates the concentration profiles of drying films

```
function [Cp,pos,thicknessFront,ca,cFront,totalThickness] =
DryingSimPde(system, filename, sheet, xlRange, fitRange,fitRange2)

%------------------------------
%Drying simulation of BCP films
%------------------------------


%Uses pdepe with various functions to solve differential equation

%Import Drying Data
%Drying Data contains time, calculated thickness, and overall weight
%fraction in rows 1, 2, and 3 respectively
%fitRange is the range over which X is an exponential function e.g. B3:BE3
data = xlsread(filename,sheet,xlRange);
datafit1 = xlsread(filename,sheet,fitRange);
datafit2 = xlsread(filename,sheet,fitRange2);
```

```
%Declare Variables, temperature is in C, rho is in kg/m3, TO is the initial
%film temp, tnum is the number of time steps, xnum is the number of
%datapoints in the finite difference method,
%t is the dimensionless time, dn is deltaEta i.e. the eta step distance
%(if there are 4 points, deta would be 0.333), dt is the dimensionless time
%step
%c0 is the inital dimensionless solvent mass density (should be 1, as the
%dimensionless solvent mass density is c = p/p0

Nt = length(datafit1);
Nt2 = length(datafit2);
Ntotal = length(data); %total length of data so that further fitting can
commence after Nt
Nx = 50;
tfinal = Nt - 1;%Debug value of time points for matrix calc
tfinal2 = Nt2 - 1;
texp = Nt;%time point up to which X is exponential
texp2 = Nt2;%time point from 1st to 2nd exponential
maxiter = 200; %maximum number of iterations
t = zeros(1,Ntotal);
dn = 1/(Nx - 1);
dt = 1/(Nt - 1);
c0 = 1;
cODT = 0.43; %ODT concentration as determined by rheology (0.59 for D1161,
0.43 for SB)
pos = ones(1,Ntotal); %pos is a 1D array showing the values for eta of the
ordering front as determined by CODT at each time point


m = 0; %geometry for pdepe (0 is for cartesian, 1 is for cylindrical
coordinates, 2 is for spherical coordinates
a1 = 0; %coefficient fitting parameter for Xfit = ae^bx
b1 = 0; %coefficient fitting parameter for Xfit = ae^bx

%Solvent Variables, Dp is the diffusion coefficient in the film, D0 is the
%initial diffusion coefficient in the film (based on self-diffusion of
%toluene in PS from http://pubs.acs.org/doi/pdf/10.1021/ma00200a025 paper)
%Dsurf is D/D0 at the upper boundary of the film D0 in paper is 16.9E-10
%Dstar is D/D0
%B is the exponent for calculating Dstar
%D0 = 7.66 E-12 for D1161, 0.246 E-10 for SB

D0 = 0.246 *(10^(-10));
Dsurf = ones(1,Ntotal);
Dstar = ones(Nx,Ntotal);

%initialize arrays from imported
fitLength = length(data);
datatime = data(1,:);
thickness = data(11,1:fitLength)*10^(-2);
wtFracMean = data(2,:);
thicknessNoFit = data(11,fitLength + 1:end)*10^(-2);
```

```
%polymer density is in SI units
if strcmp(system,'SBT')
    rhoSol = 866.9;
    rhoPol = 965;
    D0 = 0.246 *(10^(-10));
    cODT = 0.43; %ODT concentration as determined by rheology (0.59 for
D1161, 0.43 for SB)
end

if strcmp(system,'SBST')
    rhoSol = 866.9;
    rhoPol = 0.94;
    D0 = 0.0219*(10^(-10));
    cODT = 0.42;
end

if strcmp(system,'SIST')
    rhoSol = 866.9;
    rhoPol = 920;
    D0 = 6.49*10^(-12);
    cODT = 0.59; %ODT concentration as determined by rheology (0.59 for
D1161, 0.43 for SB)
end

if strcmp(system, '2140')
    rhoSol = 866.9;
    rhoPol = 1105.6;
    D0 = 0.95 * (10^(-10));
    cODT = 0.53;
end

if strcmp(system, '2250')
    rhoSol = 866.9;
    rhoPol = 1113;
    D0 = 0.031 * (10^(-10));
    cODT = 0.51;
end

if strcmp(system, '4285')
   rhoSol = 866.0;
   rhoPol = 1131;
   D0 = 0.238 * (10^(-10));
   cODT = 0.41;
end

if strcmp(system,'SBCyc')
    rhoSol = 779.0;
    rhoPol = 965;
end

%Film Variables TP is the dimensionless temperature of the film, w0 is the
initial polymer wt frac of the film,
%w is average polymer wt frac of the film, X = X* or the dimensionless upper
boundary of the film,
```

```
% eta is the dimensionless thickness, L is the initial upper (currently
assuming 400microns),
%boundary, Cpp is the Cp of the film, Cp0 is the initial Cp of the film
(units of J/kgK, init is roughly the Cp of PE (2.3)),
%rhoP is the density of the film,
%while rhoP0 is the initial density of the film. dcdn is dc/deta
%Cmean is the average dimensionless SOLVENT mass density. Is an array w/
%time points - is wtFracMean * rhoFilm
%rhoPMean is the average mass density of SOLVENT
%rhoFilm0 is the initial overall TOTAL density of the FILM
%rhoFilm is  the overall TOTAL density of the FILM - is an array wrt time of
w0 = wtFracMean(1,1); %init POLYMER wt fraction
w = wtFracMean(1,:); %POLYMER wt fraction

%Variables for mean concentration calculation
MFilm = zeros(1,Ntotal); %calculated mass (arbitrary units) of the film using
Mp0 (init polymer mass if total mass/volume = 1 (arbitrary units))
Mp0 = w0; %initial polymer mass of the entire film if initial volume and mass
= 1, arbitrary units
MpSection = Mp0/(Nx-1); %initial polymer mass of each film section if initial
volume/mass = 1, arbitrary units. THIS IS CONSTANT AS THE SOLVENT IS THE ONLY
THING ASSUMED TO MOVE
MtotalSection = zeros(Ntotal,Nx - 1); %total polymer mass of a film section
of initial volume = 1, arbitrary units. Is MpSection/Cp
VolumeFilm0 = 1; %inital film volume, arbitrary units
VolumeSection0 = 1/(Nx - 1); %inital volume of a section
VolumeSection = zeros(Ntotal,Nx - 1); %matrix of section volumes
VolumeSectionSolvent = zeros(Ntotal, Nx-1); %matrix of init section volume -
polymer section volume (i.e. the volume of solvent)
rhoFilm0 = 1/((w0/rhoPol) + ((1-w0)/rhoSol));
rhoFilm = zeros(1,Ntotal);
rhoFilm1 = zeros(Nx,Ntotal); %density of film at different points vs time

%Variables for solving the differential equations
Xnums = zeros(tfinal,1); %THIS Nx vs Nt ORDERING IS FLIPPED
Xnumsrest2 = zeros(Ntotal - tfinal - tfinal2,1); %fitting for rest of
numbers. Nx vs Nt is flipped for fitting
Xnumsrest1 = zeros(tfinal2,1);
X = zeros(1,Ntotal); %TRANSPOSE OF X. THIS Nx vs Nt ORDERING IS FLIPPED SO
THAT THE FIT WILL WORK
Xrest = zeros(1,Ntotal - tfinal,1);
L = data(11,1)*10^(-2); %SIMP - Known initial film thickness
eta = zeros(1,Nx);

V = 0.001154; %USING PARTIAL SPECIFIC VOLUME
rhoP = zeros(Nx,Ntotal); %SOLVENT mass density
rhoP0 = rhoFilm0 * (1-w0); %rhoP0 is calculated using the assumption that the
volumes add (vE = 0)


%Turns the total specific volume of solvent into average partial specific
%volume AT THE INITIAL POINT

        V = V * (1-w(1,1));
```

```
for j = 1:Ntotal
    rhoFilm(1,j) = (1/((w(j)/rhoPol) + ((1-w(j))/rhoSol)));
    Cmean(1,j) = (1-w(j))*rhoFilm(1,j)/rhoP0;
end

%Boundary Conditions
%time boundary conditions
w(1,1) = w0;
X(1,1) = 1;
rhoP(:,1) = rhoP0;


%Defining the points in dimensionless x (i.e. eta)
for i = 1:(Nx)
    %eta(i) = (i - 1)/(Nx - 1);
end

eta = linspace(0,1,Nx);
x = eta;
xmesh = eta;

%Defining the points in dimensionless time
for i = 1:(Ntotal)
    t(i) = D0*datatime(i)/L^2;
end

%delt is the difference between time points
delt = t(2) - t(1);

tmatrixinit(:,1) = t(1:tfinal);
tmatrix(:,1) = t(1:end);

tmatrix2(:,1) = tmatrix(tfinal+1:tfinal2+tfinal + 1,1);

tmatrixrest(:,1) = t(tfinal2 + tfinal + 3: end);
tspan = t;

%Finite difference method for the unsteady state nonlinear partial
%differential equation for concentration wrt eta

u = zeros(Ntotal,Nx);

%declares the Cint matrix
Cint = zeros(1,Ntotal);

%This portion fits a curve to part of the exponential fn and calculates the
%derivative. The variables a and b are used for the coefficients in front
%of and in the exponent, respectively. The region to be fit was decided
%earlier within the excel file as the max number of pts before R^2 begins
%to drop rapidly. This region will be fit later using a different function.
Xnums(1:tfinal,1) = thickness(1:tfinal)/L;
e = length(thickness);
```

```
Xnumsrest2 = ones(e - Nt - Nt2 - 1,1);
for i = Nt+Nt2+1:e
   Xnumsrest2(i - Nt - Nt2,1) = thickness(i)/L;
end




for i = Nt+1:Nt+Nt2
   Xnumsrest1(i-Nt,1) =  thickness(i)/L;
end

Xfit = fit(tmatrixinit,Xnums,'exp1');
Xfitrest1 = fit(tmatrix2,Xnumsrest1,'exp1');
Xfitrest2 = fit(tmatrixrest,Xnumsrest2,'power2');
%plot(Xfitrest,tmatrixrest,Xnumsrest); %PLOT FOR DEBUG
Xcoeffs = coeffvalues(Xfit); %coefficients for the exponential fit
a1 = Xcoeffs(1);
b1 = Xcoeffs(2);
X = a1*exp(t.*b1);
Xt_1D = b1*a1*exp(t.*b1); %dX/dt, calculated from the derivative of the fited
exponential fn

Xcoeffs = coeffvalues(Xfitrest1);
a2 = Xcoeffs(1);
b2 = Xcoeffs(2);
X(tfinal+1:tfinal + Nt2) = a2*exp(t(tfinal + 1:tfinal+Nt2).*b2);
Xt_1D(tfinal+2:tfinal + Nt2) = b2*a2*exp(t(tfinal+2:tfinal+Nt2).*b2);

Xcoeffs = coeffvalues(Xfitrest2);
a3 = Xcoeffs(1);
b3 = Xcoeffs(2);
c3 = Xcoeffs(3);
X(tfinal+1+Nt2:end) = a3*(t(tfinal+Nt2 + 1:end).^b3) + c3;
Xt_1D(tfinal+Nt2+1:end) = b3*a3*(t(tfinal + Nt2 +1:end).^(b3 - 1));


excess = ones(1,Ntotal);


%At t = 0, c is flat, so dc/deta = 0, and d2c/deta2 = 0
%At eta = 0, dc/deta = 0

%Calculating the c matrix
%Go through iterations at each point in order to back calculate X* and D
%and c at eta = 1, etc

%Will do a series of iterations of pdepe so that the diffusivity can be
%calculated from the implied flux due to the weight data.

%DryingSimFun returns the parameters C, F, and S needed by pdepe

excessLast = 1000*ones(1,Ntotal);
```

```
for iter = 1:maxiter

    u = ones(Ntotal,Nx);
    Cint(1,1) = 1;
    sol = 1;
    sol = pdepe(m,@DryingSimFun,@DryingSimIC,@DryingSimBC,xmesh,tspan);
    %Extract the first solution component as u
    u = sol(:,:,1);

    %Calculates Cp from u data
        for i = 1:Ntotal
        for j = 1:Nx
            if strcmp(system,'SBT')
                Cp(i,j) = -0.069536255*u(i,j)^2 - 0.73027205*u(i,j) +
0.99967833;
                rhoFilm1(j,i) = -80.145467*u(i,j) + 965.000;
                vFilm(i,j) = 1/rhoFilm1(j,i); %specific volume at position in
film
                rhoODT = 906.526971219646; %from CODT = 0.43
                vODT = 1/rhoODT;


            end

            if strcmp(system,'SBST')
                Cp(i,j) = -0.052328478*u(i,j)^2 - 0.74753636*u(i,j) +
0.99981813;
                rhoFilm1(j,i) = -59.417833*u(i,j) + 940.000;
                vFilm(i,j) = 1/rhoFilm1(j,i);
                rhoODT = 908.5877; %from CODT = 0.41
                vODT = 1/rhoODT;
            end

            if strcmp(system,'SIST')
                Cp(i,j) = -0.03832639*u(i,j)^2 - 0.7620008*u(i,j) +
0.9999129;
                rhoFilm1(j,i) = -43.001698*u(i,j) + 920.000;
                vFilm(i,j) = 1/rhoFilm1(j,i); %specific volume at position in
film
                rhoODT = 897.461490247797; %from CODT = 0.59
                vODT = 1/rhoODT;
            end

            if strcmp(system,'SBC')
                Cp(i,j) = -0.1463536*u(i,j)^2 - 0.7186362*u(i,j) + 0.9978279;
                rhoFilm1(j,i) = -142.98058*u(i,j) + 940.000;
                vFilm(i,j) = 1/rhoFilm1(j,i); %specific volume at position in
film
            end

            if strcmp(system, '2140')
                Cp(i,j) = -0.16135943*u(i,j)^2 - 0.63906933*u(i,j) +
0.99825895;
                rhoFilm1(j,i) = -200.31319*u(i,j) + 1105.6;
```

```
                vFilm(i,j) =  1/rhoFilm1(j,i);
                rhoODT = 983.711263810985;
                vODT = 1/rhoODT;
            end

        if strcmp(system, '2250')
                Cp(i,j) = -0.31667006*u(i,j)^2 - 0.86462174*u(i,j) +
1.1836182;
                rhoFilm1(j,i) = -206.0314*u(i,j) + 1113;
                vFilm(i,j) =  1/rhoFilm1(j,i);
                rhoODT = 977.0839979;
                vODT = 1/rhoODT;
        end

        if strcmp(system, '4285')
                Cp(i,j) = -0.17446112*u(i,j)^2 - 0.622288644*u(i,j) +
0.99825999;
                rhoFilm1(j,i) = -221.67515*u(i,j) + 1131;
                vFilm(i,j) =  1/rhoFilm1(j,i);
                rhoODT = 958.683568;
                vODT = 1/rhoODT;
        end


       end
       end

     for i = 1:Ntotal

         for j = 1:Nx-1

    MtotalSection(i,j) = MpSection*2/(Cp(i,j) + Cp(i,j+1));

         end


         MFilm(1,i) = Mp0/w(1,i);
     end


    Cint(1,:) = MFilm(1,:);
    ca(1,:) = Cint(1,:);

    for i = 1:Ntotal
       M(1,i) = w0/w(1,i);
    end

    excess(1,:) = Cint(1,:) - M(1,:);

    if iter == 1
       exInit = excess;
    end

    %Changes the diffusivity at the surface based on the current
```

```
    %concentrations
    for j = 2:Ntotal - 1
        if excess(1,j) >= 0.005 && Dsurf(1,j) >= 0.99*Dsurf(1,j+1) &&
excessLast(1,j) > excess(1,j) %0.99*Dsurf(1,j+1)
            Dsurf(1,j) = Dsurf(1,j-1)*0.99;

        else if excess(1,j) <= -0.005 && excessLast(1,j) < excess(1,j) &&
Dsurf(1,j) >= 1.01*Dsurf(1,j+1)%1.01*Dsurf(1,j+1)
                Dsurf(1,j) = Dsurf(1,j)*1.01;


            end
        end
    end

    if excess(1,Ntotal) >= 0.005 && excessLast(1,Ntotal) > excess(1,Ntotal)
        Dsurf(1,Ntotal) = Dsurf(1,Ntotal)*0.99;

    else if excess(1,Ntotal) <= -0.005 && excessLast(1,Ntotal) <
excess(1,Ntotal)
              Dsurf(1,Ntotal) = Dsurf(1,Ntotal)*1.01;

        end
    end

    %Linear diffusivity function in order to calculate diffusivities to
    %start reflexive portion of program

    %Diffusivity interpolation - logarithmic diffusivity wrt c
    %logD1 = logD0 + B(C1-C0)




    for j = 2:Ntotal
        %Calculates exponent coefficient B from D0 ASSUMES THAT
        %THERE IS NO CHANGE IN MODEL BEFORE VS AFTER ODT

        %Also calculates the derivative
        B(1,j) = (log(Dsurf(1,j)))/(u(j,Nx) - 1);

        for i = 1:Nx

            Dstar(i,j) = Dsurf(1,j)*exp(B(1,j)*(u(j,i) - u(j,Nx)));

        end
    end

    excessLast = excess;
end


%Calculates pos from Cp data, calculates thicknessFront
```

```
%totalFilmVol and nonLayerFilmVol are the
totalFilmVol = zeros(1,Ntotal);
nonLayerFilmVol = zeros(1,Ntotal);

%Variables for calculating the wt fraction of the front. MFront is total
%mass of front, and MpFront is the polymer mass of the front, and MnotFront
%and MpnotFront are mass not in the front. cFront is the wt fraction of
%polymer in the front
MFront = zeros(1,Ntotal);
MpFront = zeros(1,Ntotal);
MnotFront = zeros(1,Ntotal);
MpnotFront = zeros(1,Ntotal);
cFront = zeros(1,Ntotal);
cFront1 = zeros(1,Ntotal);
coeff = zeros(Ntotal,3);
etafit(:,1) = linspace(0,1,Nx);
Cpfit = Cp';
VolumeLayer = zeros(1,Ntotal);
debug = zeros(1,Ntotal);

%Calculates pos for situations before the ordering front forms and after it
%reaches the bottom of the film

for i = 1:Ntotal
            if Cp(i,1) > cODT
                pos(1,i) = 0;
                thicknessFront(1,i) = thickness(1,i)*100/L;
                cFront(1,i) = w(1,i);
                else if Cp(i,Nx) < cODT
                   pos(1,i) = 2;

                   thicknessFront(1,i) = 0;
                end

            end
end



%Here it is assumed that the polymer in a giver section doesn't move and that
%the volume change is due entirely to lost solvent. The inital volume is
%assumed to be 1(arbitrary units), so that Mp0 = w0/Nx - 1. Mpsection = M
%VolumeSection0 * rhoFilm(1,1)* (Nx-1) is a constant that's used to make
%VolumeFilm0 = 1
for i = 1:Ntotal
    for j = 1:Nx - 1

        %Calculates the total mass of each section, along with the total
volume of each section
        VolumeSectionSolvent(i,j) = ((MtotalSection(i,j) - MpSection)/rhoSol)
* VolumeSection0 * rhoFilm0 * (Nx - 1);
        VolumeSection(i,j) = (MpSection/rhoPol)* VolumeSection0 * rhoFilm0 *
(Nx - 1) + VolumeSectionSolvent(i,j);

        if Cp(i,j) <= cODT && Cp(i,j+1) >= cODT
```

```
            %interpolation to find eta(ODT) at each time point
            pos(1,i) = (j/Nx) + ((1/Nx)*((cODT*vODT -
(Cp(i,j)*vFilm(i,j)))/((Cp(i,j+1)*vFilm(i,j+1)) - (Cp(i,j)*vFilm(i,j)))));
        end


        if eta(j+1) >= pos(1,i) && eta(j) < pos(1,i) %find position of pos
wrt eta

            vFront = zeros(1, Nx - j + 1);
            vFront(2:end) = vFilm(i,j+1:end);
            vFront(1) = (vFront(2) - 1/rhoODT);
            vFrontTest(i) = sum(vFront);



        end

        if pos(1,i) == 0
            vFront = zeros(1,Nx);
            vFront(:) = vFilm(i,:);
            vFrontTest(i) = sum(vFront);
        end




        if Cp(i,j) <= cODT && Cp(i,j+1) >= cODT


            for aj = 1:(floor(Nx*pos(1,i)) - 1)
                nonLayerFilmVol(1,i) = nonLayerFilmVol(1,i) +
VolumeSection(i,aj);
                MpnotFront(1,i) = MpnotFront(1,i) + MpSection;
                MnotFront(1,i) = MnotFront(1,i) + MtotalSection(i,aj);
                nonLayerFilmVoltest(1,i) = nonLayerFilmVol(1,i);

            end



            nonLayerFilmVol(1,i) = nonLayerFilmVol(1,i) + ((pos(1,i) - ((j-
1)/(Nx-1))))*VolumeSection(i,j)*(Nx-1); %Interpolation for bit between last
section and pos
            MnotFront(1,i) = MnotFront(1,i) + ((pos(1,i) - ((j-1)/(Nx-
1))))*MtotalSection(i,j)*(Nx);
            MpnotFront(1,i) = MpnotFront(1,i) + ((pos(1,i) - ((j-1)/(Nx-
1))))*MpSection*(Nx);
            postest(i,j) = pos(1,i) - ((j - 1)/(Nx-1));

            MFront(1,i) = MFilm(1,i) - MnotFront(1,i);
            MpFront(1,i) = Mp0 - MpnotFront(1,i);
```

```
            cFront(1,i) = MpFront(1,i)/MFront(1,i);

            f = fit(etafit(j-1:end,1), Cpfit(j-1:end,i),'poly2'); %fitting to
curve of Cp vs eta from 1 section below pos to 1
            fcoeffs = coeffvalues(f);
            coeff(i,1) = fcoeffs(1);
            coeff(i,2) = fcoeffs(2);
            coeff(i,3) = fcoeffs(3);

            cFront(1,i) = (((coeff(i,1)/3) + (coeff(i,2)/2) + (coeff(i,3))) -
((coeff(i,1)*(pos(1,i))^3/3) + (coeff(i,2)*(pos(1,i))^2/2) +
(coeff(i,3)*pos(1,i))))/(1-pos(1,i));
            VolumeLayer(1,i) = ((1-pos(1,i))*cFront(1,i)/rhoPol)*MFilm(1,i) +
(((1-pos(1,i))*(1-cFront(1,i))*MFilm(1,i)/rhoSol));



        end


    end

          if pos(1,i) == 0
            MFront(1,i) = MFilm(1,i);
            MpFront(1,i) = Mp0;
            %cFront(1,i) = MpFront(1,i)/MFront(1,i);
            cFront(1,i) = w(1,i);
            cFront1(1,i) = cFront(1,i);
                        vFront = zeros(1,Nx);
            vFront(:) = vFilm(i,:);
            vFrontTest(i) = sum(vFront);


            f = fit(etafit(1:end,1), Cpfit(1:end,i),'poly2'); %fitting to
curve of Cp vs eta from 1 section below pos to 1
            fcoeffs = coeffvalues(f);
            coeff(i,1) = fcoeffs(1);
            coeff(i,2) = fcoeffs(2);
            coeff(i,3) = fcoeffs(3);

            cFront(1,i) = ((coeff(i,1)/3) + (coeff(i,2)/2) + (coeff(i,3)));


            VolumeLayer(1,i) = ((1-pos(1,i))*cFront(1,i)/rhoPol)*MFilm(1,i) +
(((1-pos(1,i))*(1-cFront(1,i))*MFilm(1,i)/rhoSol));


          end

            cFrontTest(1,i) = cFront1(1,i) - cFront(1,i);
            totalThickness(1,i) = X(1,i)*100;
```

```
            totalFilmVol(1,i) = MFilm(1,i)*w(1,i)/rhoPol + (MFilm(1,i)*(1-
w(1,i))/rhoSol);
            thicknessFront(1,i) =
(VolumeLayer(1,i))*thickness(1,i)*100/(L*totalFilmVol(1,i));
            debug(1,i) = VolumeLayer(1,i)/totalFilmVol(1,i);


end

%--------------------------------------------------------------------------

%%%%%%%%%%%%%%%%%%%%%%%%%%%%%%%%%%%%%%%%%%%%%%%%%%%%%%%%%%%%%%%%%%%%%%%%%%%
%END OF MAIN FUNCTION
%BEGINNING OF PDE FUNCTIONS
%%%%%%%%%%%%%%%%%%%%%%%%%%%%%%%%%%%%%%%%%%%%%%%%%%%%%%%%%%%%%%%%%%%%%%%%%%%

%%%%%%%%%%%%%%%%%%%%%%%%%%%%%%%%%%%%%%%%%%%%%%%%%%%%%%%%%%%%%%%%%%%%%%%%%%%
%INITIAL CONDITION FUNCTION
%%%%%%%%%%%%%%%%%%%%%%%%%%%%%%%%%%%%%%%%%%%%%%%%%%%%%%%%%%%%%%%%%%%%%%%%%%%
%--------------------------------------------------------------------------
function u0 = DryingSimIC(x)
%--------------------------------------------------------------------------
%Initial conditions for the pdepe function for the differential equation
%--------------------------------------------------------------------------

%at t = 0, c = 1

u0 = 1;


end



%%%%%%%%%%%%%%%%%%%%%%%%%%%%%%%%%%%%%%%%%%%%%%%%%%%%%%%%%%%%%%%%%%%%%%%%%%%
%BOUNDARY CONDITIONS FUNCTION
%%%%%%%%%%%%%%%%%%%%%%%%%%%%%%%%%%%%%%%%%%%%%%%%%%%%%%%%%%%%%%%%%%%%%%%%%%%
function [pl,ql,pr,qr] = DryingSimBC(xl,ul,xr,ur,t)
%----------------------------------------------------------
%Boundary Conditions for the pdepe function
%----------------------------------------------------------
%Neumann boundary condition for the bottom
%Boundary condition from eqn 67 in Vrentas paper for top of film
%D is D/D0 in Vrentas paper

%Time index for Diff
tindex = t/delt + 1;
tindex = int64(tindex);

%at eta = 0
pl = 0;
ql = 1;

if tindex <= texp
```

```
Xstar = a1*exp(b1*t); %scaler of X(tIndex) that is calculated for use in
these equations
dXstardt = a1*b1*exp(b1*t); %scaler of Xt_1D that is used in these equations
else if tindex > texp && tindex <= texp + texp2
Xstar = a2*exp(b2*t); %middle fit
dXstardt = a2*b2*exp(b2*t); %middle fit
    else
Xstar = a3*t^b3 + c3; %3rd fit
dXstardt = a3*b3*t^(b3 - 1); %3rd fit
end


end
Vp = (1-Xstar)/(1-(Xstar*Cmean(1,tindex)));


%at eta = 1
pr = Xstar*dXstardt*(1-Vp*ur);
qr = -Vp;

if ur < 0
   pr = ur;
   qr = 0;
end
end
%%%%%%%%%%%%%%%%%%%%%%%%%%%%%%%%%%%%%%%%%%%%%%%%%%%%%%%%%%%%%%%%%%%%%%%%%%%%%%%
%PDE PARAMETER FUNCTION
%%%%%%%%%%%%%%%%%%%%%%%%%%%%%%%%%%%%%%%%%%%%%%%%%%%%%%%%%%%%%%%%%%%%%%%%%%%%%%%

function [c, f, s] = DryingSimFun(x,t,u,DuDx)
%returns parameters needed by pdepe for calculating concentration profile
%as a function as time, here given by u.
%D is diffusivity ratio
%Time index for Diff

tindex = t/delt + 1;
tfloor = floor(tindex);
tceiling = tfloor + 1;


%Space index for Diff

xindex = x*(Nx-1) + 1;
xfloor = floor(xindex);
xceiling = xfloor + 1;


if tindex <= texp
Xstar = a1*exp(b1*t); %scaler of X(tIndex) that is calculated for use in
these equations
dXstardt = a1*b1*exp(b1*t); %scaler of Xt_1D that is used in these equations
else if tindex > texp && tindex <= texp + texp2
Xstar = a2*exp(b2*t); %middle fit
dXstardt = a2*b2*exp(b2*t); %middle fit
```

```
    else
Xstar = a3*t^b3 + c3; %3rd fit
dXstardt = a3*b3*t^(b3 - 1); %3rd fit
    end
end


%interpolation of Dstar
if xceiling <= Nx && tceiling <= Ntotal
dfloor = Dstar(xfloor,tfloor) + ((Dstar(xceiling,tfloor) -
Dstar(xfloor,tfloor))*((xindex - xfloor)/(xceiling - xfloor)));
dceiling = Dstar(xfloor,tceiling) + ((Dstar(xceiling,tceiling) -
Dstar(xfloor,tceiling))*((xindex - xfloor)/(xceiling - xfloor)));

d = dfloor + ((dceiling - dfloor)*((tindex - tfloor)/(tceiling - tfloor)));

else if xceiling > Nx && tceiling <= Ntotal
        d = Dstar(Nx,tfloor) + ((Dstar(Nx,tceiling) -
Dstar(Nx,tfloor))*((tindex - tfloor)/(tceiling - tfloor)));
    else if tceiling > Ntotal && xceiling <= Nx
        d = Dstar(xfloor,Ntotal) + ((Dstar(xceiling,Ntotal) -
Dstar(xfloor,Ntotal))*((xindex - xfloor)/(xceiling - xfloor)));
        else
        d = Dstar(Nx,Ntotal);
        end
    end
end

c = Xstar^2;
f = d*DuDx;
s = x*Xstar*dXstardt*DuDx;

end


end
```

Calculates the concentration profile of the film for systems that have slow diffusivity

```
function [Cp,pos,thicknessFront,ca,cFront,totalThickness,u,Cint,M] =
DryingSimPdeSlowDiff(system, filename, sheet, xlRange, fitRange,fitRange2)

%------------------------------
%Drying simulation of BCP films
%------------------------------

%Uses pdepe with various functions to solve differential equation

%Import Drying Data
%Drying Data contains time, calculated thickness, and overall weight
```

```
%fraction in rows 1, 2, and 3 respectively
%fitRange is the range over which X is an exponential function e.g. B3:BE3
data = xlsread(filename,sheet,xlRange);
datafit1 = xlsread(filename,sheet,fitRange);
datafit2 = xlsread(filename,sheet,fitRange2);


%Declare Variables, temperature is in C, rho is in kg/m3, TO is the initial
%film temp, tnum is the number of time steps, xnum is the number of
%datapoints in the finite difference method,
%t is the dimensionless time, dn is deltaEta i.e. the eta step distance
%(if there are 4 points, deta would be 0.333), dt is the dimensionless time
%step
%c0 is the inital dimensionless solvent mass density (should be 1, as the
%dimensionless solvent mass density is c = p/p0
%Nt = length(data); %SIMP? - is equal to the number of time steps -
simplified by making time steps equal to the number of time points in the
data
Nt = length(datafit1); %Modified so that X is fit to a function to simplify
calculations.
Nt2 = length(datafit2);
Ntotal = length(data); %total length of data so that further fitting can
commence after Nt
Nx = 50;
tfinal = Nt - 1;%Debug value of time points for matrix calc
tfinal2 = Nt2 - 1;
texp = Nt;%time point up to which X is exponential
texp2 = Nt2;%time point from 1st to 2nd exponential
maxiter = 200; %maximum number of iterations
t = zeros(1,Ntotal);
dn = 1/(Nx - 1);
dt = 1/(Nt - 1);
c0 = 1;
cODT = 0.43; %ODT concentration as determined by rheology (0.59 for D1161,
0.43 for SB)
pos = ones(1,Ntotal); %pos is a 1D array showing the values for eta of the
ordering front as determined by CODT at each time point


m = 0; %geometry for pdepe (0 is for cartesian, 1 is for cylindrical
coordinates, 2 is for spherical coordinates
a1 = 0; %coefficient fitting parameter for Xfit = ae^bx
b1 = 0; %coefficient fitting parameter for Xfit = ae^bx

%Solvent Variables, Dp is the diffusion coefficient in the film, D0 is the
%initial diffusion coefficient in the film (based on self-diffusion of
%toluene in PS from http://pubs.acs.org/doi/pdf/10.1021/ma00200a025 paper)
%Dsurf is D/D0 at the upper boundary of the film D0 in paper is 16.9E-10
%Dstar is D/D0
%B is the exponent for calculating Dstar
%D0 = 7.66 E-12 for D1161, 0.246 E-10 for SB

D0 = 0.246 *(10^(-10));
Dsurf = ones(1,Ntotal);
Dstar = ones(Nx,Ntotal);
```

```
%initialize arrays from imported
fitLength = length(data);
datatime = data(1,:);
thickness = data(11,1:fitLength)*10^(-2);
wtFracMean = data(2,:);
thicknessNoFit = data(11,fitLength + 1:end)*10^(-2);


%Polymer Variables in different systems
%polymer density is in SI units
if strcmp(system,'SBT')
    rhoSol = 866.9;
    rhoPol = 965;
    D0 = 0.246 *(10^(-10));
    cODT = 0.43; %ODT concentration as determined by rheology (0.59 for
D1161, 0.43 for SB)
end

if strcmp(system,'SBST')
    rhoSol = 866.9;
    rhoPol = 0.94;
    D0 = 0.0219*(10^(-10));
    cODT = 0.42;
end

if strcmp(system,'SIST')
    rhoSol = 866.9;
    rhoPol = 920;
    D0 = 6.49*10^(-12);
    cODT = 0.59;
end

if strcmp(system, '2140')
    rhoSol = 866.9;
    rhoPol = 1105.6;
    D0 = 0.91 * (10^(-10));
    cODT = 0.53;
end

if strcmp(system, '2250')
    rhoSol = 866.9;
    rhoPol = 1113.0;
    D0 = 0.032 * (10^(-10));
    cODT = 0.51;
end

if strcmp(system, '4285')
   rhoSol = 866.0;
   rhoPol = 1131;
   D0 = 0.238 * (10^(-10));
   cODT = 0.41;
end

if strcmp(system,'SBCyc')
```

```
    rhoSol = 779.0;
    rhoPol = 965;
end

%Film Variables TP is the dimensionless temperature of the film, w0 is the
initial polymer wt frac of the film,
%w is average polymer wt frac of the film, X = X* or the dimensionless upper
boundary of the film,
% eta is the dimensionless thickness, L is the initial upper (currently
assuming 400microns),
%boundary, Cpp is the Cp of the film, Cp0 is the initial Cp of the film
(units of J/kgK, init is roughly the Cp of PE (2.3)),
%rhoP is the density of the film,
%while rhoP0 is the initial density of the film. dcdn is dc/deta
%Cmean is the average dimensionless SOLVENT mass density. Is an array w/
%time points - is wtFracMean * rhoFilm
%rhoPMean is the average mass density of SOLVENT
%rhoFilm0 is the initial overall TOTAL density of the FILM
%rhoFilm is  the overall TOTAL density of the FILM - is an array wrt time of
w0 = wtFracMean(1,1); %init POLYMER wt fraction
w = wtFracMean(1,:); %POLYMER wt fraction

%Variables for mean concentration calculation
MFilm = zeros(1,Ntotal); %calculated mass (arbitrary units) of the film using
Mp0 (init polymer mass if total mass/volume = 1 (arbitrary units))
Mp0 = w0; %initial polymer mass of the entire film if initial volume and mass
= 1, arbitrary units
MpSection = Mp0/(Nx-1); %initial polymer mass of each film section if initial
volume/mass = 1, arbitrary units. THIS IS CONSTANT AS THE SOLVENT IS THE ONLY
THING ASSUMED TO MOVE
MtotalSection = zeros(Ntotal,Nx - 1); %total polymer mass of a film section
of initial volume = 1, arbitrary units. Is MpSection/Cp
VolumeFilm0 = 1; %inital film volume, arbitrary units
VolumeSection0 = 1/(Nx - 1); %inital volume of a section
VolumeSection = zeros(Ntotal,Nx - 1); %matrix of section volumes
VolumeSectionSolvent = zeros(Ntotal, Nx-1); %matrix of init section volume -
polymer section volume (i.e. the volume of solvent)
rhoFilm0 = 1/((w0/rhoPol) + ((1-w0)/rhoSol));
rhoFilm = zeros(1,Ntotal);
rhoFilm1 = zeros(Nx,Ntotal); %density of film at different points vs time

%Variables for solving the differential equations
Xnums = zeros(tfinal,1); %THIS Nx vs Nt ORDERING IS FLIPPED FOR FITTING
Xnumsrest2 = zeros(Ntotal - tfinal - tfinal2,1); %fitting for rest of
numbers. Nx vs Nt is flipped for fitting.
Xnumsrest1 = zeros(tfinal2,1);
X = zeros(1,Ntotal); %TRANSPOSE OF X. THIS Nx vs Nt ORDERING IS FLIPPED SO
THAT THE FIT WILL WORK.
Xrest = zeros(1,Ntotal - tfinal,1);
L = data(11,1)*10^(-2);
eta = zeros(1,Nx);

V = 0.001154; %PARTIAL SPECIFIC VOLUME, Units are in m3/kg
rhoP = zeros(Nx,Ntotal); %SOLVENT mass density
rhoP0 = rhoFilm0 * (1-w0); %rhoP0 is calculated using the assumption that the
volumes add (vE = 0)
```

```
%Turns the total specific volume of solvent into average partial specific
%volume AT THE INITIAL POINT

        V = V * (1-w(1,1));

for j = 1:Ntotal
    rhoFilm(1,j) = (1/((w(j)/rhoPol) + ((1-w(j))/rhoSol)));
    Cmean(1,j) = (1-w(j))*rhoFilm(1,j)/rhoP0;
end

%Boundary Conditions
%time boundary conditions
w(1,1) = w0;
X(1,1) = 1;
rhoP(:,1) = rhoP0;


%Defining the points in dimensionless x (i.e. eta)
for i = 1:(Nx)
    %eta(i) = (i - 1)/(Nx - 1);
end

eta = linspace(0,1,Nx);
x = eta;
xmesh = eta;

%Defining the points in dimensionless time
for i = 1:(Ntotal)
    t(i) = D0*datatime(i)/L^2;
end

%delt is the difference between time points
delt = t(2) - t(1);

tmatrixinit(:,1) = t(1:tfinal);
tmatrix(:,1) = t(1:end);

tmatrix2(:,1) = tmatrix(tfinal+1:tfinal2+tfinal + 1,1);

tmatrixrest(:,1) = t(tfinal2 + tfinal + 3: end);
tspan = t;

%Finite difference method for the unsteady state nonlinear partial
%differential equation for concentration wrt eta

%Initial guesses for c - initial guess is 0.99 in a step function after
%initial time, as c is a dimensionless solvent mass density
%Average
u = zeros(Ntotal,Nx);

%declares the Cint matrix
Cint = zeros(1,Ntotal);
```

```
%This portion fits a curve to part of the exponential fn and calculates the
%derivative. The variables a and b are used for the coefficients in front
%of and in the exponent, respectively. The region to be fit was decided
%earlier within the excel file as the max number of pts before R^2 begins
%to drop rapidly. This region will be fit later using a different function.
Xnums(1:tfinal,1) = thickness(1:tfinal)/L;
e = length(thickness);

Xnumsrest2 = ones(e - Nt - Nt2 - 1,1);
for i = Nt+Nt2+1:e
   Xnumsrest2(i - Nt - Nt2,1) = thickness(i)/L;
end




for i = Nt+1:Nt+Nt2
   Xnumsrest1(i-Nt,1) =  thickness(i)/L;
end

Xfit = fit(tmatrixinit,Xnums,'exp1');
Xfitrest1 = fit(tmatrix2,Xnumsrest1,'exp1');
Xfitrest2 = fit(tmatrixrest,Xnumsrest2,'power2');
Xcoeffs = coeffvalues(Xfit); %coefficients for the exponential fit
a1 = Xcoeffs(1);
b1 = Xcoeffs(2);
X = a1*exp(t.*b1);
Xt_1D = b1*a1*exp(t.*b1); %dX/dt, calculated from the derivative of the fited
exponential fn

Xcoeffs = coeffvalues(Xfitrest1);
a2 = Xcoeffs(1);
b2 = Xcoeffs(2);
X(tfinal+1:tfinal + Nt2) = a2*exp(t(tfinal + 1:tfinal+Nt2).*b2);
Xt_1D(tfinal+2:tfinal + Nt2) = b2*a2*exp(t(tfinal+2:tfinal+Nt2).*b2);

Xcoeffs = coeffvalues(Xfitrest2);
a3 = Xcoeffs(1);
b3 = Xcoeffs(2);
c3 = Xcoeffs(3);
X(tfinal+1+Nt2:end) = a3*(t(tfinal+Nt2 + 1:end).^b3) + c3;
Xt_1D(tfinal+Nt2+1:end) = b3*a3*(t(tfinal + Nt2 +1:end).^(b3 - 1));

%Initial guesses for D, Assuming that D = D0
%Dsurf is the nondimensionalized D (Dp/D0) at the surface. The initial
%guess is 1.
%dDdc is the partial derivative d/dc(Dp/D0) ie the partial derivative of
%the nondimensionalized D (Dp/D0) with respect to concentration. The initial
%guess is 0.
%dDdn is the partial derivative d/dn(Dp/D0), initial guess is 0.
%Uint is a placeholder that will be integrated into Cint that will be
%compared to Cmean to solve for D

excess = ones(1,Ntotal);
```

```
%At t = 0, c is flat, so dc/deta = 0, and d2c/deta2 = 0
%At eta = 0, dc/deta = 0

%Calculating the c matrix
%Go through iterations at each point in order to back calculate X* and D
%and c at eta = 1, etc

%Tested Heat Conduction Equation by assuming a c of 1 and dropping to a
%c of 0.1

%Will do a series of iterations of pdepe so that the diffusivity can be
%calculated from the implied flux due to the weight data.

%DryingSimFun returns the parameters C, F, and S needed by pdepe to do its
%job

excessLast = 1000*ones(1,Ntotal);

for iter = 1:maxiter

    u = ones(Ntotal,Nx);
    Cint(1,1) = 1;
    sol = 1;
    sol = pdepe(m,@DryingSimFun,@DryingSimIC,@DryingSimBC,xmesh,tspan);
    %Extract the first solution component as u
    u = sol(:,:,1);

    %Calculates Cp from u data
        for i = 1:Ntotal
        for j = 1:Nx
            if strcmp(system,'SBT')
                Cp(i,j) = -0.069536255*u(i,j)^2 - 0.73027205*u(i,j) +
0.99967833;
                rhoFilm1(j,i) = -80.145467*u(i,j) + 965.000;
                vFilm(i,j) = 1/rhoFilm1(j,i); %specific volume at position in
film
                rhoODT = 906.526971219646; %from CODT = 0.43
                vODT = 1/rhoODT;


            end

            if strcmp(system,'SBST')
                Cp(i,j) = -0.052328478*u(i,j)^2 - 0.74753636*u(i,j) +
0.99981813;
                rhoFilm1(j,i) = -59.417833*u(i,j) + 940.000;
                vFilm(i,j) = 1/rhoFilm1(j,i);
                rhoODT = 908.5877; %from CODT = 0.41
                vODT = 1/rhoODT;
            end

            if strcmp(system,'SIST')
```

```
                Cp(i,j) = -0.03832639*u(i,j)^2 - 0.7620008*u(i,j) +
0.9999129;
                rhoFilm1(j,i) = -43.001698*u(i,j) + 920.000;
                vFilm(i,j) = 1/rhoFilm1(j,i); %specific volume at position in
film
                rhoODT = 897.461490247797; %from CODT = 0.59
                vODT = 1/rhoODT;
            end

            if strcmp(system,'SBC')
                Cp(i,j) = -0.1463536*u(i,j)^2 - 0.7186362*u(i,j) + 0.9978279;
                rhoFilm1(j,i) = -142.98058*u(i,j) + 940.000;
                vFilm(i,j) = 1/rhoFilm1(j,i); %specific volume at position in
film
            end

            if strcmp(system, '2140')
                Cp(i,j) = -0.16135943*u(i,j)^2 - 0.63906933*u(i,j) +
0.99825895;
                rhoFilm1(j,i) = -200.31319*u(i,j) + 1105.6;
                vFilm(i,j) =  1/rhoFilm1(j,i);
                rhoODT = 983.711263810985;
                vODT = 1/rhoODT;
            end

            if strcmp(system, '2250')
                Cp(i,j) = -0.16019632*u(i,j)^2 - 0.62881622*u(i,j) +
0.99861424;
                rhoFilm1(j,i) = -204.28343*u(i,j) + 1113;
                vFilm(i,j) =  1/rhoFilm1(j,i);
                rhoODT = 977.0839979;
                vODT = 1/rhoODT;
            end

            if strcmp(system, '4285')
                Cp(i,j) = -0.17446112*u(i,j)^2 - 0.622288644*u(i,j) +
0.99825999;
                rhoFilm1(j,i) = -221.67515*u(i,j) + 1131;
                vFilm(i,j) =  1/rhoFilm1(j,i);
                rhoODT = 958.683568;
                vODT = 1/rhoODT;
            end

        end
        end

     for i = 1:Ntotal

         for j = 1:Nx-1

    MtotalSection(i,j) = MpSection*2/(Cp(i,j) + Cp(i,j+1));

         end
```

```
        MFilm(1,i) = Mp0/w(1,i);
    end
    for i = 1:Ntotal
        ca(i) = mean(u(i,:));

    end
    plot(vFilm)
    hold on
    plot(ca)
    hold on
    plot(Cint)

   Cint(1,:) = MFilm(1,:);

   for i = 1:Ntotal
      M(1,i) = w0/w(1,i);
      M(1,i) = ca(1,i);
   end


   %Excess is the difference between the mean and the integrated mean
   %from the data

   excess(1,:) = Cint(1,:) - M(1,:);
   exc = excess;

   if iter == 1
      exInit = excess;
   end

   %Changes the diffusivity at the surface based on the current
   %concentrations
   for j = 2:Ntotal - 1
       if excess(1,j) >= 0.005 && Dsurf(1,j) >= 0.99*Dsurf(1,j+1) &&
excessLast(1,j) > excess(1,j) %0.99*Dsurf(1,j+1)
           Dsurf(1,j) = Dsurf(1,j-1)*0.99;

       else if excess(1,j) <= -0.005 && excessLast(1,j) < excess(1,j) &&
Dsurf(1,j) >= 1.01*Dsurf(1,j+1)%1.01*Dsurf(1,j+1)
               Dsurf(1,j) = Dsurf(1,j)*1.01;


           end
       end
   end

   if excess(1,Ntotal) >= 0.005 && excessLast(1,Ntotal) > excess(1,Ntotal)
       Dsurf(1,Ntotal) = Dsurf(1,Ntotal)*0.99;

   else if excess(1,Ntotal) <= -0.005 && excessLast(1,Ntotal) <
excess(1,Ntotal)
              Dsurf(1,Ntotal) = Dsurf(1,Ntotal)*1.01;

       end
```

```
    end


    %Diffusivity interpolation - logarithmic diffusivity wrt c
    %logD1 = logD0 + B(C1-C0)




    for j = 2:Ntotal
        %Calculates exponent coefficient B from D0 ASSUMES THAT
        %THERE IS NO CHANGE IN MODEL BEFORE VS AFTER ODT

        %Also calculates the derivative
        B(1,j) = (log(Dsurf(1,j)))/(u(j,Nx) - 1);

        for i = 1:Nx

            Dstar(i,j) = Dsurf(1,j)*exp(B(1,j)*(u(j,i) - u(j,Nx)));

        end
    end

    excessLast = excess;

end


%Calculates pos from Cp data, calculates thicknessFront
%totalFilmVol and nonLayerFilmVol are the
totalFilmVol = zeros(1,Ntotal);
nonLayerFilmVol = zeros(1,Ntotal);

%Variables for calculating the wt fraction of the front. MFront is total
%mass of front, and MpFront is the polymer mass of the front, and MnotFront
%and MpnotFront are mass not in the front. cFront is the wt fraction of
%polymer in the front
MFront = zeros(1,Ntotal);
MpFront = zeros(1,Ntotal);
MnotFront = zeros(1,Ntotal);
MpnotFront = zeros(1,Ntotal);
cFront = zeros(1,Ntotal);
cFront1 = zeros(1,Ntotal);
coeff = zeros(Ntotal,3);
etafit(:,1) = linspace(0,1,Nx);
Cpfit = Cp';
VolumeLayer = zeros(1,Ntotal);
debug = zeros(1,Ntotal);

%Calculates pos for situations before the ordering front forms and after it
%reaches the bottom of the film

for i = 1:Ntotal
```

```
            if Cp(i,1) > cODT
                pos(1,i) = 0;
                thicknessFront(1,i) = thickness(1,i)*100/L;
                cFront(1,i) = w(1,i);

                else if Cp(i,Nx) < cODT
                   pos(1,i) = 2;
                   thicknessFront(1,i) = 0;
                end

            end


end



%Here it is assumed that the polymer in a giver section doesn't move and that
%the volume change is due entirely to lost solvent. The inital volume is
%assumed to be 1(arbitrary units), so that Mp0 = w0/Nx - 1. Mpsection = M
%VolumeSection0 * rhoFilm(1,1)* (Nx-1) is a constant that's used to make
%VolumeFilm0 = 1
for i = 1:Ntotal
    for j = 1:Nx - 1

        %Calculates the total mass of each section, along with the total
volume of each section
        VolumeSectionSolvent(i,j) = ((MtotalSection(i,j) - MpSection)/rhoSol)
* VolumeSection0 * rhoFilm0 * (Nx - 1);
        VolumeSection(i,j) = (MpSection/rhoPol)* VolumeSection0 * rhoFilm0 *
(Nx - 1) + VolumeSectionSolvent(i,j);

        if Cp(i,j) <= cODT && Cp(i,j+1) >= cODT

            %interpolation to find eta(ODT) at each time point
            pos(1,i) = (j/Nx) + ((1/Nx)*((cODT*vODT -
(Cp(i,j)*vFilm(i,j)))/((Cp(i,j+1)*vFilm(i,j+1)) - (Cp(i,j)*vFilm(i,j)))));
        end


        if eta(j+1) >= pos(1,i) && eta(j) < pos(1,i) %find position of pos
wrt eta

            vFront = zeros(1, Nx - j + 1);
            vFront(2:end) = vFilm(i,j+1:end);
            vFront(1) = (vFront(2) - 1/rhoODT);
            vFrontTest(i) = sum(vFront);



        end

        if pos(1,i) == 0
```

```
            vFront = zeros(1,Nx);
            vFront(:) = vFilm(i,:);
            vFrontTest(i) = sum(vFront);
        end




        if Cp(i,j) <= cODT && Cp(i,j+1) >= cODT


            for aj = 1:(floor(Nx*pos(1,i)) - 1)
                nonLayerFilmVol(1,i) = nonLayerFilmVol(1,i) +
VolumeSection(i,aj);
                MpnotFront(1,i) = MpnotFront(1,i) + MpSection;
                MnotFront(1,i) = MnotFront(1,i) + MtotalSection(i,aj);
                nonLayerFilmVoltest(1,i) = nonLayerFilmVol(1,i);

            end



            nonLayerFilmVol(1,i) = nonLayerFilmVol(1,i) + ((pos(1,i) - ((j-
1)/(Nx-1))))*VolumeSection(i,j)*(Nx-1); %Interpolation for bit between last
section and pos
            MnotFront(1,i) = MnotFront(1,i) + ((pos(1,i) - ((j-1)/(Nx-
1))))*MtotalSection(i,j)*(Nx);
            MpnotFront(1,i) = MpnotFront(1,i) + ((pos(1,i) - ((j-1)/(Nx-
1))))*MpSection*(Nx);
            postest(i,j) = pos(1,i) - ((j - 1)/(Nx-1));

            MFront(1,i) = MFilm(1,i) - MnotFront(1,i);
            MpFront(1,i) = Mp0 - MpnotFront(1,i);
            cFront(1,i) = MpFront(1,i)/MFront(1,i);

            f = fit(etafit(j-1:end,1), Cpfit(j-1:end,i),'poly2'); %fitting to
curve of Cp vs eta from 1 section below pos to 1
            fcoeffs = coeffvalues(f);
            coeff(i,1) = fcoeffs(1);
            coeff(i,2) = fcoeffs(2);
            coeff(i,3) = fcoeffs(3);

            cFront(1,i) = (((coeff(i,1)/3) + (coeff(i,2)/2) + (coeff(i,3))) -
((coeff(i,1)*(pos(1,i))^3/3) + (coeff(i,2)*(pos(1,i))^2/2) +
(coeff(i,3)*pos(1,i))))/(1-pos(1,i));
            VolumeLayer(1,i) = ((1-pos(1,i))*cFront(1,i)/rhoPol)*MFilm(1,i) +
(((1-pos(1,i))*(1-cFront(1,i))*MFilm(1,i)/rhoSol));



        end
```

```
    end

            if cFront(1,i) < w(1,i) && i>15
                thicknessFront(1,i) = thickness(1,i)*100/L;
                pos(1,i) = 0;
            end

          if pos(1,i) == 0
            MFront(1,i) = MFilm(1,i);
            MpFront(1,i) = Mp0;
            cFront(1,i) = w(1,i);
            cFront1(1,i) = cFront(1,i);
            vFront = zeros(1,Nx);
            vFront(:) = vFilm(i,:);
            vFrontTest(i) = sum(vFront);



            VolumeLayer(1,i) = ((1-pos(1,i))*cFront(1,i)/rhoPol)*MFilm(1,i) +
(((1-pos(1,i))*(1-cFront(1,i))*MFilm(1,i)/rhoSol));


          end

            cFrontTest(1,i) = cFront1(1,i) - cFront(1,i);
            totalThickness(1,i) = X(1,i)*100;
            totalFilmVol(1,i) = MFilm(1,i)*w(1,i)/rhoPol + (MFilm(1,i)*(1-
w(1,i))/rhoSol);
            thicknessFront(1,i) =
(VolumeLayer(1,i))*thickness(1,i)*100/(L*totalFilmVol(1,i));
            debug(1,i) = VolumeLayer(1,i)/totalFilmVol(1,i);



end

%%%%%%%%%%%%%%%%%%%%%%%%%%%%%%%%%%%%%%%%%%%%%%%%%%%%%%%%%%%%%%%%%%%%%%%%%%%%%%%
%END OF MAIN FUNCTION
%BEGINNING OF PDE FUNCTIONS
%%%%%%%%%%%%%%%%%%%%%%%%%%%%%%%%%%%%%%%%%%%%%%%%%%%%%%%%%%%%%%%%%%%%%%%%%%%%%%%

%%%%%%%%%%%%%%%%%%%%%%%%%%%%%%%%%%%%%%%%%%%%%%%%%%%%%%%%%%%%%%%%%%%%%%%%%%%%%%%
%INITIAL CONDITION FUNCTION
%%%%%%%%%%%%%%%%%%%%%%%%%%%%%%%%%%%%%%%%%%%%%%%%%%%%%%%%%%%%%%%%%%%%%%%%%%%%%%%
%--------------------------------------------------------------------------
function u0 = DryingSimIC(x)
%--------------------------------------------------------------------------
%Initial conditions for the pdepe function for the differential equation
%--------------------------------------------------------------------------

%at t = 0, c = 1

u0 = 1;
```

```
end



%%%%%%%%%%%%%%%%%%%%%%%%%%%%%%%%%%%%%%%%%%%%%%%%%%%%%%%%%%%%%%%%%%%%%%%%%%%%%%%
%BOUNDARY CONDITIONS FUNCTION
%%%%%%%%%%%%%%%%%%%%%%%%%%%%%%%%%%%%%%%%%%%%%%%%%%%%%%%%%%%%%%%%%%%%%%%%%%%%%%%
function [pl,ql,pr,qr] = DryingSimBC(xl,ul,xr,ur,t)
%-------------------------------------------------------
%Boundary Conditions for the pdepe function
%-------------------------------------------------------
%Neumann boundary condition for the bottom
%Boundary condition from eqn 67 in Vrentas paper for top
%D is D/D0 in Vrentas paper

%Time index for Diff
tindex = t/delt + 1;
tindex = int64(tindex);

%at eta = 0
pl = 0;
ql = 1;

if tindex <= texp
Xstar = a1*exp(b1*t); %scaler of X(tIndex) that is calculated for use in
these equations
dXstardt = a1*b1*exp(b1*t); %scaler of Xt_1D that is used in these equations
else if tindex > texp && tindex <= texp + texp2
Xstar = a2*exp(b2*t); %middle fit
dXstardt = a2*b2*exp(b2*t); %middle fit
    else
Xstar = a3*t^b3 + c3; %3rd fit
dXstardt = a3*b3*t^(b3 - 1); %3rd fit
end



end
Vp = (1-Xstar)/(1-(Xstar*Cmean(1,tindex)));


%at eta = 1
pr = Xstar*dXstardt*(1-Vp*ur);
qr = -Vp;

if ur < 0
   pr = ur;
   qr = 0;
end
end
%%%%%%%%%%%%%%%%%%%%%%%%%%%%%%%%%%%%%%%%%%%%%%%%%%%%%%%%%%%%%%%%%%%%%%%%%%%%%%%
%PDE PARAMETER FUNCTION
%%%%%%%%%%%%%%%%%%%%%%%%%%%%%%%%%%%%%%%%%%%%%%%%%%%%%%%%%%%%%%%%%%%%%%%%%%%%%%%
```

```
function [c, f, s] = DryingSimFun(x,t,u,DuDx)
%returns parameters needed by pdepe for calculating concentration profile
%as a function as time, here given by u.
%D is diffusivity ratio
%Time index for Diff

tindex = t/delt + 1;
tfloor = floor(tindex);
tceiling = tfloor + 1;


%Space index for Diff

xindex = x*(Nx-1) + 1;
xfloor = floor(xindex);
xceiling = xfloor + 1;


if tindex <= texp
Xstar = a1*exp(b1*t); %scaler of X(tIndex) that is calculated for use in
these equations
dXstardt = a1*b1*exp(b1*t); %scaler of Xt_1D that is used in these equations
else if tindex > texp && tindex <= texp + texp2
Xstar = a2*exp(b2*t); %middle fit
dXstardt = a2*b2*exp(b2*t); %middle fit
    else
Xstar = a3*t^b3 + c3; %3rd fit
dXstardt = a3*b3*t^(b3 - 1); %3rd fit
    end
end


%interpolation of Dstar
if xceiling <= Nx && tceiling <= Ntotal
dfloor = Dstar(xfloor,tfloor) + ((Dstar(xceiling,tfloor) -
Dstar(xfloor,tfloor))*((xindex - xfloor)/(xceiling - xfloor)));
dceiling = Dstar(xfloor,tceiling) + ((Dstar(xceiling,tceiling) -
Dstar(xfloor,tceiling))*((xindex - xfloor)/(xceiling - xfloor)));

d = dfloor + ((dceiling - dfloor)*((tindex - tfloor)/(tceiling - tfloor)));

else if xceiling > Nx && tceiling <= Ntotal
        d = Dstar(Nx,tfloor) + ((Dstar(Nx,tceiling) -
Dstar(Nx,tfloor))*((tindex - tfloor)/(tceiling - tfloor)));
    else if tceiling > Ntotal && xceiling <= Nx
        d = Dstar(xfloor,Ntotal) + ((Dstar(xceiling,Ntotal) -
Dstar(xfloor,Ntotal))*((xindex - xfloor)/(xceiling - xfloor)));
        else
        d = Dstar(Nx,Ntotal);
        end
    end
end
```

```
c = Xstar^2;
f = d*DuDx;
s = x*Xstar*dXstardt*DuDx;



end

end
```

Code that inputs data from Excel file that was produced earlier by `DataWriteIq2LSLarge` and exports it so that it can be analyzed.

```
function datafileEr = DataReadEr(filein, lowangle, timestart, range)

%------------------------------------------------------------------------
%This function reads normalized Excel compiled files and outputs arrays
%for data analysis
%------------------------------------------------------------------------

%timestart is an integer that lists the number of the datapoint in the
%spreadsheet where the ordering begins

%imports the file
datain = xlsread(filein, 'Sheet1', range);


%--------------------
%Variable Declaration
%--------------------

%gives the low angle of the angle range of the data (200 for 200-250,
%210 for 210-240, etc) determines which row of the array is taken
angle = 0;

%number of datapoints after start of ordering
l = length(datain) - timestart;

%output that lists time, wt frac and integrated Iq2 in that order
datafileEr = zeros(5,l);

%sets variable for the time step from the second column in the time row
time = datain(1,:);

%sets variable for the wt data and the weight error data
wtfrac = datain(2,:);
pe = datain(5,:);
ne = datain(6,:);

%C-C(ODT)
wtfracODT = zeros(l);
```

```
%t-t(ODT)
timeODT = zeros(l);

%data from ODT
dataODT = zeros(l);



%sets variables for angle specific datasets
if lowangle == 195;
    intdata = datain(3,:);
end

if lowangle == 210;
    intdata = datain(4,:);
end


%puts wt frac, time values, and integrated date into wtfracODT and timeODT
%and dataODT and assigns values for the output variable (datafile)
for i = 1:l
    wtfracODT(i) = wtfrac(i + timestart - 1);
    timeODT(i) = time(i + timestart - 1);
    dataODT(i) = intdata(i + timestart - 1);
    peODT(i) = pe(i + timestart - 1);
    neODT(i) = ne(i + timestart - 1);

    datafileEr(1,i) = timeODT(i);
    datafileEr(2,i) = wtfracODT(i);
    datafileEr(3,i) = dataODT(i);
    datafileEr(4,i) = peODT(i);
    datafileEr(5,i) = neODT(i);

end
end
```

Code that performs the solvent partitioning and uses it to normalize the integrated data.

```
function [output,pos,wtFront,Vol,wtfrac,divisor,wtPhaseTotal1,wtPhaseTotal2]
= SolPartDryingPDI(system, filein, lowangle, timestart, range, fitRange,
fitRange2)

%-------------------------------------------------------------------------
%This function analyzes the data using F-H theory to determine the curve of
%phi with the solvent partitioning. It also outputs to Sheet2 of the input
%file
%-------------------------------------------------------------------------

%Import Data
datafile = DataReadEr(filein, lowangle, timestart, range);
```

```
%Import Drying Model
[Cp, pos, thicknessFront,ca,wtFront,totalThickness] = DryingSimPde(system,
filein, 'Sheet1', range, fitRange, fitRange2);


%Variable declaration
l = length(datafile);

%length and width of Cp calculated from drying model
[tIndexCp, xIndexCp] = size(Cp);

%variable average
ave = 1;

%Densities
%RhoS is the styrene density, etc
RhoSt = 1.07;
RhoBu = 0.915;
RhoIs = 0.913;
RhoTo = 0.867;
RhoCh = 0.778;
RhoPMMA = 1.18;
RhoPBA = 1.087;

%RhoPMMA
%RhoPBA

%Electron Densities
edSt = 90700000000;
edBu = 93500000000;
edIs = 94100000000;
edTo = 91500000000;
edCh = 96200000000;
edPMMA = 91000000000;
edPBA = 92100000000;

%Molecular Weights
MSt = 104.16;
MBu = 54.1;
MIs = 68.12;
MTo = 92.15;
MCh = 84.16;
MPMMA = 100.11;
MPBA = 128.16;
%Declaring the densities of the various blocks that will be used in the
%actual calculations. Block 1 is the structure forming block. For instance,
%for SBS, Rho1 would be the density of styrene, etc.
Rho1 = 0;
Rho2 = 0;
RhoS = 0;

%Declaring the densities, specific volumes, and the solvent partitioning
coeff of the various phases to be used in the actual
%calculations. Block 1 is the structure forming block. For example, for
%SBS, RhoPhase1 would be the phase density of styrene, etc. Part uses
```

```
%row 1 for the partitioning into phase 1 and row 2 for partitioning into
%phase 2. Only one array is used to allow for easy debugging.
RhoPhase1 = zeros(1,l);
RhoPhase2 = zeros(1,l);
vPhase1 = zeros(1,l);
vPhase2 = zeros(1,l);
wtPhaseTotal1 = zeros(1,l);
wtPhaseTotal2 = zeros(1,l);
Part = zeros(2,l);

%Declaring Ns, X1Ns and X2Ns, rN1, and rN2. These reperesnt the number of
solvent
%molecules used in the FH theory
X1Ns = zeros(1,l);
X2Ns = zeros(1,l);
Ns = zeros(1,l);
rN1 = zeros(1,l);
rN2 = zeros(1,l);

%Declaring the electron densities of the two phases and the difference
edPhase1 = zeros(1,l);
edPhase2 = zeros(1,l);
delEdSq = zeros(1,l);

%Declaring the phase volumes and the volume fractions
v1 = zeros(1,l);
v2 = zeros(1,l);
Phi1 = zeros(1,l);
Phi2 = zeros(1,l);

%Declaring the total volume, the normalized total volume of ordered phase.
%The output array is also declared
Vol = zeros(1,l);
NormVol = zeros(1,l);
output = zeros(7,l);

%Declaring the molecular weights that will be used in actual calculations.
%Here M1 is the molecular weight of the structure forming block, and MS is
%the molecular weight of the solvent
M1 = 0;
M2 = 0;
MS = 0;

%Declaring the segment lengths and block fraction. Here, the structure
forming
%block is 1, so for SBS, r1 would be the number of repeat units in the
%styrene blocks (both of them combined). f is the weight fraction of block 1.
r1 = 0;
r2 = 0;
f = 0;

%Declaring electron densities that will be used in actual calculations. The
%phase forming block is 1, so for SBS, ed1 would be the electron density of
%the styrene block. edsol is the electron density of the solvent
edsol = 0;
```

```
ed1 = 0;
ed2 = 0;

%Chi Interaction Parameters
%ChiST is the styrene-toluene interaction, etc
%PBA has a delta of 18.5 MPa^1/2, and PMMA has one of 19.0 MPa^1/2
ChiST = 0.3469;
ChiBT = 0.4018;
ChiIT = 0.4647;
ChiBC = 0.3439;
ChiSC = 0.4821;
ChiPMMAT = 0.3676;
ChiPBAT = 0.3439;


%Declaring chi interaction parameters
%Chi1 is the interaction of the solvent with the structure forming block
Chi1 = 0;
Chi2 = 0;

%Pulling wt, time and integrated data from the datafile and creating the
%array for the solvent weight fractions
time = datafile(1,:);
wtfrac = datafile(2,:);
data = datafile(3,:);
perrorfrac = datafile(4,:);
nerrorfrac = datafile(5,:);
solfrac = zeros(1,l);


%Creating an array for the last 50 or so values of the dataset. This will
%be used to normalize the data
aveset = zeros(1,50);

%sets parameter values for a given system
if strcmp(system,'SBT')

    cODT = 0.43;
    %num fractions -> x_tri = 0.1156, x_di = 0.8844
    %wt fractions -> wtri = 0.2309, wdi = 0.7691
    %wt fractions
    wtri = 0.2309;
    wdi = 0.7691;

    %diblock
    r1 = 236;
    r2 = 561;
    f = 0.33;

    %triblock uses capital letters for r and f
    %triblock
    R1 = 277;
    R2 = 1289;
    F = 0.33;
```

```
    Rho1 = RhoSt;
    Rho2 = RhoBu;
    RhoS = RhoTo;

    M1 = MSt;
    M2 = MBu;
    MS = MTo;

    ed1 = edSt;
    ed2 = edBu;
    edsol = edTo;

    %Chi values. Chi3 is the chi interaction parameter between the two
    %different MW chains
    Chi1 = ChiST;
    Chi2 = ChiBT;
    Chi3 = 0;

end

if strcmp(system,'SBST')

    cODT = 0.42;
    %num fractions -> x_tri = 0.1156, x_di = 0.8844
    %wt fractions -> wtri = 0.8723, wdi = 0.1277
    %MWs -> Mns = 170.7 and 79.5kDa
    %Mws = 181.6 and 81.3kDa
    %f = 0.1836
    wtri = 0.8723;
    wdi = 0.1277;

    %diblock
    r1 = 145;%145.3
    r2 = 552;%552.4
    f = 0.1836;

    %triblock uses capital letters for r and f
    %triblock
    R1 = 156;%311.9 total
    R2 = 593;%1186.2
    F = 0.1836;

    Rho1 = RhoSt;
    Rho2 = RhoBu;
    RhoS = RhoTo;

    M1 = MSt;
    M2 = MBu;
    MS = MTo;

    ed1 = edSt;
    ed2 = edBu;
    edsol = edTo;
```

```
    %Chi values. Chi3 is the chi interaction parameter between the two
    %different MW chains
    Chi1 = ChiST;
    Chi2 = ChiBT;
    Chi3 = 0;

end


if strcmp(system, 'SIST')

        %num fractions -> x_tri = 0.1156, x_di = 0.8844
        %wt fractions -> wtri = 0.2309, wdi = 0.7691
        %wt fractions
        wtri = 0.81;
        wdi = 0.19;

        %r VALUES ARE WRONG FOR ISOPRENE. FIX THEM!!!!
        %diblock
        r1 = 104;
        r2 = 692;
        f = 0.15;

        %r VALUES ARE WRONG FOR ISOPRENE. FIX THEM!!!!
        %triblock uses capital letters for r and f
        %triblock
        R1 = 95;
        R2 = 1261;
        F = 0.15;

        Rho1 = RhoSt;
        Rho2 = RhoIs;
        RhoS = RhoTo;

        M1 = MSt;
        M2 = MIs;
        MS = MTo;

        ed1 = edSt;
        ed2 = edIs;
        edsol = edTo;

        Chi1 = ChiST;
        Chi2 = ChiIT;

        %value for ODT
        cODT = 0.59;
end


if strcmp(system,'SBCyc')
        r1 = 378;
        r2 = 1477;
        f = 0.33;
```

```
        Rho1 = RhoSt;
        Rho2 = RhoBu;
        RhoS = RhoCh;

        M1 = MSt;
        M2 = MBu;
        MS = MCh;

        ed1 = edSt;
        ed2 = edBu;
        edsol = edCh;

        Chi1 = ChiSC;
        Chi2 = ChiBC;

end

if strcmp(system,'2140')

        wtri = 0.999;
        wdi = 0.001;

        r1 = 106;
        r2 = 459;
        f = 0.20;

        %triblock uses capital letters for r and f
        %triblock
        R1 = 106;
        R2 = 918;
        F = 0.20;

        Rho1 = RhoPMMA;
        Rho2 = RhoPBA;
        RhoS = RhoTo;

        M1 = MPMMA;
        M2 = MPBA;
        MS = MTo;

        ed1 = edPMMA;
        ed2 = edPBA;
        edsol = edTo;

        Chi1 = ChiPMMAT;
        Chi2 = ChiPBAT;

        %value for ODT
        cODT = 0.53;

end

if strcmp(system,'2250')
```

```
        wtri = .999;
        wdi = 0.001;

        r1 = 167;
        r2 = 369;
        f = 0.33;

        %triblock uses capital letters for r and f
        %triblock3
        R1 = 167;
        R2 = 737;
        F = 0.33;

        Rho1 = RhoPMMA;
        Rho2 = RhoPBA;
        RhoS = RhoTo;

        M1 = MPMMA;
        M2 = MPBA;
        MS = MTo;

        ed1 = edPMMA;
        ed2 = edPBA;
        edsol = edTo;

        Chi1 = ChiPMMAT;
        Chi2 = ChiPBAT;

end

if strcmp(system,'4285')

        wtri = .999;
        wdi = 0.001;

        r1 = 239;
        r2 = 249;
        f = 0.51;

        %triblock uses capital letters for r and f
        %triblock3
        R1 = 239;
        R2 = 499;
        F = 0.51;

        Rho1 = RhoPMMA;
        Rho2 = RhoPBA;
        RhoS = RhoTo;

        M1 = MPMMA;
        M2 = MPBA;
        MS = MTo;
```

```
        ed1 = edPMMA;
        ed2 = edPBA;
        edsol = edTo;

        Chi1 = ChiPMMAT;
        Chi2 = ChiPBAT;

end


%Calculating the weight fraction of the ordering layer
%xPos is the index of the ordering front (is NOT an integer)

xPos = zeros(1,tIndexCp);

%Puts wtFront data into wtfrac

for k = timestart:tIndexCp
    if wtFront(k) ~= 0

        wtfrac(1 + k - timestart) = wtFront(k);

        %DEBUG
       % wtfrac(1+k-timestart) = 0.7;

    end

end
%F-H Calculations
%Will try to put this into a function

%This  includes the error involved

for a = 1:3
for i = 1:l
        if a==2
            wtfrac(i) = 1.047*wtfrac(i);
        else if a==3
                wtfrac(i) = 0.955*wtfrac(i)/1.047;
            end
        end

        %RN1 is the triblock rN1, and RN2 is the triblock rN2
        solfrac(i) = 1 - wtfrac(i);
        Ns(i) = solfrac(i)/MS;
        rN1(i) = f*wtfrac(i)*wdi/M1;
        rN2(i) = (1-f)*wtfrac(i)*wdi/M2;
        RN1(i) = F*wtfrac(i)*wtri/M1;
        RN2(i) = (1-F)*wtfrac(i)*wtri/M2;

        %parameter that will be used for the fsolve function used to
calculate the solvent partition by setting the activities equal to each other
        FHparam(1) = r1;
        FHparam(2) = r2;
```

```
        FHparam(3) = Chi1;
        FHparam(4) = Chi2;
        FHparam(5) = Ns(i);
        FHparam(6) = rN1(i);
        FHparam(7) = rN2(i);
        FHparam(8) = R1;
        FHparam(9) = R2;
        FHparam(10) = RN1(i);
        FHparam(11) = RN2(i);

        %X1Ns (solvent frac in ordered phase 1) guess (to calculate initial
activity)
        %Initial guess is set to equal partitioning where the densities are
        %equal. x0 is the initial guess for fsolve.
        X1Ns(i) = Ns(i)*f;
        x0 = X1Ns(i);



        %Uses an anonymous function handle to make a function of one variable
        %with a second input to the function FH
        Z = @(x0) FH(x0, FHparam);

        %Solves for X1Ns to make a1 = a2
        [x, fval] = fsolve(Z, x0);

        %Put the values obtained in fsolve into X1Ns and X2Ns
        X1Ns(i) = x;
        X2Ns(i) = Ns(i) - X1Ns(i);

        %Calculate the solvent partitioning
        Part(1,i) = ((X1Ns(i)/Ns(i))/(rN1(i)/(rN1(i)+rN2(i))));
        Part(2,i) = ((X2Ns(i)/Ns(i))/(rN2(i)/(rN1(i)+rN2(i))));
        X(1,i) = X1Ns(i)/Ns(i);
        X(2,i) = X2Ns(i)/Ns(i);

        %Calculate the phase densities
        %Factored in the total weight of the solution into the weight
fraction of the solvent and the polymer.
        wtPhaseTotal1(i) = (solfrac(i)*Part(1,i))+wtfrac(i);
        wtPhaseTotal2(i) = (solfrac(i)*Part(2,i))+wtfrac(i);

        vPhase1(i) = (wtfrac(i)/Rho1*wtPhaseTotal1(i)) +
((solfrac(i)*Part(1,i))/(RhoS*wtPhaseTotal1(i)));
        vPhase2(i) = (wtfrac(i)/Rho2*wtPhaseTotal2(i)) +
((solfrac(i)*Part(2,i))/(RhoS*wtPhaseTotal2(i)));

        RhoPhase1(i) = 1/vPhase1(i);
        RhoPhase2(i) = 1/vPhase2(i);

        %Calculate the electron densities of the two phases and the
difference
        edPhase1(i) = ((ed1*RhoPhase1(i)*wtfrac(i)/Rho1) +
(edsol*RhoPhase1(i)*solfrac(i)*Part(1,i)/RhoS))/wtPhaseTotal1(i);
        edPhase2(i) = ((ed2*RhoPhase2(i)*wtfrac(i)/Rho2) +
(edsol*RhoPhase2(i)*solfrac(i)*Part(2,i)/RhoS))/wtPhaseTotal2(i);
```

```
        delEdSq(i) = ((edPhase1(i) - edPhase2(i))^2)/1000000000000000000;

        %Calculate the phase volumes and volume fractions
        %Here, partitioning is done by calculating the theoretical solvent
        %concentration w/o partitioning using the volume fraction in each
        %phase. The volume fractions are calculated assuming that excess
volume
        %is zero.
        %If something is wrong, change the way the the partitioning is done
        v1(i) = (f*wtfrac(i)/Rho1) +
(Part(1,i)*solfrac(i)*((f/Rho1)/((f/Rho1)+((1-f)/Rho2)))/RhoS);
        v2(i) = ((1-f)*wtfrac(i)/Rho2) + (Part(2,i)*solfrac(i)*(((1-
f)/Rho2)/((f/Rho1)+((1-f)/Rho2)))/RhoS);
        Phi1(i) = v1(i)/(v1(i) + v2(i));
        Phi2(i) = v2(i)/(v1(i) + v2(i));

        %Calculating the total volume fraction ordered phase
        Vol(i) = data(i)/(delEdSq(i)*Phi1(i)*Phi2(i));

        divisor(i) = delEdSq(i)*Phi1(i)*Phi2(i);
end
        if a==1
           for j = 1:30
              aveset(j) = Vol(l+1-j)/thicknessFront(1 + l - j);

          end

        end

%Normalizing data using the last 50 pts of the range. An array with the
%last 30 values in it (aveset) is used to do this


%Find the mean of aveset in order to perform the normalization. ave is
%apparently an array for whatever reason.

%Performs normalization and produces the output
ave = mean(aveset);
%ave = 1;

for k = 1:l

        if a==1

        NormVol(k) = Vol(k)/(totalThickness(1,timestart+k)*ave);
        %NormVol(k) = Vol(k)/(ave);

        output(1,k) = time(k);
        outputwrite(1,k) = time(k);
        output(2,k) = wtfrac(k);
        outputwrite(2,k) = wtfrac(k);
        output(3,k) = NormVol(k);
        outputwrite(3,k) = NormVol(k);
        else if a==2
```

```
                NormVol(k) = Vol(k)/(totalThickness(1,timestart+k)*ave);
                %NormVol(k) = Vol(k)/(ave);

                output(4,k) = wtfrac(k);
                output(5,k) = NormVol(k);
                outputwrite(4,k) = NormVol(k);
            else
                NormVol(k) = Vol(k)/(totalThickness(1,timestart+k)*ave);
                %NormVol(k) = Vol(k)/(ave);

                output(6,k) = wtfrac(k);
                output(7,k) = NormVol(k);
                outputwrite(5,k) = NormVol(k);
            end
        end
end

end



plot(outputwrite(1,:), outputwrite(3,:),outputwrite(1,:),
outputwrite(4,:),outputwrite(1,:), outputwrite(5,:));

%Outputs into Sheet2 of the input file
xlswrite(filein, outputwrite, 'Sheet2', range);
xlswrite(filein, Part, 'Sheet3', range);
end



%Here, for SB and SIS, can probably consider the styrene blocks to be the
%same, but the butadiene and isoprene blocks as having a length of 1/2 r
%and the number of styrene blocks in the triblocks should be double that in
%the diblocks, although the volume ratio between them and the
isoprene/butadiene should be the same
% sssss-------- vs
% sssss----------------sssss
%can model the diene block as being a blend
%R1 and R2 are r values for triblock
function diff = FH(XNs, param)
%uses a modification of the Flory-Huggins theory for ternary systems with
%the blocks from the triblock being one of the components and the diblocks
%being the other
    r1 = param(1);
    r2 = param(2);
    Chi1 = param(3);
    Chi2 = param(4);
    Ns = param(5);
    rN1 = param(6);
    rN2 = param(7);
    R1 = param(8);
    R2 = param(9);
    RN1 = param(10);
    RN2 = param(11);
```

```
    %calculates the phi values using chemical potential from Geveke and
Danner paper from 1993 instead of activity
    %phi1 is the phi of the diblock polymer in phase 1
    %phiS1 is the phi of the solvent in phase 1
    %phiT1 = triblock phi in phase 1
    phi1 = rN1/(rN1 + XNs + RN1);
    phi2 = rN2/(rN2 + Ns - XNs + RN2);
    phiT1 = RN1/(rN1 + XNs + RN1);
    phiT2 = RN2/(rN2 + Ns - XNs + RN2);
    phiS1 = XNs/(rN1 + XNs + RN1);
    phiS2 = (Ns - XNs)/(rN2 + Ns - XNs + RN2);

    %Assumptions: chis are the same for each component and its counterpart
    %in the triblock, chis are not dependent on composition or molecular
weight, along with the other F-H assumptions
    diff = 298 * 8.3145 * ((log(phiS1) + phi1 + phiT1 - (phi1/r1) -
(phiT1/R1) + (Chi1*(phi1 + phiT1)^2)) - (log(phiS2) + phi2 + phiT2 -
(phi2/r2) - (phiT2/R2) + (Chi2*(phi2 + phiT2)^2)));

end
```

A2. Chapter 5 Appendix

The same diffusivity calculation procedure was used to calculate the diffusivity of the two triblock copolymers as was used in the diblock copolymers. The SIS diffusivity data is shown below.

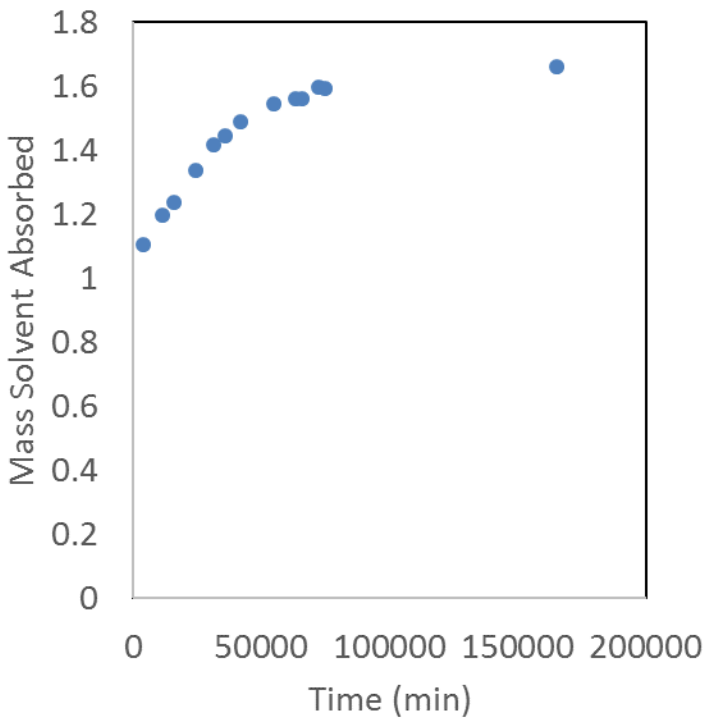

Figure A5: Mass of the SIS polymer film during sorption to determine equilibrium total mass solution

Table A2: Diffusivity calculation data for toluene in styrene/isoprene triblock copolymer

Mass	Mass Solvent	Time (min)	Thickness (m)	Solvent Concentration	M/Minf	Thickness Error	Calculated Diffusivity (m^2/s)	Error (m^2/s)
1.454	1.106	4293	1.03E-03	0.761	0.666	9.15E-08	6.45E-12	3.15E-14
1.546	1.198	11517	1.10E-03	0.775	0.721	9.73E-08	6.46E-12	9.65E-14
1.586	1.238	15926	1.13E-03	0.781	0.746	9.99E-08	6.46E-12	1.45E-13
1.685	1.337	24582	1.20E-03	0.793	0.805	1.06E-07	6.48E-12	2.59E-13
1.764	1.416	31625	1.26E-03	0.803	0.853	1.11E-07	6.49E-12	3.70E-13
1.794	1.446	36082	1.28E-03	0.806	0.871	1.13E-07	6.50E-12	4.49E-13
1.837	1.489	41774	1.31E-03	0.811	0.897	1.16E-07	6.52E-12	5.60E-13
1.893	1.545	54827	1.35E-03	0.816	0.930	1.19E-07	6.56E-12	8.55E-13
1.907	1.559	63255	1.36E-03	0.817	0.939	1.20E-07	6.59E-12	1.08E-12
1.910	1.562	66123	1.36E-03	0.818	0.940	1.21E-07	6.45E-12	3.15E-14
1.946	1.598	72158	1.39E-03	0.821	0.962	1.23E-07	6.46E-12	9.65E-14

1.942	1.594	74908	1.38E-03	0.821	0.960	1.23E-07	6.46E-12	1.45E-13

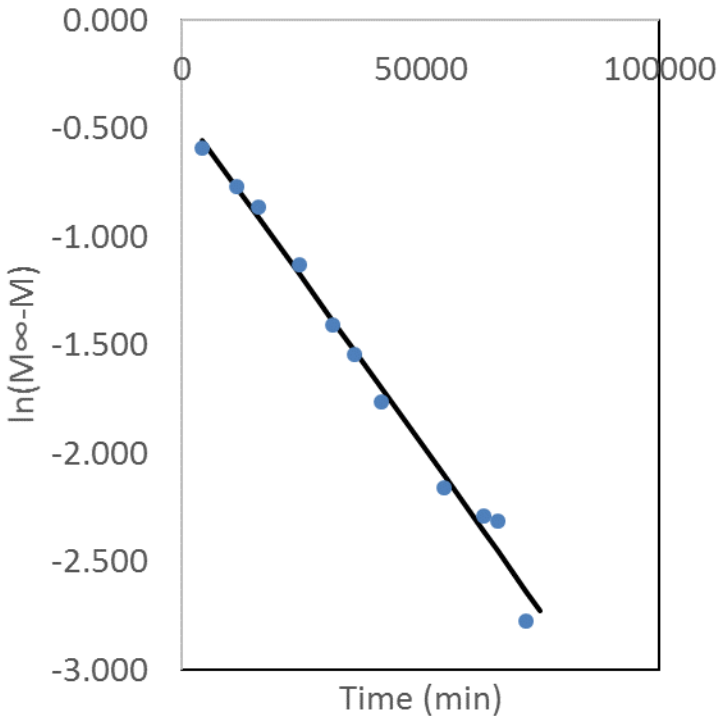

Figure A6: Fit of natural log of mass difference with respect to time for diffusivity calculation for SIS

The SBS data are shown below.

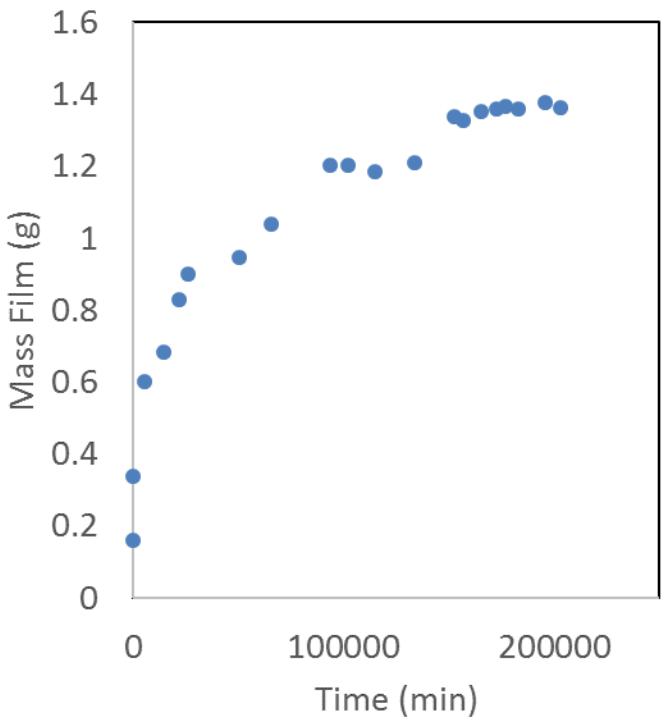

Figure A7: Mass of the SBS polymer film during sorption to determine equilibrium total mass solution

Table A3: Diffusivity calculation data for toluene in styrene/butadiene triblock copolymer

Mass	Mass Solvent	Time (min)	Thickness (m)	Solvent Concentration	M/Minf	Thickness Error	Calculated Diffusivity (m^2/s)	Error (m^2/s)
0.517	0.357	22	3.64E-04	0.691	0.379	3.22E-08	-4.14E-12	1.21E-15
0.607	0.447	1175	4.28E-04	0.736	0.444	3.79E-08	-3.91E-12	2.84E-14
0.612	0.452	1509	4.32E-04	0.738	0.448	3.82E-08	-3.85E-12	3.71E-14
0.645	0.485	2549	4.55E-04	0.752	0.472	4.03E-08	-3.64E-12	6.68E-14
0.647	0.487	2908	4.57E-04	0.753	0.474	4.05E-08	-3.58E-12	7.79E-14
0.673	0.513	4040	4.76E-04	0.762	0.493	4.22E-08	-3.37E-12	1.16E-13
0.762	0.602	7566	5.40E-04	0.790	0.558	4.78E-08	-2.77E-12	2.63E-13
0.781	0.620	9071	5.53E-04	0.795	0.571	4.90E-08	-2.53E-12	3.38E-13
0.785	0.625	10070	5.56E-04	0.796	0.574	4.93E-08	-2.39E-12	3.93E-13
0.820	0.660	12825	5.81E-04	0.805	0.600	5.15E-08	-2.01E-12	5.61E-13
0.895	0.735	18748	6.36E-04	0.821	0.655	5.63E-08	-1.37E-12	1.01E-12
0.893	0.733	20158	6.34E-04	0.821	0.654	5.62E-08	-1.24E-12	1.14E-12

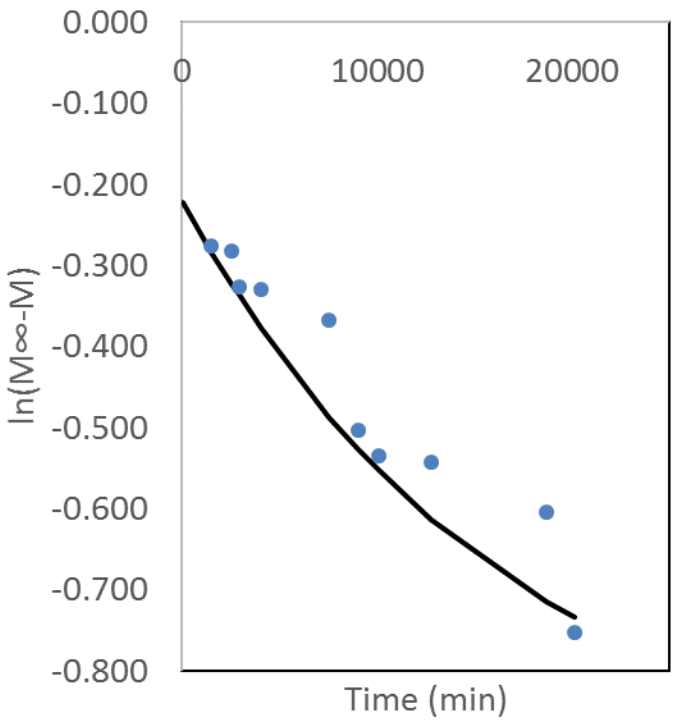

Figure A8: Fit of natural log of mass difference with respect to time for diffusivity calculation for SBS

Integrated Iq^2 data from SIS and SBS are shown below

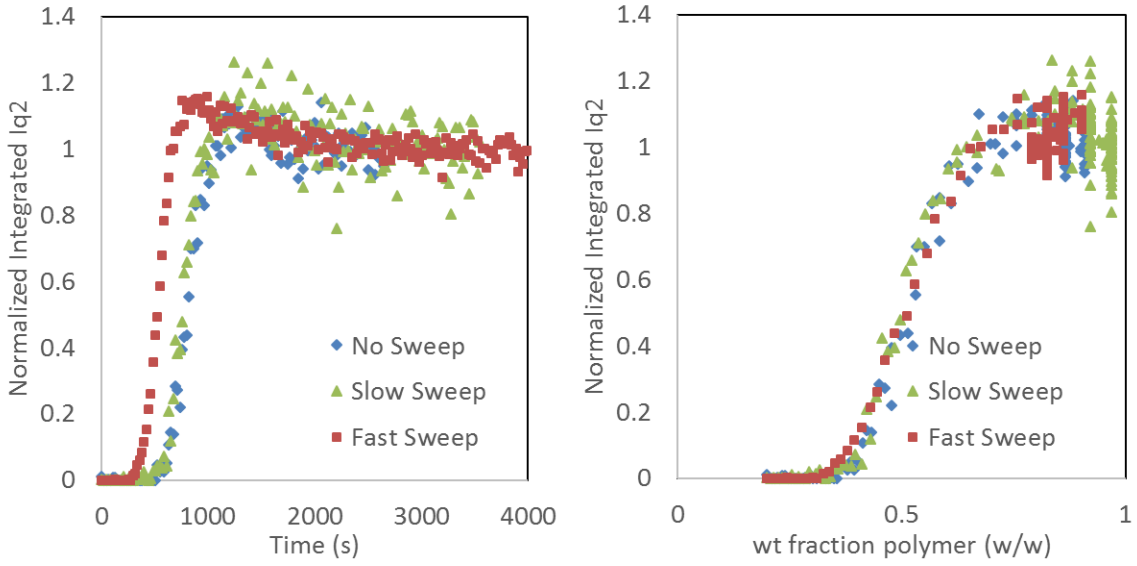

Figure A9: Integrated Iq^2 of SIS film in toluene vs time and total film concentration

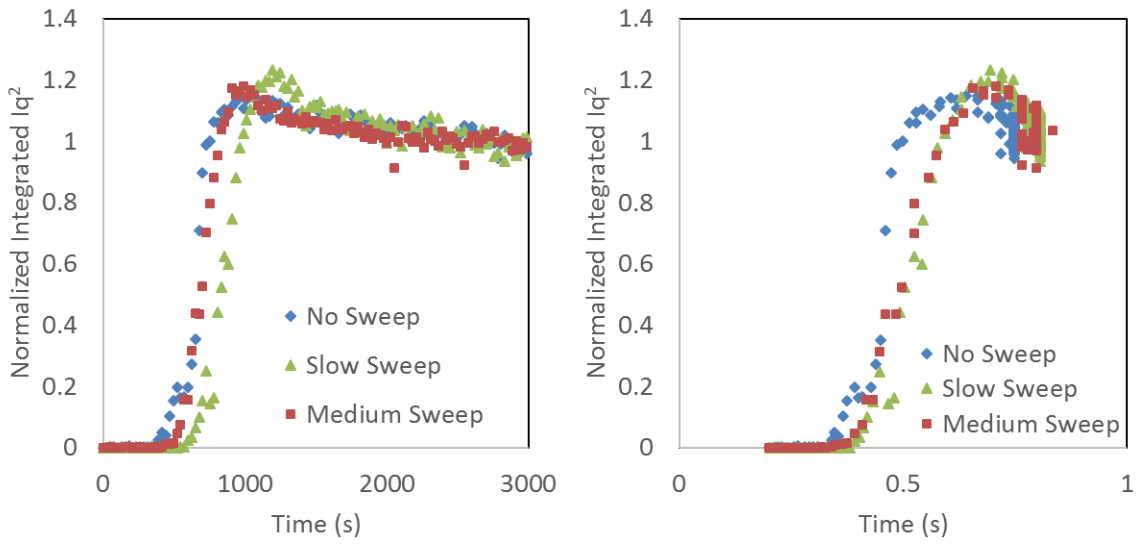

Figure A10: Integrated Iq^2 of SBS film in toluene vs time and total film concentration

A3. Chapter 6 Appendix

Polyacrylate diffusivity data is shown below. Unlike the data for the styrene/diene block copolymers, the data for calculating the maximum sorption mass is the same as that for calculating the diffusivity.

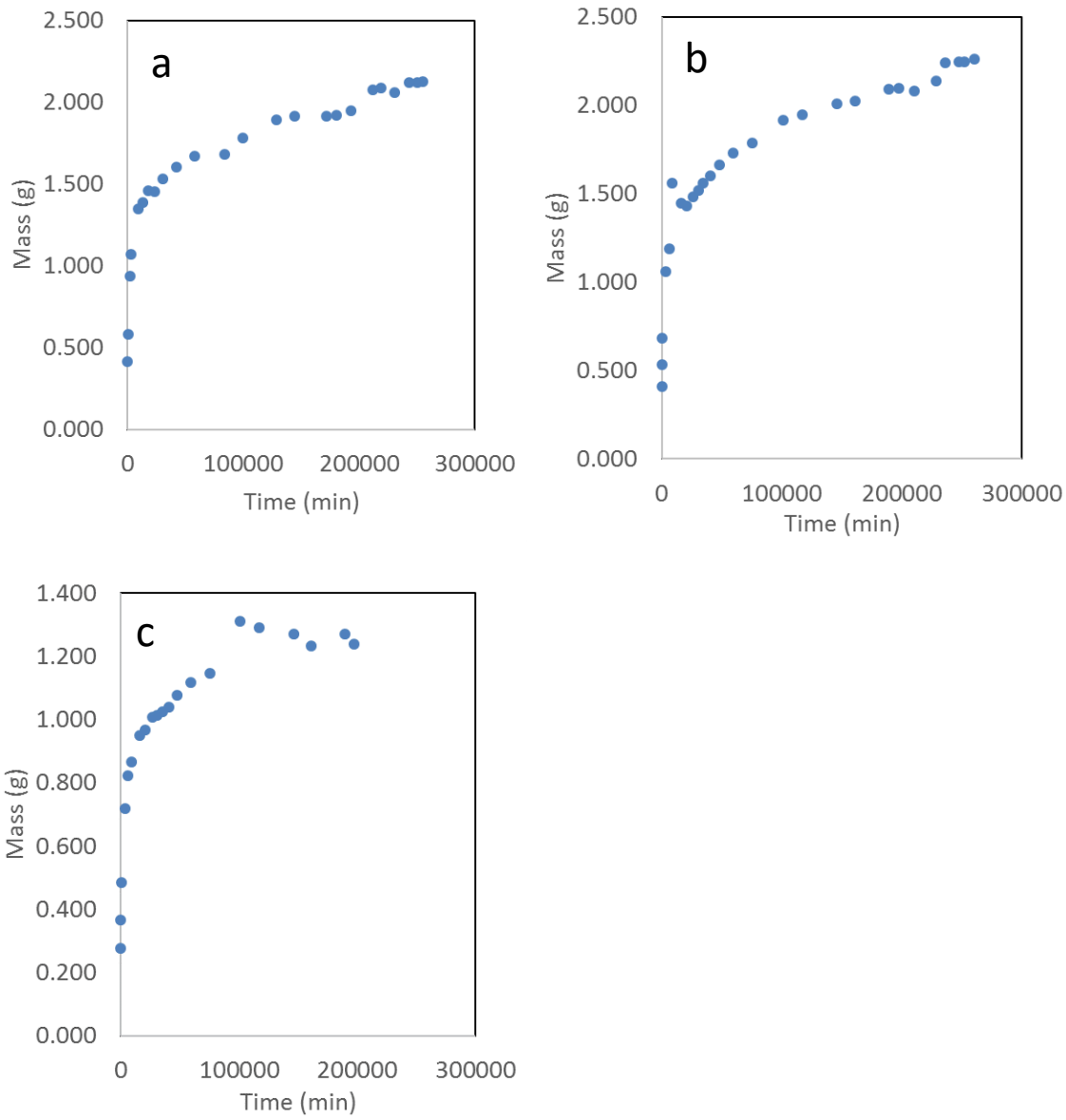

Figure A11: Mass of film during toluene sorption experiment. a) 20% PMMA b) 33% PMMA c) 51% PMMA

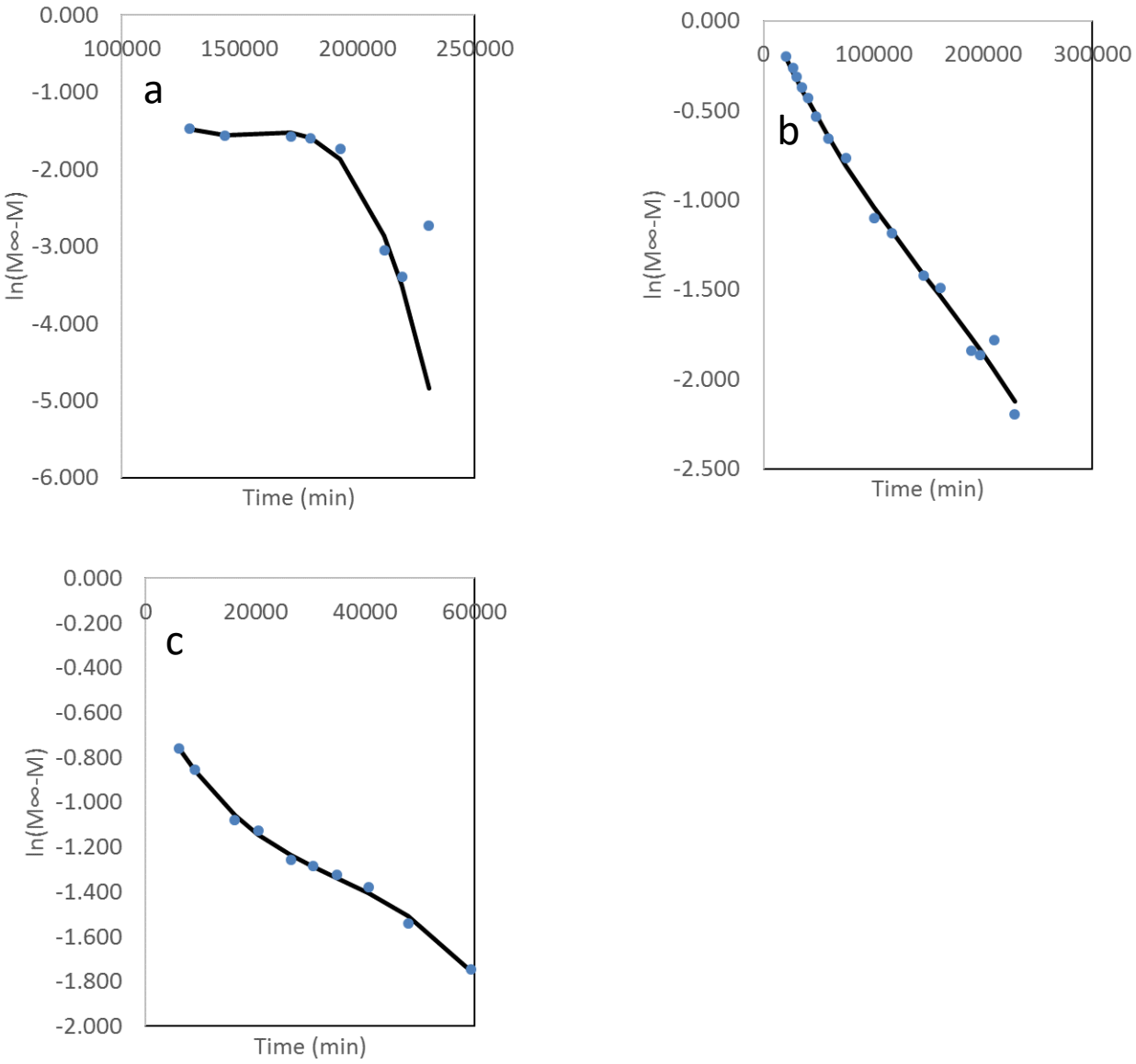

Figure A12: Fit of natural log of mass difference with respect to time for diffusivity calculation for a) 20% PMMA b) 33% PMMA c) 51% PMMA

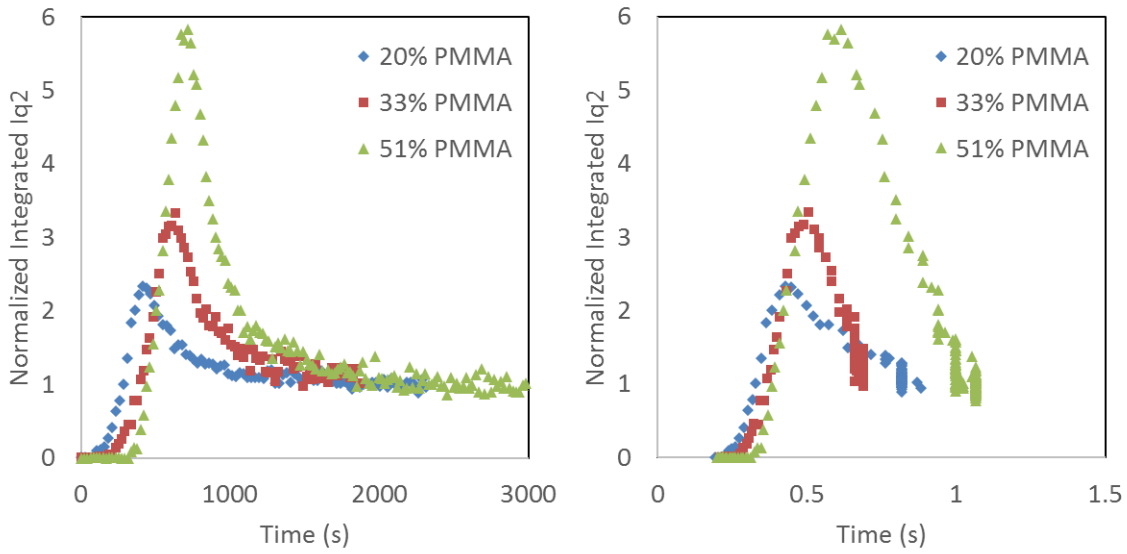

Figure A13: Integrated Iq^2 of acrylate film in toluene vs time and total film concentration

A4. Chapter 7 Appendix

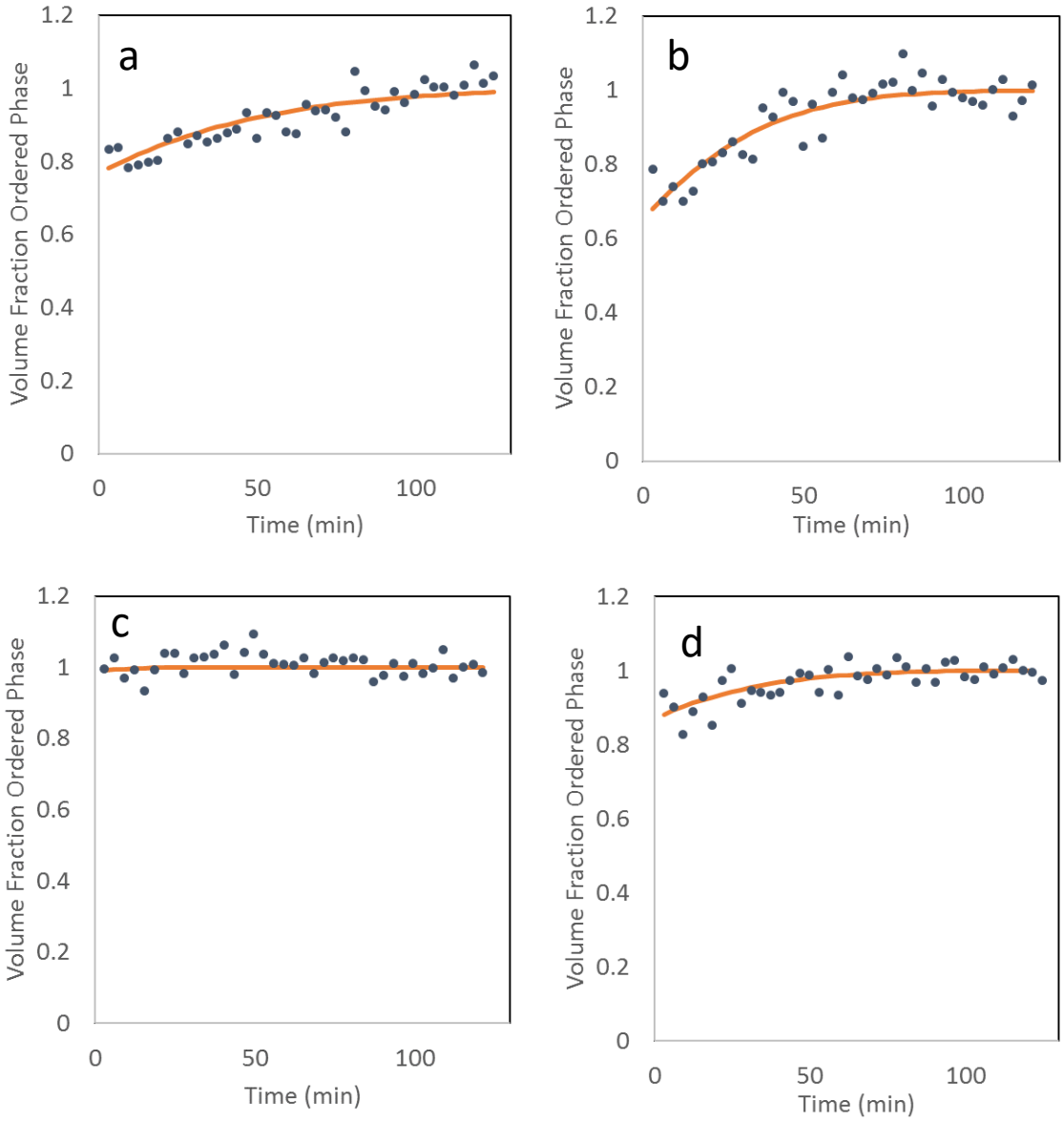
a
b
c
d
Volume Fraction Ordered Phase
Time (min)
0
0.2
0.4
0.6
0.8
1
1.2
0
50
100

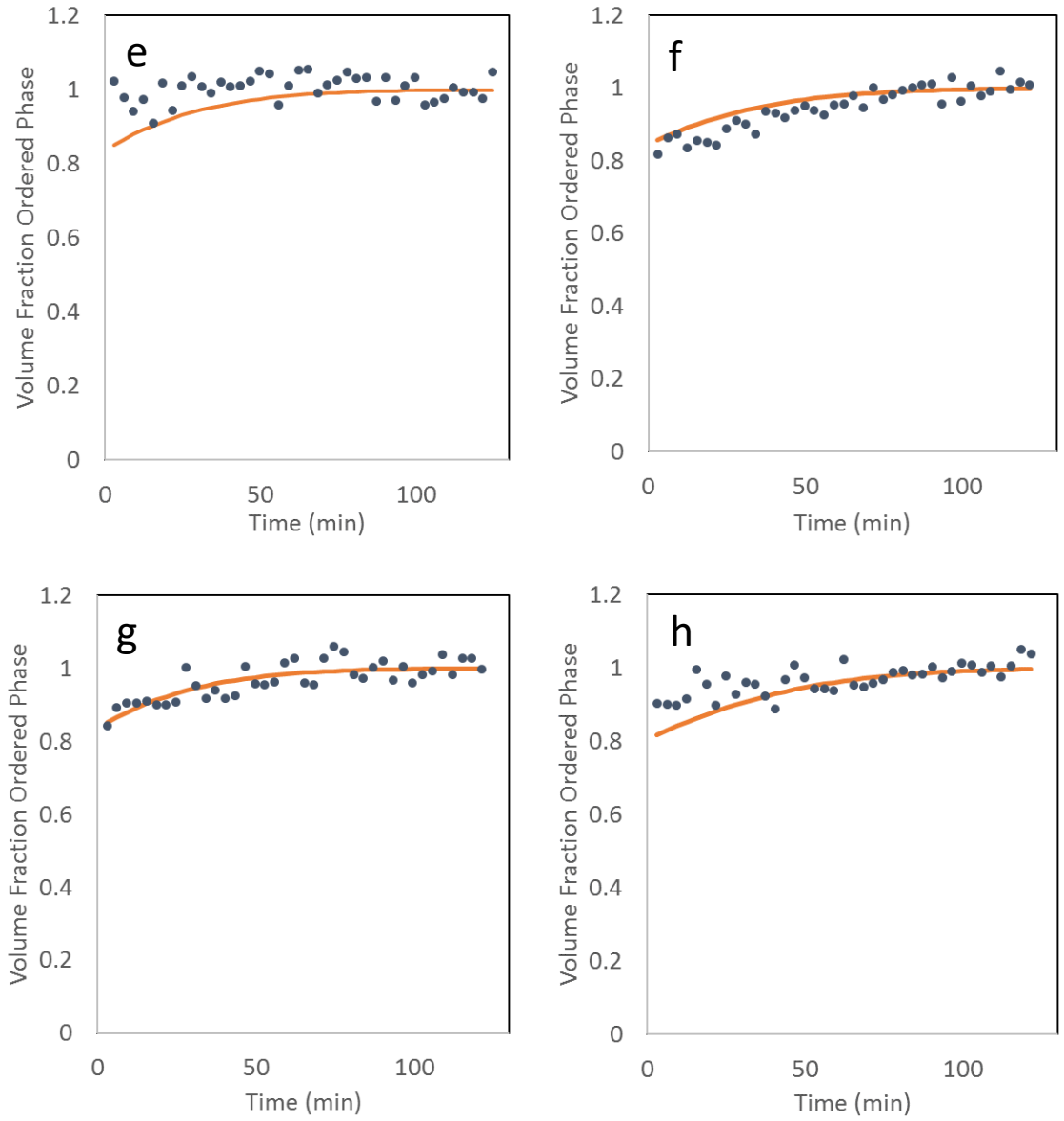

Figure A14: Volume fraction ordered phase in a) 61.3wt% b) 63.1% c) 67.7% d) 69.2% e) 69.3% f) 70.0% g) 76.4% h) 80.7%